広島大学学位請求論文

Biogeochemical cycles of iron, carbon, and trace elements in biogenic iron oxyhydroxides

（微生物生成水酸化鉄を介して生じる
鉄・炭素・微量元素の生物地球化学的循環）

2015 年

広島大学大学院理学研究科
地球惑星システム学専攻

菊池　早希子

目次

1) 主論文

Biogeochemical cycles of iron, carbon, and trace elements in biogenic iron oxyhydroxides

（微生物生成水酸化鉄を介して生じる鉄・炭素・微量元素の生物地球化学的循環）

Sakiko Kikuchi

（菊池　早希子）

2) 公表論文

1. Application of synchrotron based μ-XRF-XAFS to the speciation of Fe on single stalk in bacteriogenic iron oxides (BIOS)

   S. Kikuchi, H Makita, S Mitsunobu, Y Terada, N Yamaguchi, K Takai, and Y Takahashi

   Chemistry Letters, **40**, (2011), 680–681.

2. Characterization of biogenic iron oxides collected by the newly designed liquid culture method using diffusion chambers

   S. Kikuchi, H Makita, S Mitsunobu, N Yamaguchi, K Takai, and Y Takahashi

   Geobiology, **12**, (2014), 133–145.

3) 参考論文

1. Bacteriogenic Fe(III) (oxyhydr)oxides characterized by synchrotron microprobe coupled with spatially resolved phylogenetic analysis

   S Mitsunobu, F Shiraishi, H Makita, BN Orcutt, S Kikuchi, BB Jorgensen, Y Takahashi

   Environmental Science & Technology, **46**(2012), 3304–3311.

2. Prokaryotic abundance and community composition in a freshwater iron-rich microbial mat at circumneutral pH

   S Kato, S Kikuchi, T Kashiwabara, Y Takahashi, K Suzuki, T Itoh, M Ohkuma A Yamagishi

   Geomicrobiology Journal, **29**(2012), 896–905.

主論文

Biogeochemical cycles of iron, carbon, and trace elements in biogenic iron oxyhydroxides

By

Sakiko Kikuchi

Department of Earth and Planetary Systems Science,
Graduate School of Science,
Hiroshima University

学位論文要旨

Biogeochemical cycles of iron, carbon, and trace elements in biogenic iron oxyhydroxides
（微生物生成水酸化鉄を介して生じる鉄・炭素・微量元素の生物地球化学的循環）

広島大学大学院理学研究科　地球惑星システム学専攻　菊池　早希子

本博士論文は、微生物生成水酸化鉄(Biogenic iron oxyhydroxides: 以下 BIOS)の沈殿から堆積作用に伴う一連の微生物活動から生まれる鉄・炭素・微量元素の循環を地球化学・分子生物学的分析手法を用いて解明した研究であり、6 章に分けてまとめている。1 章では鉄鉱物が天然環境に与える影響についてまとめるとともに、鉄鉱物の生成・溶解に寄与する微生物についてまとめた。2 章では、さまざまな環境下で採取した BIOS が持つ鉄鉱物種についてまとめた。3 章では、鉄酸化菌を液体培養し BIOS を大量に採取する方法を新たに確立することで、天然の BIOS と比較して初期沈殿や吸着の少ない BIOS の鉄鉱物種・鉱物構造を分子レベルで解明した。4 章では、2 章で採取した天然の BIOS および 3 章で確立した室内合成 BIOS を用いてヒ素・イットリウム・セリウムの吸着実験を行うことで、BIOS の微量元素吸着特性を明らかにした。5 章では、BIOS が長年沈殿することで堆積作用を伴った際の鉄鉱物種変化・有機物の分解プロセスとこれらに寄与する微生物代謝について議論している。6 章は全体のまとめである。以下に各章の要旨を示す。

１章．研究背景

鉄は地球上で最も多く存在する元素の一つであり、天然で主に二価もしくは三価の価数を持つ鉱物や溶存イオンとして存在する。酸化還元電位や pH 変化に起因する鉄鉱物の沈殿・溶解は炭素など地球上の他の主用元素の循環とも深く関わる。また、鉄鉱物は吸着を通して微量元素の挙動を支配する物質として、また鉄を還元して生きる微生物の電子受容体として働いており、地球化学・環境化学・環境微生物学を含む多岐の分野から注目されてきた。中でも微生物活動により生成される水酸化鉄は Biogenic iron (oxhydr)oxides (以下 BIOS)と呼ばれ、(1) 天然に普遍的に存在すること、(2) 微量元素吸着能の高い水酸化鉄と有機物の混合体であることが知られている。一方で BIOS が天然で担う役割を理解するための基礎情報となる (i) BIOS の鉱物種、(ii) BIOS が示す吸着特性とその要因、(ii) 沈殿後の BIOS の鉱物変化や有機物分解は充分理解されておらず、合成水酸化鉄が BIOS を模擬する物質として使用され続けてきた。そこで本研究は BIOS が天然で担う役割を決定づける上記(i)〜(iii)の項目について明らかにすることで、BIOS を介した鉄・炭素・微量元素循環を総合的に理解し、BIOS が地球化学、環境化学および環境微生物学で担う役割について考察することを目的とした。

２章．天然で採取した BIOS が持つ鉄鉱物種

鉄鉱物種は、BIOS の微量元素吸着特性や生物利用性を解明する上で最も基本となる情報である。よって 2 章では、(i)地下水浸出口、(ii)海底熱水孔、(iii)温泉で採取した BIOS の全 9 試料に対し X 線吸収微細構造法を適応することで、天然 BIOS が持つ鉄鉱物種を定量的に評価した。結果として、分析対象とした天然の BIOS は異なる水温・溶存イオン条件で採取されたにもかかわらず、全てのサイトにおいて非晶質性が高い水酸化鉄から成ることが明らかになった。また、これらは BIOS を模擬する物質としてこれまで使用されてきた合成水酸化鉄の Ferrihydrite よりも結晶性が低いことが明らかになった。

３章．微好気性鉄酸化菌の液体培養により得た BIOS の詳細な鉱物種・鉱物構造

BIOS が沈殿する環境下では非結晶質な水酸化鉄の生成を促進するシリカやリンなどのイオンが多く存在しており、天然サンプルの分析のみから BIOS の非晶質性を特徴づける要因を把握することは困難である。また、天然の BIOS に含まれる多くの不純物は、BIOS そのものの吸着特性の理解も複雑にしている。よって本章では、海底で活動する微好気性鉄酸化菌である *Mariprofundus ferrooxydans* PV-1 の新たな液体培養法を確立することで、初期吸着・沈殿の少ない BIOS の大量合成を実現し、溶存イオンの違いや培養日数の違いによる鉄鉱物種変化の有無を検討した。拡散セルを使用した *M. ferrooxydans* の培養により得た BIOS は、培養初期は主に非晶質な水酸化鉄から成るが、培養日数の増加とともにより結晶性の高い水酸化鉄である Lepidocrocite の沈殿がみられた。よって鉄酸化菌の活動は沈殿当初の BIOS を非晶質化する可能性はあるが、天然 BIOS が非晶質な水酸化物として維持されるためにはシリカなどの無機イオンの寄与が重要であることが示唆された。

４章．BIOS が持つヒ素・イットリウム・セリウムの吸着特性とその要因の解明

BIOS は水酸化鉄と有機物の混合体であることで 2 つの吸着サイトを持ち、BIOS を模擬する物質として使用されてきた合成水酸化鉄(Ferrihydrite)とは異なる吸着挙動を示すことが近年の研究によりわかってきている。しかしその要因となる具体的な物理化学的性質は明らかにされていない。本研究では、陰イオンであるヒ素、陽イオンであるイットリウムとセリウムを対象として、(i)天然で採取した BIOS (in situ BIOS), (ii)室内で鉄酸化菌を培養することにより得た BIOS (in vitro BIOS), (iii)合成 ferrihydrite の 3 つの吸着媒で吸着挙動を比較することで、BIOS が持つ吸着特性とそれら特性を生み出す要因を明らかにすることを試みた。海水条件下でのバッチ吸着実験の結果、ヒ素吸着量は in situ、in vitro BIOS ともに合成 ferrihydrite より低いことが明らかになった。EXAFS より求められたヒ素吸着構造は、全ての吸着媒に対して内圏錯体構造であった。また、等電点は合成 ferrihydrite の pH8.0 に対して in situ, in vitro BIOS はそれぞれ 4.5, 5.5 であった。更に、BIOS は極めて細粒な水酸化鉄から構成されるにも関わらず、BET 表面積は合成 ferrihydrite よりも小さな値を示した。これらの結果より、BIOS へのヒ素吸着量の減少は BIOS に含まれるリンや有機物が(i)水酸化鉄に吸着することでヒ素の吸着サイトを奪うこと、(ii)水酸化鉄の凝集を促すことで表面積を減少させること、(iii)表面電荷を負にすることでヒ素と BIOS の静電的反発を生じさせることの３つであることが示された。陽イオンであるイットリウムとセリウムに対しても in situ で吸着量の低下がみられることから、上記３つの要因の中でも特に水酸化鉄の凝集効果が BIOS への微量元素吸着を阻害する要因として働くことを本研究は明らかにした。

５章．BIOS が堆積作用を経た際に生じる鉄鉱物種変化や有機物分解

2 章から 4 章で明らかにした BIOS が持つ鉱物種や吸着特性は BIOS の“沈殿時”に BIOS が示す微量元素循環を理解する上で極めて重要である。しかし、BIOS は堆積作用中に生じる微生物活動により、鉄還元や有機物分解を生じる。特に、BIOS 中の水酸化鉄や有機物は微量元素の吸着ホスト相や吸着を阻害する要因として働くため、BIOS の堆積作用中に生じる鉄還元や有機物分解は BIOS に吸着した微量元素の挙動を変化させる重要な要因となる。よって第 5 章では、BIOS を主成分とする天然の堆積物を対象として、BIOS の沈殿から堆積作用中に生じる(i)鉄鉱物種の変化、(ii)有機物分解、(iii)微生物種の変化を捉えることで、BIOS の初期続成作用時に生じる鉄・炭素の循環について考察した。XAFS 解析、TEM 観察、DNA 解析により、BIOS の沈殿後は鉄還元菌により鉄還元および有機物分解が生じる結果、水酸化鉄の一部が Siderite($FeCO_3$)や Goethite(α-FeOOH)へと変化することが明らかになった。しかし、これらの鉱物が水酸化鉄の周囲を覆ってしまうことで鉄の生物利用性が低下し、還元的な堆積物中でも多くの水酸化鉄は保存されることが明らかになった。一方鉄還元が抑制された下層堆積物中でも BIOS 中の有機物は利用

可能なため、鉄還元菌に代わってメタン生成古細菌が有機物分解を担うことがわかった。

本研究の地球化学的・環境微生物学的意義

本研究により、天然に広く分布する水酸化鉄と有機物の混合体である BIOS は(1)これまで BIOS を模擬する物質として使用されてきた無機水酸化鉄よりも結晶性が低い一方で、微量元素吸着量はそれらより低いこと、(2) BIOS 中の水酸化鉄は堆積・続成作用を経てもその大部分が変化することなく残る一方で、有機物は連続的に減少していくことが明らかとなった。本研究から得られた BIOS 中で生じる微量元素の吸着挙動・微生物代謝の素過程は、BIOS の沈殿から溶解、二次鉱物生成までの一連の変化の中で生じる微量元素の循環を理解する上で重要な知見となる。

また本研究から得られた結果は、現在の環境のみならず古環境で生じた鉄を介した微量元素循環・微生物活動の理解にもつながると考えられる。例えば先カンブリア紀に全球規模で生じた縞状鉄鉱床(Banded iron formation: BIF)の生成は微生物由来の水酸化鉄が初生鉱物であったことが指摘されている。BIF の形成やそれらに関わる微生物の関与については酸化還元状態、鉱物種と堆積層序といった地質学・地球化学的な解釈・分析に基づいて、漠然とした定性的な仮説が示されるに留まっている。これらは時間的・空間的に多くの続成作用を受けた地質試料である BIF から堆積当時の条件を復元しなければならなかったことが要因の一つとして挙げられる。本研究のように BIOS を主成分とする堆積物中の鉄と炭素の時間的・空間的変化を追った研究は極めて少なく、BIF 堆積当初にどのような微生物活動・微量元素循環が生じていたかを知る手がかりになりうる。

CONTENTS

Abstract

Biogenic iron oxyhydroxides (BIOS) are minerals that (1) scavenge various trace elements onto their surfaces and (2) work as an electron donor for microbial activities. This thesis aims to understand the cycles of iron, carbon, and trace elements within BIOS-rich sediment, from their precipitation to long-term diagenesis. Topics are divided into six chapters. Geochemical and microbiological importance of iron oxyhydroxides and microorganisms involved in BIOS precipitation-dissolution are summarized in Chapter 1. Chapter 2 describes mineral species of natural BIOS collected from a variety of location with different environmental condition. Chapter 3 describes molecular-level mineral structures of BIOS by analyzing BIOS collected from newly-designed cultivation method of Fe(II)-oxidizing bacteria. Chapter 4 is dedicated to anion and cation adsorption characteristics of BIOS focusing on physicochemical factors causing the adsorption features. Chapter 5 deals with the change of iron mineral species and organic content during BIOS sedimentation. Chapter 6 is a summary of this thesis. Following is a brief abstract of each chapter.

Chapter 1. Background and aim of this thesis

Biogenic iron oxyhydroxides (BIOS) are minerals that are precipitated by the activities of Fe(II)-oxidizing bacteria. BIOS is commonly intermixed with bacterial-induced organic materials and are widely distributed at surface environment. Since inorganic iron oxyhydroxides work as (A) scavengers for trace elements and (B) electron donors for microorganisms, one of the iron oxyhydroxides in nature (BIOS) is also suggested to have physicochemical properties similar to inorganic iron oxyhydroxides. However, there are many uncharacterized features of BIOS that may show environmental roles different from inorganic iron oxyhydroxides. This thesis identifies (i) iron mineral species, (ii) trace element adsorption characteristics, and (iii) iron and carbon bioavailability of BIOS to reveal contribution of BIOS to iron, carbon, and trace element cycles in natural environment.

Chapter 2. Mineral species and local structures of natural biogenic iron oxyhydroxides

Mineral species of BIOS are most fundamental information to characterize

physicochemical feature of BIOS. This study identified mineral species of BIOS using X-ray absorption fine structure. Microbial communities of natural BIOS are also identified to reveal ecological similarities or differences between BIOS at different sampling site. Samples are collected from various environmental conditions including hydrothermal vents, groundwater discharge points, and hot springs (total 9 samples). X-ray diffraction patters of BIOS show two broad peaks, similar to standard two-line ferrihydrite. However, extended X-ray absorption fine structure analysis showed that mineral species of natural BIOS are consisting of amorphous iron oxyhydroxides that are less ordered than standard two-line ferrihydrite. The similar mineral species among BIOS regardless of sampling site may suggest similar geochemical and ecological roles of BIOS in natural environment.

Chapter 3. Establishment of new cultivation method for Fe(II)-oxidizing bacteria and characterization of in vitro biogenic iron oxyhydroxides (BIOS)

To study the formation and mineralogical characteristics of BIOS which has less initial adsorption and co-precipitation of trace elements, a new culture method for microaerophilic Fe(II)-oxidizing bacteria is designed. An Fe(II)-oxidizing bacterium, *Mariprofundus ferrooxydan*s PV-1^{T} (ATCC, BAA–1020), was cultured by a set of diffusion chambers to prepare broad anoxic–oxic interface, in which BIOS formation is typically observed in natural environments. Iron oxide precipitates were generated during bacterial growth. Scanning electron microscopy analysis indicated that the morphological features of iron oxide precipitates in the medium (*in vitro* BIOS) were similar to those of the BIOS collected from natural deep-sea hydrothermal environments in the Northwest Eifuku Seamount field in northern Mariana Arc (*in situ* BIOS). Further chemical speciation of both *in vitro* and *in situ* BIOS using XAFS showed that both BIOS minerals were composed mainly of ferrihydrite and oligomeric stages of amorphous iron oxides with edge-sharing octahedral linkages. Cultivation of *M. ferrooxydan*s at various phosphate concentrations and at various incubation periods showed variability in mineral species, suggesting strong dependence of iron mineral species by water chemistry. Thus, inorganic ions such as silica and phosphate present in natural BIOS are suggested to be an important role for the preservation of amorphous iron oxyhydroxides in BIOS.

Chapter 4. Decrease of arsenate adsorption onto biogenic ferrihydrite: Effect of specific surface area and surface charge

Biogenic iron oxyhydroxides (BIOS) possess multiple sorption sites for trace elements and they show different adsorption behavior to that of synthetic ferrihydrite. Here I compared adsorption behavior of arsenate (As(V)) onto (i) BIOS collected from a hydrothermal vent (in situ BIOS), (ii) BIOS collected by the incubation of Fe(II)-oxidizing bacteria, *Mariprofundus ferrooxydans* (in vitro BIOS), and (iii) synthetic ferrihydrite, to identify adsorptive characteristics of BIOS. Batch adsorption experiments under seawater condition revealed that adsorption of As(V) onto both in situ and in vitro BIOS were ca. 20 to 30% lower than that of synthetic ferrihydrite between pH 4 to 10. Arsenic K-edge extended EXAFS analysis showed that local structure of As(V) adsorbed onto each adsorbent was nearly identical, forming inner-sphere complexes. However, isoelectrostatic point of in situ and in vitro BIOS showed 4.5 and 5.5 respectively, which is less than synthetic ferrihydrite (8.0). Moreover, BET specific surface area (SSA) of both in situ and in vitro BIOS showed reduced value than synthetic ferrihydrite, in spite of their fine mineral particles similar to synthetic ferrihydrite. My results suggest that reduced As(V) adsorption onto BIOS is caused mainly by phosphate and organic carbons which are commonly present in both in situ and in vitro BIOS. These ions (i) reduce active surface sites by directly masking the adsorption site, (ii) promote aggregation of particulate iron oxyhydroxides, and (iii) change surface charge of BIOS more negative to induce repulsion between ferrihydrite and As(V). Further adsorption experiment using yttrium and cerium as adsorbate showed lesser amount of adsorption for in situ BIOS, but higher amount of adsorption for in vitro BIOS compared to that for synthetic ferrihydrite. The different cation adsorption behavior among in situ and in vitro BIOS imply initial masking of surface site for in situ BIOS. These results suggest that trace element adsorption onto BIOS also depends on the availability of adsorption site even though physicochemical properties show similar results. These adsorption characteristics of BIOS will expand our understanding of trace element cycles occurring in natural environment.

Chapter 5. Biogeochemical cycles of iron and carbon during the sedimentation of biogenic

iron oxyhydroxides

Iron and carbon bioavailability in biogenic iron minerals controls the microbial community development, which affects the formation of secondary iron mineral species. In this chapter, freshwater biogenic iron-rich sediment was analyzed to investigate iron and carbon cycles in biogenic iron minerals. Microelectrode measurements revealed that redox state changed from oxic to anoxic environment at an interval of 3 cm in the sediment. The dominance of ferrihydrite in the surface sediment (depths of 0 cm to 2 cm) was replaced by goethite and siderite in deeper sediment zone (depths of 2 cm to 5 cm); this dominance was quantitatively characterized by XAFS. However, abundant ferrihydrite was preserved even in the reduced sediment. Transmission electron microscope observations revealed that siderite and goethite precipitated on the surface areas of stalks and sheaths, suggesting that the encrustation of secondary minerals around ferrihydrite may decrease ferrihydrite bioavailability. Stable isotope analysis results of methane indicated that potential microbial aceticlastic and/or methylotrophic methane significantly increased as iron reduction decreased (depth of 6 cm). 16S rRNA gene analysis results revealed the predominance of iron-oxidizing chemolithoautotrophic bacteria, particularly *Gallionellaceae* at surface sediment (depths from 0 cm to 2 cm). By contrast, 16S rRNA gene phylotype composition indicated the presence of iron-reducing bacteria (*Geobacteraceae*) and fermenting bacteria (*Syntrophaceae*) at a depth of 4 cm; uncultured *Deltaproteobacteria* and methanogenic archaea were observed at a depth of 10 cm. My results suggest that iron-reducing bacteria are implicated in organic carbon decomposition and siderite precipitation within a limited subsurface area of the sediment. Microorganisms that decompose organic carbon are replaced by methanogenic archaea in deeper sediment layers. Limited reduction of iron oxyhydroxides and continuous oxidation of organic carbon in biogenic iron-rich sediment may provide further insights into iron phase transformation and carbon cycles in modern and ancient iron deposits.

Geochemical and microbiological implication of biogenic iron oxyhydroxides from this thesis

Through this thesis, following conclusions are suggested.

(1) Biogenic iron oxyhydroxides (BIOS) consist of less poorly-ordered iron oxyhydroxides than 2-line ferrihydrite which is the mineral that have been used to mimic BIOS in previous studies. In spite of their amorphous and fine mineral particle, BIOS show smaller adsorption capacities to trace elements, especially As(V), compared to synthetic ferrihydrite.

(2) Most of the amorphous iron oxyhydroxides present in BIOS are preserved without being reduced, whereas organic materials co-exist with BIOS are gradually decomposed during the sedimentation.

These results provide better understanding of trace element cycles controlled by BIOS. Moreover, these results can be extended to microbial ecosystems and mineralogical transformation in ancient environment. For example, banded iron formations (BIFs) are common Precambrian sedimentary succession wherer biogenic iron oxyhydroxides are suggested to be initial mineral species. Since many hypotheses have been proposed for the formation of BIFs (e.g. microbial activities, iron phase transformation, and trace element cycles), there is still lack of information such as how microbial activities and iron phase transformation interact with each other. This study not only confirmed close relationship between trace element adsorption, iron phase transformation, and microbial activities, but also identified their physicochemical factors and processes to control the reaction, which can have implications to ancient environment.

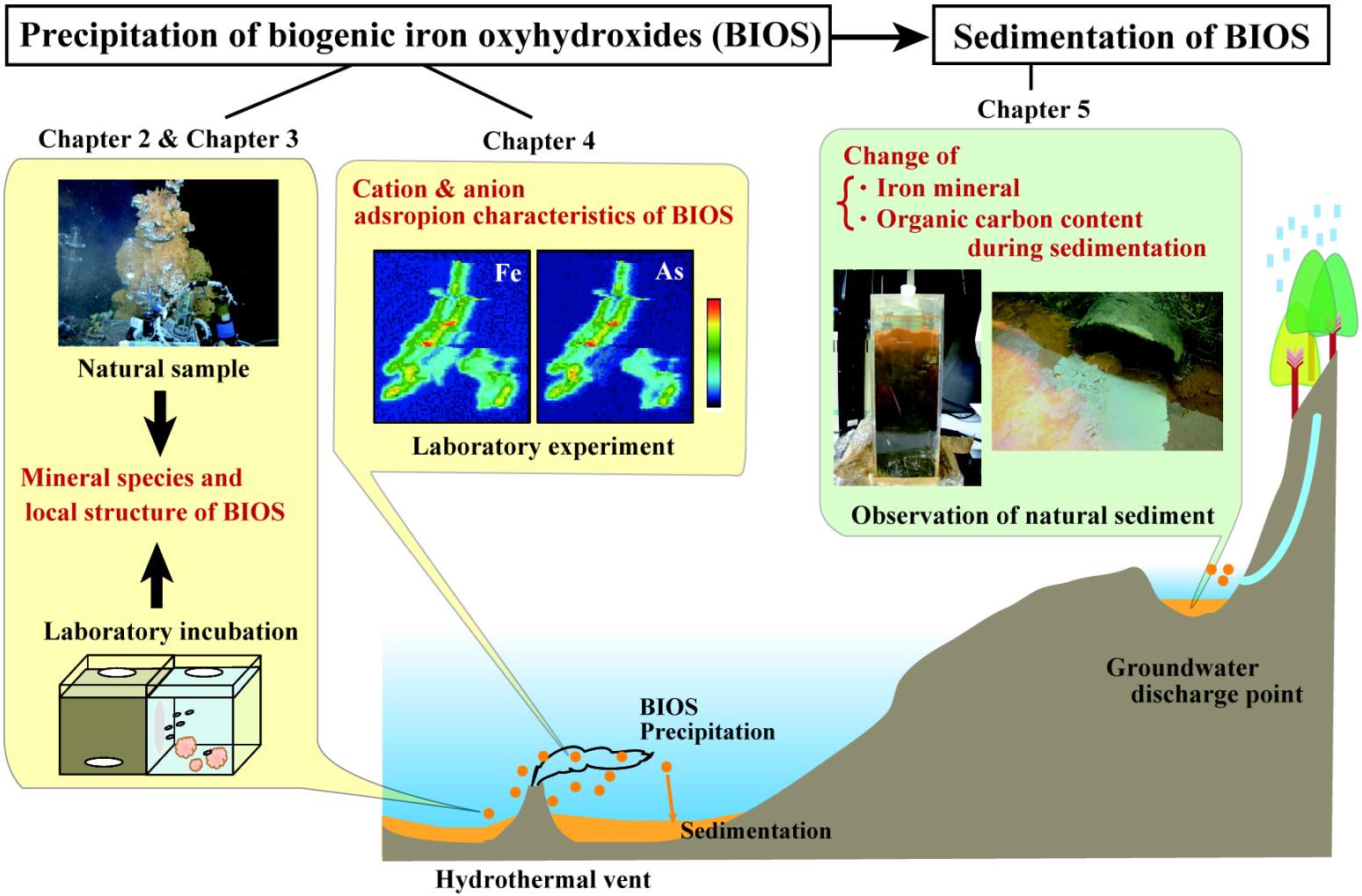

Figure. Schematic illustration of this thesis. Thesis reveals iron, carbon, trace elements cycles from precipitation of biogenic iron oxyhydroxides (BIOS) to their sedimentation.

Chapter 1. Introduction

1.1. Geochemical and ecological importance of iron oxyhydroxides

Iron is fourth abundant element in the earth's crust. Iron is involved in many reactions occurring at atmosphere, biosphere, hydrosphere, and lithosphere (Cornell and Schwertmann, 2000). The oxidation state of iron ranges from –II to +VI, but iron is mainly present as +II [ferrous iron: Fe(II)] or +III [ferric iron: Fe(III)] in most of natural conditions. The changes of these two oxidation states affect not only physicochemical properties of iron itself but also a large number of element cycles such as sulfur and carbon (Roden et al., 2004).

Iron is mainly present as mineral or dissolved iron in the environment. The distribution of iron depends on the redox potential (Eh), pH, and presence or absence of inorganic and organic ions that are strongly bound to Fe(II) and Fe(III) (Kendall et al., 2012). Each mineral has its own solubility and dissolution-precipitation processes of these iron minerals drive global cycle of iron. Under anoxic but not sulfidic condition, dissolved Fe(II) is thermodynamically stable. Concentration of dissolved Fe(II) under such condition is relatively high (up to mM range) such as in hydrothermal vents (Emerson and Moyer, 1997; Holden and Adams, 2003), groundwater discharge points (Duckworth et al., 2009; Gault et al., 2010; Kato et al., 2012), and acid mine drainages (Ferris et al., 1989; Edwards et al., 2000). Under oxygen saturated condition, however, Fe(III) is thermodynamically favored and Fe(II) ions are oxidized rapidly under neutral pH. The Fe(III) ions are then immediately hydrolyzed to form iron oxyhydroxides precipitates because of their low solubility (Stumm and Morgan, 1981). Concentration of dissolved Fe(III) hardly exceeds 10^{-9} M level (Kappler and Straub, 2005) except for colloidal formation or complexation by organic compounds (Cornell and Schwertmann, 2003).

A role of iron oxyhydroxides in environment is their high adsorption capacity to trace elements (Jambor and Dutrizac, 1998). Iron oxyhydroxides possess surface hydroxyl functional groups on their mineral surface. This fact induces electrostatic interaction between trace elements and iron oxyhydroxides (Balistrieri and Chao, 1990; Langley et al., 2009). In addition, various trace elements are adsorbed via surface complexes by ligand exchange (Waychunas et al., 1993; Sun and Doner, 1996; Rrivedi et al., 2003; Chitrakar et al., 2006).

Toxic elements such arsenic, selenium, uranium, and cadmium have been studied all over the world, which have motivated various studies such as a matter of environmental contaminations (e.g. Pierce and Moore, 1982; Balistrieri and Chao, 1990; Waychunas et al., 1993; Waite et al., 1994; Raven et al., 1998; Moyes et al., 2000; Spadini et al., 2003; Mustafa et al., 2004; Das et al., 2013). Their high adsorptive properties toward trace elements have been used as iron-based technologies to reduce the risks of contamination in water (Cundy et al., 2008).

Another role of iron oxyhydroxides in environment is that they work as electron donors for Fe(III)-reducing bacteria (Lovley, 1991). Various types of Fe(III)-reducing bacteria have been detected and isolated from natural sediments (Weiss et al., 2003; Nevin et al., 2005; Zavarzina et al., 2006; Blothe and Roden, 2009; Emerson, 2009; Langley et al., 2009; Weelink et al., 2009). Microbial Fe(III) reduction occurs with (1) organic carbon decomposition (Lovley, 1991), (2) sulfate reduction (Afonso and Stumm, 1992), and/or possibly (3) methane oxidation (Beal et al., 2009; Egger et al., 2015). Moreover, trace elements initially adsorbed onto iron oxyhydroxides desorbed from solid phase or change their host phases during microbial Fe(III) reduction, suggesting that reduction of iron oxyhydroxides impacts cycles of trace elements (Parmar et al., 2001; Zachara et al., 2001; Muehe et al., 2013a, 2013b). The utilization of iron oxyhydroxides depends on the mineral species of iron oxyhydroxides, surface area, and particle size (Roden et al., 1996; Amstaetter et al., 2012; Lentini et al., 2012).

1.2. Bacteriogenic iron oxides

The word “bacteriogenic iron oxides (BIOS)” is initially proposed by Ferris et al (1999) when they characterize natural iron oxyhydroxides that coexist with typical organic materials produced by Fe(II)-oxidizing bacteria. BIOS represent minerals that are precipitated by the activities of Fe(II)-oxidizing bacteria. There are other words such as biogenic iron minerals (Hansel et al., 2004; Kleinert et al., 2011), biogenic iron (oxyhydr)oxides (Langley et al., 2009; Toner et al., 2009), biogenically produced Fe(III) (oxyhydr)oxides (Klueglein et al., 2014; Omoregie et al., 2014), and microbial iron-mat (Emerson, 2009; Kato et al., 2012; Toner et al., 2012; Fleming et al., 2013b) that represent similar meaning as BIOS. There can

be two end member of BIOS depending on how microorganisms are involved in the BIOS formation (Konhauser, 1997; Konhauser and Ridwing, 2012). One is "biologically controlled BIOS" where bacterial activities themselves regulate iron precipitation. Since this process occurs within microenvironment which is isolated from the external environment, mineral precipitation occurs even under a condition that is not preferred under bulk environment (Konhauser, 1997). The other endmember of BIOS is "biologically induced mineralization" which causes BIOS precipitation as secondary events from interactions between the activities of microorganisms and their surrounding environment. This process is common among natural BIOS (Konhauser et al., 1997). A fundamental question about how we can distinguish BIOS from inorganic iron oxyhydroxides in natural sample is difficult to answer. Previous laboratory-based studies suggested that iron oxyhydroxides present within BIOS are relatively smaller in size compared to abiotic iron oxyhydroxides (Larese-Casanova et al., 2010). However, we cannot adapt the results to natural samples since particle size depends on water chemistry (Voegelin et al., 2010; Mikutta et al., 2008). Moreover, BIOS always contain certain amount of inorganic iron oxyhydroxides which is precipitated by autocatalytic Fe(II) oxidation (James and Ferris, 2004; Rentz et al., 2007; Druschel et al., 2008). Thus, our common recognitions about BIOS are (1) known Fe(II)-oxidizing bacteria are detected within iron oxyhydroxides by DNA analysis and/or (2) organic materials characteristics for Fe(II)-oxidizing bacteria are distributed within iron oxyhydroxides.

Common difference between BIOS and abiotic iron oxyhydroxides is that BIOS are intermixed with bacterial-induced organic materials (Chan et al., 2009; Klueglein and Kappler, 2012; Wu et al., 2014). This fact have great implications to characterize physicochemical properties of BIOS, since organic materials coexisting with iron oxyhydroxides change (1) mineral species, (2) adsorption behavior of trace elements, and (3) iron bioavailability compared to abiotic iron oxyhydroxides (Bauer and Blodau, 2006; Wang and Mulligan, 2006; Mikutta et al., 2008, Mikutta and Kretzschmar, 2008; Sharma et al., 2010; Amstaetter et al., 2012; Toner et al., 2012; Shimizu et al., 2013; Braunschweig et al., 2014; Karlsson and Persson, 2012; Lalonde et al., 2013). Although various studies have examined interconnection between organic materials and iron oxyhydroxides, only a few studies have confirmed whether the results are valid for natural BIOS (Langley et al., 2009;

Kennedy et al., 2011).

1.3. Neutrophilic Fe(II)-oxidizing bacteria involve in BIOS precipitation

Formation of BIOS occur both anoxic and oxic conditions at neutral pH. When Fe(II) is provided in the presence of oxygen and/or other oxidants, Fe(II) is oxidized into Fe(III). The kinetics of Fe(II) oxidation can be expressed by

$$\frac{-d[\mathrm{Fe(II)}]}{dt} = k[\mathrm{Fe(II)}][(\mathrm{OH}^-)]^2\ \mathrm{pO_2} \quad (1)$$

where k = $(8 \pm 2.5) \times 10^{13}$ $\mathrm{min^{-1}\ atm^{-1}\ mol^{-2}\ liter^{-2}}$ (Emerson et al., 2000). Therefore, oxidation of Fe(II) is strongly dependent on the concentration of dissolved oxygen and pH. Iron oxidation is accelerated under more oxygenated and higher pH condition which means that Fe(II)-oxidizing bacteria living under neutral pH have to compete with rapid inorganic oxidation of dissolved Fe(II). Up to now, three types of aerobic and anaerobic Fe(II)-oxidizing bacteria are suggested to produce BIOS at neutral pH: (1)microaerophilic neutrophilic Fe(II)-oxidizing bacteria, (2)anaerobic nitrate-reducing, Fe(II)-oxidizing bacteria, and (3)anaerobic photoferrotrophic Fe(II)-oxidizing bacteria (Weber et al., 2006; Emerson et al., 2010; Melton et al., 2014).

1.3.1. Microaerophilic Fe(II)-oxidizing bacterium

Microaerophilic Fe(II)-oxidizing bacteria utilize Fe(II) as electron donor and oxygen as electron acceptor. The chemical reaction of this process is explained by the following equation (Emerson et al., 2010),

$$\mathrm{Fe^{2+} + 0.25\ O_2 + H^+ \rightarrow Fe^{3+} + 1/2\ H_2O} \quad (2)$$

Most challenging thing for aerobic Fe(II)-oxidizing bacteria living at neutral pH is that they have to compete with inorganic Fe(II) oxidation. As a consequence, they found their niche at microaerophilic conditions (dissolved oxygen concentration < 50 μM) where abiotic Fe(II) oxidation is kinetically slow (Emerson and Moyer, 1997; Druschel et al., 2008). Most of microaerophilic Fe(II)-oxidizing bacteria that have been recognized so far are within a member of *Proteobacteria* and their isolates have been obtained from wetlands, hydrothermal vents, groundwater, and rhizosphere (Emerson and Moyer, 1997; Weber et al., 2006;

Emerson et al., 2007; Singer et al., 2011; Krepski et al., 2012; Woyke et al., 2013). They are within *Gallionellales (G. ferruginea*, *G. capsiferriformans*, and *Sideroxydans lithotrophicus*) in *Betaproteobacteria*, *Burkholderiales* (*Leptothrix ochracea*) in *Betaproteobacteria* (Woyke et al., 2013), and *Mariprofundales* (*Mariprofundus ferrooxydans*) in *Zetaprotebocateria*. Most of these species grow at near neutral (normally pH 6.0-6.5) and microaerobic condition in the environment (Emerson and Moyer, 1997; Weber et al., 2006; Singer et al., 2011; Krepski et al., 2012; Woyke et al., 2013). However, there are some exceptions for the habitation of *Gallionella*ceae under acidic (pH = 4.4) and fully oxic condition (de Vet et al., 2011; Fabisch et al., 2013). Phylotypes of *Gallionellales* and *Mariprofundales* are lithoautotrophic bacteria and they fix all their carbon from aqueous CO_2 (Emerson and Moyer, 1997; Singer et al., 2011; Krepski et al., 2012). The physiology and ecology of *Leptothrix ochracea* are understood to a lesser extent compared to other microaerophilic Fe(II)-oxidizng bacteria, for which both chemolithoautotrophic and heterotrophic growth are suggested (Emerson et al., 2010).

One characteristic metabolism for aerobic Fe(II)-oxidizing bacteria is that they produce unique twisted or tubular organic materials during their growth (Chan et al., 2011; Singer et al., 2011; Krepski et al., 2012). These organic materials can be a biosignature and indicator of local oxygen concentration at the time of iron precipitation (Krepski et al., 2013). Inclusion of stalks are observed at ancient rocks such as hydrothermal Fe-Si deposit (Krepski et al., 2013), cherts (Little et al., 2004), and stromatolites (Crosby et al., 2014), suggesting common presence of microaerophilic Fe(II)-oxidizing bacteria in the ancient environment. Metabolic role of the organic materials produced by the bacteria is suggested to be that the stalk works as a template where iron minerals precipitate (Chan et al., 2004). Simultaneously, selective precipitation of iron minerals onto stalks protect encrustation of the cell by the iron minerals (Chan et al., 2011). Another possibility of the role of stalk is that it works as a positioning apparatus to stay at their optimum environment (Emerson et al., 2010). However, stalk-forming Fe(II)-oxidizing bacteria does not always produce stalks (Hallbeck and Pedersen, 1990; Krepski et al., 2013) which may suggest that stalk is a byproduct of specific environmental condition. The stalks mainly consist of carboxyl-rich polysaccharides (Chan et al., 2011).

1.3.2. Anaerobic Nitrate-reducing Fe(II)-oxidizing bacteria

A few kinds of Fe(II)-oxidizing bacteria successfully oxidize Fe(II) ion anoxically with the coupling of nitrate reduction. The metabolism is expressed by the following equation (Straub et al., 1996):

$$10Fe^{2+} + 2NO_3^- + 24H_2O \rightarrow 10Fe(OH)_3 + N_2 + 18H^+ \quad (3)$$

They are recognized as nitrate-reducing Fe(II)-oxidizing bacteria which was firstly isolated by Straub et al. in 1996. Up to now, isolates have been obtained from freshwater, brackish environments and they are within the members of *Alphaproteobacteria*, *Betaproteobacteria*, *Gammaproteobacteria*, and *Deltaproteobacteria* (Straub et al., 2004; Kappler et al., 2005; Benzine et al., 2013). Most of nitrate-reducing Fe(II)-oxidizing bacteria grow mixotrophically which they need some organic materials such as acetate as carbon sources. One exception is lithoautotrophic nitrate-reducing Fe(II)-oxidizing bacterium, *Pseudogulbenkiania* sp. strains 2002 (Weber et al., 2006). Some species of nitrate-reducing Fe(II)-oxidizing bacteria are capable of utilizing Fe(II) from Fe(II) minerals such as siderite, biotite, and reduced smectite (Benzine et al., 2013).

One of the important physiological differences between nitrate-reducing Fe(II)-oxidizing bacteria and microaerophilic bacteria is that nitrate-reducing Fe(II)-oxidizing bacteria do not produce any solid organic minerals such as stalks and sheaths (Schädler et al., 2009). Instead, it is reported that they produce dissolved extracellular polysaccharides (EPS; Klueglein et al., 2014). Although iron precipitation is inhibited within the local areas of EPS, encrustation of iron minerals at cell walls and within periplasm are commonly observed in nitrate-reducing Fe(II)-oxidizing bacteria under laboratory conditions (Miot et al., 2011; Klueglein et al., 2014). However, heavy cell encrustation is only observed at high concentration of organic substrate in culture medium, suggesting successful habitances of nitrate-reducing Fe(II)-oxidizing bacteria under environmentally relevant concentration of organic substrate (Chakraborty et al., 2011).

1.3.2. Anaerobic phototrophic Fe(II)-oxidizing bacteria

In anoxic and light penetrated environments, oxidation of Fe(II) ion occurs biotically as shown by the following reaction (Ehrenreich and Widdel, 1994),

$$4Fe^{2+} + HCO_3^- + 10H_2O + hv \rightarrow 4Fe(OH)_3 + (CH_2O) + 7H^+ \quad (4)$$

Light penetrates only about 2–3 mm in modern sediment, suggesting phototrophic Fe(II) oxidizing bacteria have to find very restricted and specialized environment within sediment (Konhauser et al., 2011). Instead, light can penetrate up to one hundred meters in water column (Kappler et al., 2005). Thus, phototrophic Fe(II)-oxidizing bacteria are considered to play an important role in ancient anoxic and ferruginous ocean, especially when Precambrian banded iron formations were formed (Crowe et al., 2008).

Bacterial species of Fe(II)-oxidizing bacteria includes green sulfur bacterium, purple sulfur bacterium, and purple non-sulfur bacterium in a group of *Proteobacteria* (Melton et al., 2014). None of the isolated phototrophic Fe(II)-oxidizing bacteria produce stalk or sheath, but they produce EPS during their growth (Wu et al., 2014). They precipitate ferrihydrite which gradually transformed into goethite and lepidocrocite (Kappler and Newman, 2004).

1.4. Objective of this thesis

As overviewed above, iron oxyhydroxides are important scavengers for various trace elements and work as electron donors for microorganisms. Iron oxyhydroxides in natural environment (BIOS) can be produced by various kinds of Fe(II)-oxidizing bacteria at neutral pH and they have possibilities to scavenge various trace elements and stimulate microbial Fe(III) reduction under anoxic condition. In spite of their importance, environmental and microbiological roles of BIOS are still not clear. Especially, previous studies used inorganic ferrihydrite to mimic BIOS without fully confirming the similarities or differences of their (i) mineralogy, (ii) adsorptive characteristics, and (ii) iron and carbon bioavailability.

In the present thesis, I attempted on to reveal cycles of iron, carbon, and trace elements controlled by BIOS, from their precipitation to diagenesis, especially focusing on (1) initial iron mineral species, (2) trace elements adsorption characteristics, and (3) iron and carbon transformation/decomposition during sedimentation of BIOS.

In Chapter 2, I firstly identified mineral species and local structures of BIOS using X-ray absorption fine structures (XAFS) to get basic mineralogical information of BIOS. I collected samples in various environmental setting such as hydrothermal vents, groundwater discharge points, and hot springs. A part of this chapter is collaborated with Dr. Hiroko Makita and Dr. Satoshi Mitsunobu which was published in *Environmental Science & Technology*, **46**, 3304–3311 (*Published as* S Mitsunobu, F Shiraishi, H Makita, BN Orcutt, S Kikuchi, BB Jorgensen, Y Takahashi, Bacteriogenic Fe(III) (oxyhydr)oxides characterized by synchrotron microprobe coupled with spatially resolved phylogenetic analysis).

Chapter 3 deals with local structure of BIOS collected from newly-designed cultivation method of Fe(II)-oxidizing bacteria (*Mariprofunds ferrooxydans*). Successful establishment of new liquid cultivation method of *M. ferrooxydans* enables to understand local structure of BIOS that have less initial adsorption and co-precipitation of trace elements. I also identified mineral species of BIOS at different phosphate concentration and different incubation period. Some parts of this chapter were published in *Chemistry Letters* **40**, 680–681 [*Published as* S Kikuchi, H Makita, S Mitxunobu, Y Terada, N Yamaguchi, K Takai, Y Takahashi, Application of synchrotron μ-XRF-XAFS to the speciation of Fe on a single stalk in bacteriogenic iron oxides (BIOS)] and *Geobiology* **12**, 133–145 (*Published as* S Kikuchi, H Makita, K Takai, N Yamaguchi, Y Takahashi, Characterization of biogenic iron oxides collected by the newly designed liquid culture method using diffusion chambers).

Chapter 4 describes adsorptive characteristics of BIOS using oxyanion (arsenate) and cation (yttrium and cerium) as adsorbates. I also investigated physicochemical factors to characterize different adsorptive properties between BIOS and synthetic ferrihydrite, by analyzing specific surface area, surface charge, and local adsorption structure of arsenate.

Chapter 5 describes iron phase transformation and carbon decomposition during sedimentation of BIOS, based on the analysis of BIOS-rich sediment in freshwater environment. I used XAFS for the change of iron mineral species, transmission electron microscope for identification of mineral species, and 16S rRNA gene analysis to reveal microbial community during sedimentation of BIOS. Main part of this chapter was submitted to *Geobology* (*in revision* as S Kikuchi, H Makita, U Konno, F Shiraishi, K Takai, M Maeda, Y Takahashi, Biogeochemical cycles of iron and carbon in biogenic iron-rich sediment in a

freshwater pond).

Chapter 6 summarizes conclusions obtained throughout this thesis.

Chapter 2. Mineral species and local structures of natural biogenic iron oxyhydroxides

2.1. Introduction

Iron is present as various kinds of mineral forms including sulfides, oxides, hydroxides, carbonates, phosphates, and silicates at earth's surface (Jambor and Dutrizac, 1998; Taylor and Konhauser, 2011). Each mineral species possesses its physical and chemical properties and their characteristics show different environmental influences on natural environment. For instance, one of the iron oxyhydroxides, ferrihydrite has large surface area (up to 600 m^2/g; Jambor and Dutrizac, 1998) compared to other iron minerals (e.g. goethite and hematite) and ferrihydrite shows high adsorption capacity to trace elements (Schwertmann and Cornell, 1991). Microorganisms use ferrihydrite more effectively than the other iron oxyhydroxides which also cause cycles of trace elements during microbial reduction of ferrihydrite (Blöthe & Roden, 2009; Langley et al., 2009; Emerson et al., 2009).

Since various field- and laboratory-based studies have been updating our knowledge about geochemical, microbiological, and industrial implications of iron minerals, successful isolation of Fe(II)-oxidizing bacteria and the development of analytical techniques for microbial samples in recent decades greatly expand our knowledge about the role of biogenic iron oxides (BIOS) in natural environment (Chan et al., 2004, 2009; Singer et al., 2011; Woyke et al., 2013). Finding of Fe(II)-oxidizing bacteria that can successfully gain energy under anoxic to microaerophilic condition have changed our previous speculation that most of Fe(II) oxidation occurring in natural environment is abiotic. Further studies about the trace element adsorptive characteristics of BIOS and metabolisms of Fe(II)-oxidizing bacteria suggest that (1) BIOS adsorb various trace elements onto their surface (Ferris et al., 2000; Martinez et al., 2003; Rentz et al., 2009; Langley et al., 2009; Kennedy et al., 2011), (2) BIOS can be readily reduced by microorganisms (Langley et al., 2009), and (3) Fe(II)-oxidizing bacteria produce solid and liquid form of organic materials when they oxidize Fe(II) (Chan et al., 2011; Klueglein et al., 2014; Wu et al., 2014). Thus, BIOS have great implications on microbial activities and trace element cycles, and their mineralogical characteristic might be able to apply to various research fields such as bioremediation (Rentz

et al., 2009).

Mineral species are most fundamental information to characterize physicochemical feature of BIOS. One of the most standard analytical techniques to identify mineral species of natural sample is X-ray diffraction (XRD) analysis. The XRD patterns of BIOS collected from natural environments show poorly ordered iron oxyhydroxides, indicative of 2-line ferrihydrite (Kasama and Murakami, 2001; Kennedy et al., 2003). More detailed and spatially-resolved analytical techniques such as X-ray absorption fine structure (XAFS), X-ray photoelectron emission spectroscopy (X-PEEM), and Mossbauer spectroscopy revealed that BIOS contain goethite, lepidocrocite, akaganeite, and poorly ordered iron oxyhydroxides which is less ordered than synthetic ferrihydrite (Chan et al., 2004, 2009, 2011; Toner et al., 2009; Edwards et al., 2011). These previous studies have suggested that BIOS basically consisted of amorphous iron oxyhydroxides with some amount of crystalline iron (oxyhydr)oxides. However, detailed fractions of each mineral species and environmental functions involved in BIOS mineralogy are still not clear. It has been suggested that there is an active Fe(II) oxidation and reduction within BIOS and their activities might affect iron mineralogy. There may be some common environmental background (e.g. pH, dissolved ions, water temperature, and concentration of dissolved Fe^{2+}) at the site of BIOS precipitation.

In this study, I aimed to understand mineral species of BIOS at various sampling site (hydrothermal vents, groundwater discharged points, and hot spring). I used XRD analysis as well as XAFS to understand the details of the mineral composition and local structure of BIOS.

2.2. Materials and Methods

2.2.1. Natural sample collection

Natural samples used in this study were collected from hydrothermal vent (5 samples), groundwater discharge area (3 samples), and hot spring (1 sample). Details for the location are summarized in Table 2–1. BIOS from hydrothermal vent were collected using a remotely operated vehicle (ROV), Hyper-Dolphin, owned by the Japan Agency for Marine-Earth Science and Technology. BIOS from groundwater discharge points and hot springs were collected into 50 mL of centrifuge tube. All samples were stored at –80 °C before analysis.

2.2.2. X-ray diffraction analysis

Mineralogical properties of samples were examined by X-ray diffraction (XRD). Prior to measurements, samples were washed with MQ water and then freeze-dried. Samples were then ground into powder. Measurements were performed using M18XHF with Cu Kα radiation.

2.2.3. X-ray absorption fine structure analysis

XAFS measurements were conducted at BL01B1 in SPring-8 (Hyogo, Japan) or BL12C in KEK photon factory (Tsukuba, Japan). For measurement, wet paste samples were mounted on mixed cellulose membrane (pore size, 0.2 μm; Advantec). Standard samples were mixed with boron nitrate and formed them into pellets.

2.3. Results

2.3.1. Composition and morphologies of natural biogenic iron minerals

BIOS examined in this study ranged in color from orange to brown (Fig. 2–1A to F). At NW Eifuku and Tarama site, BIOS were precipitated at diffusing zone of hydrothermal vent where low-temperature hydrothermal water comes from sea floor. At Urashima and Snail site, BIOS covered blackish or whitish chimney mound. There was a difference in BIOS mineral colors at few cm range within BIOS at Urashima site: one was white and the other was orange in color (named as Urashima-1 and Urshima-2, respectively). At groundwater discharge points and hot spring (Budo-pond, Mizugami, Sakuragaoka, and Sambe), samples spread near the water source over the range of few meters. All the samples showed fluffy textures which were easily suspended and dispersed in water. Physicochemical conditions of natural biogenic iron minerals are displayed in Table 2–1. Water temperature ranges from 2.7 to 55 ˚C. The pH of the water was slightly acidic (6.0) to neutral. Concentrations of Fe^{2+} were 0.01 to 0.29 mM.

Iron was most abundant element in most of the samples which ranged from 44 to 75 wt% (calculated as Fe_2O_3). One exception is observed at Snail site where the content of silicate (50 wt%) exceeded the abundance of iron (30 wt%). Second abundant element among the BIOS

was silica which was ranging from 12 to 50 wt%. Phosphate was also abundant among the BIOS which ranging from 0.3 to 3.7 wt%.

2.3.2. X-ray diffraction patterns of BIOS

Bulk mineral species of natural samples were firstly examined by most standard analytical technique for mineralogy: power XRD (Fig. 2–2). Most of the samples show only broad peaks, typical for amorphous minerals. Snail site shows exceptional result compared with the other samples in that it had prominent peaks at 31.8˚, 45.5˚, and 56.5˚ 2θ with a broad peak at ca. 22˚. These peaks were attributed to the presence of crystalline silica mineral and amorphous silica, consistent with the abundant composition (50 wt%) of SiO_2 obtained from XRF analysis. XRD patterns of Budo-pond, Sakuragaoka, Mizukgami showed two broad peaks which were similar to standard 2-line ferrihydrite. However, peaks were much more broadened than standard ferrihydrite. Sambe, NW Eifuku, and Urashima-2 also showed two broad peaks although the strongest peak positions shifted to smaller angles compared to standard ferrihydrite. Thus, XRD analyses of BIOS samples indicate that BIOS were mainly consisted of amorphous phase of iron oxyhydroxides.

2.3.3. X-ray absorption structure of BIOS

Samples were examined by iron K-edge XAFS to obtain quantitative mineral composition (Figs. 2–3 and 2–4). Peak of X-ray absorption near edge structure (XANES) were within the areas of ferric iron, suggesting that ferric minerals dominate iron mineral species of BIOS (Fig. 2–3A). All natural BIOS showed similar XANES spectra in each other, but different from spectra obtained from standard iron oxyhydroxides such as goethite and 2-line ferrihydrite. There is XANES peak at 7128 eV and broad shoulder at ca. 7134 eV. This feature showed a similarity to XANES spectra obtained from iron-carboxylate (co-precipitate of organic material and ferric iron) and iron phosphate. The similarities of spectra between BIOS samples and iron phosphate were also recognized by first derivative of normalized absorption (Fig. 2–3B). There is no prominent peak at 7134 eV in ferrihydrite whereas there is small peak at 7134 eV for iron phosphate. Derivative of normalized absorption in BIOS have broad shoulder around 7134 eV, suggesting more similar structures to iron phosphate

than to ferrihydrite.

Iron extended X-ray absorption fine structure (EXAFS) is displayed in Fig. 2–4. EXAFS spectra showed similar structures among the samples despite that their sampling sites were different. However, none of the EXAFS spectra for natural BIOS were identical to standard minerals that we measured. This result suggests that BIOS are a mixture of two or more minerals. Since XANES spectra have limitations in determining the fraction of minerals, linear combination fitting of EXAFS spectra was conducted. We selected 2-line ferrihydrite and iron-phosphate as reference minerals. Iron phosphate represents small iron oligomers whereas 2-line ferrihydrite represents iron oxyhydroxide that have been considered as most possible mineral for BIOS (Kikuchi et al., 2014). Goodness of the fitting was calculated by the following equation,

$$R = \frac{\sum(I_{sample}(E) - I_{calc}(E))^2}{\sum I_{sample}(E)^2} \quad (1)$$

where I_{sample} and I_{calc} are the normalized absorption of samples and calculated spectra. The fitting result suggests that BIOS contain 31 to 53% of ferrihydrite in addition to the inclusion of 47 to 69% of iron oligomers.

To understand local structures of BIOS that characterize the inclusion of iron oligomers, shell-by-shell fitting of iron K-edge EXAFS spectra was conducted for natural BIOS. In addition, results were compared with local structures of standard ferrihydrite. The radial structure functions (RSFs) of BIOS are shown in Figure 2–5 and the shell-by-shell fittings are shown in Table 2–3. The RSFs exhibited one prominent shell at distance of 1.95 Å, which was attributed to Fe-O atom pairs (Toner et al., 2009). There were another shells at radial distance of 3.06 Å and 3.42 Å. They are attributed to edge- and corner-sharing linkages of octahedral iron, respectively (Mikkuta et al., 2008; Toner et al., 2009). Although edge- and corner-sharing linkages can be fitted in every natural BIOS, coordination number of corner-sharing linkages were reduced in BIOS compared to standard ferrihydrite.

2.4. Discussion

In this study, mineral species and local structures of BIOS collected from groundwater discharge points, hydrothermal vents, and hot springs were identified. The XRD and XAFS

analysis of BIOS showed similar results regardless of the sampling sites. However, mineral species of BIOS were not identical to standard 2-line ferrihydrite which is one of the minerals that have been used to mimic natural iron oxyhydroxides (Roden et al, 1998; Jambor et al., 1998). Characteristic features of natural BIOS which are different from standard ferrihydrite are (1) shift of XRD peak to smaller angle and/or decrease of intensity of XRD peak and (2) inclusion of oligomeric stages of iron oxyhydroxides which is characterized by reduced corner-sharing Fe–O_6 linkages. The results are consistent with previous XAFS measurement of BIOS collected from hydrothermal vent (Toner et al., 2009; 2012). Given that water chemistry and physicochemical properties (e.g. pH, temperature, and Eh) significantly control mineral species of iron in the environment (Yee, 2006; Dyer et al., 2010; Voegelin et al., 2010; Cismasu et al., 2011), similar mineral species of BIOS regardless of sampling sites may reveal the importance of geochemical setting where BIOS precipitation occurs.

There are some common features of BIOS among those collected from the different sampling sites. One is abundant inclusion of silica which ranging from 12 to 50wt% (calculated as SiO_2). Silica contained in natural BIOS likely originates from hydrothermal water or groundwater which contains high concentration of silicic acid (DeMaster et al., 1995). Amorphous and crystalline silica (e.g. quartz and opal) were not identified by XRD analysis except at Snail site, indicating that silicic acid is adsorbed and/or co-precipitated with BIOS at most of the sampling sites, where concentration of silicic acid ranged from 0.2 to 0.6 mM. On the contrary, high concentration of silicic acid (2.9 mM) at Snail site promoted precipitation of the silica minerals. The other common feature of BIOS is the inclusion of phosphate which ranged from 0.3 to 3.7 wt%. Phosphate has a high affinity for iron oxyhydroxides (Thibault et al., 2009), suggesting common accumulation of phosphate by natural iron oxyhydroxides (Perret et al., 2000; Rose et al., 1997). Oligomeric stages of iron oxyhydroxides which is characterized by the reduced corner-sharing linkages of iron have been reported in the presence of silicate (Voegelin et al., 2010), phosphate (Rose et al., 1997), and organic carbons (Mikutta et al., 2008), suggesting the effect of inorganic and organic ions on the formation of less-ordered iron oxyhydroxides than 2-line ferrihydrite within BIOS (Toner et al., 2012).

To identify most possible ligands to induce oligomeric stages of iron oxyhydroxides

within BIOS, I further examined correlations between mineral fractions and the concentration of three inorganic and organic ions that inhibit polymerization of iron as discussed above: silicate, phosphate, and organic carbon (OC). Since OC and phosphate did not show any prominent correlation to ferrihydrite fraction (data not shown), a correlation has been identified in the case of silica (Fig. 2–6). Strong negative correlation ($R^2 = 0.998$) have been obtained when Si/Fe molar ratio is less than 1.0, whereas correlation between Si/Fe and ferrihydrite fraction seems to reach equilibrium at Si/Fe molar ratios larger than 1.0. These trends are characteristic feature when SiO_4 ligands involved into the growth of iron species (Doelsch et al., 2003). At Si/Fe ratio less than 1.0, increasing silica concentration leads to a gradual increase of inhibition of iron polymerization, which means that the effect gradually reduces ferrihydrite fraction within BIOS. In contrast, inhibition effect of iron polymerization did not increase further at Si/Fe molar ratio larger than 1.0. I thus suggest that silica contained in natural BIOS shows the most prominent role to induce oligomeric stages of iron oxyhydroxides.

Figures and Tables

Table 2–1. Description and water chemistry of natural BIOS.

Area	sample name	Sample color	Location	Depth or altitude (m)	Temperature (˚C)	pH	Fe^{2+} (mM)	Si (mM)	K^{+} (mM)	Na^{+} (mM)	Mg^{2+} (mM)	Alkalinity (mM)
hydrothermal vent	NW Eifuku	Orange	21°15.0'N, 144°00.0'E	-1676	2.7	7.4	NA	NA	NA	NA	NA	ND
	Tarama	Orange	25°05.2113N,124°32.0322E	-1532	NA	6.4	0.240	1.04	NA	NA	NA	6.84
	Urashima-1	White	12°55.264'N,143°38.863'E	-2899	5.6	6.0	0.150	0.550	9.80	442	53.7	2.30
	Urashima-2	Orange	12°55.264'N,143°38.863'E	-2899	5.6	6.0	0.150	0.550	9.80	442	53.7	2.30
	Snail	Orange	12°57.151'N, 143°37.128'E	-2868	55.1	6.2	0.01	2.923	12.9	428	44.0	2.00
Groundwater discharge point	Budo-pond	Brown	34°24.04'N, 132°42.47'E	+211	17	6.8	0.290	0.06	0.0593	0.482	0.0896	1.91
	Mizugami	Brown	35°35.44'N,139°43.59'E	+3	NA	NA	NA	NA	NA	NA	NA	ND
	Sakuragaoka	Brown	35°38.08'N,139°27.44'E	+100	NA	NA	NA	NA	NA	NA	NA	ND
Hot spring	Sambe	Orange	35°06.54'N,132°37.46'E	+478	41	6.4	0.05	ND	1.5	20.9	2.53	ND

Table 2–2. Elemental composition of natural BIOS.

Area	sample name	Fe_2O_3	MnO	MgO	CaO	Na_2O	K_2O	TiO_2	P_2O_5	SiO_2	Al_2O_3	Organic carbon
hydrothermal vent	NW Eifuku	75	0.28	0.73	1.9	1.61	0.34	0.005	1.6	15	0.54	1.58
	Tarama	56	0.16	0.63	1.3	0.69	0.27	0.026	3.7	14	0.83	NA
	Urashima-1	44	0.59	1.14	0.4	0.92	0.33	< 0.001	0.3	42	0.04	0.70
	Urashima-2	44	0.59	1.14	0.4	0.92	0.33	< 0.001	0.3	42	0.04	0.70
	Snail	30	0.44	0.47	0.6	0.61	0.26	0.003	1.6	50	0.12	0.31
Groundwater discharge point	Budo-pond	60	NA	NA	NA	NA	NA	NA	NA	NA	NA	3.05
	Mizugami	NA	NA	NA	NA	NA	NA	NA	NA	NA	NA	NA
	Sakuragaoka	76	5.41	0.23	3.5	NA	0.15	0.05	0.8	12	0.85	NA
Hot spring	Sambe	67	1.72	0.18	2.9	0.43	0.42	NA	3.6	19	0.13	0.90

Table 2–3. Results of EXAFS fitting. Ferrihydrite and iron phosphate are used as standard mineral. Ferrihydrite represents amorphous iron oxyhydroxides with edge- and corner-sharing linkage of octahedral iron(III) and iron phosphate represents small iron oligomers.

Area	sample name	Ferrihydrite	Iron-phosphate	R
hydrothermal vent	NW Eifuku	53(2)	47(2)	0.007
	Tarama	40(2)	60(2)	0.008
	Urashima-1	27(3)	73(1)	0.063
	Urashima-2	26(3)	74(3)	0.021
	Snail	27(3)	73(3)	0.021
Groundwater discharge point	Budo-pond	69(2)	31(2)	0.008
	Mizugami	45(2)	55(2)	0.008
	Sakuragaoka	62(2)	38(2)	0.007
Hot spring	Sambe	31(2)	69(2)	0.007

Table 2–4. Results from shell-by-shell fitting of Fe K-edge EXAFS spectra. Fits are performed in *k*-space from 2.5 to 12 Å.

sample	Atom	CN[a]	R(Å)[b]	σ^2(Å^2)[c]	ΔE_0[d]
synFH[e]	Fe-O	4.3 ± 0.4	1.95 ± 0.01	0.110	-5.6
	Fe-Fe	3.2 ± 0.6	3.06 ± 0.02	0.020	
	Fe-Fe	1.5 ± 0.6	3.42 ± 0.02	0.011	
NW Eifuku[e]	Fe-O	5.2 ± 0.4	1.97 ± 0.01	0.012	-4.9
	Fe-Fe	3.3 ± 0.6	3.09 ± 0.02	0.020	
	Fe-Fe	0.8 ± 0.6	3.40 ± 0.02	0.011	
Tarama	Fe-O	4.9 ± 0.4	1.97 ± 0.01	0.011	-4.8
	Fe-Fe	3.5 ± 0.7	3.10 ± 0.02	0.021	
	Fe-Fe	0.9 ± 0.4	3.42 ± 0.03	0.011	
Urashima-1	Fe-O	5.2 ± 0.4	1.98 ± 0.01	0.011	-4.7
	Fe-Fe	4.7 ± 1.3	3.12 ± 0.03	0.029	
	Fe-Fe	0.4 ± 0.2	3.47 ± 0.03	0.001	
Urashima-2	Fe-O	4.7 ± 0.4	1.97 ± 0.01	0.009	-5.9
	Fe-Fe	3.1 ± 0.9	3.10 ± 0.03	0.023	
	Fe-Fe	0.3 ± 0.1	3.44 ± 0.04	0.001	
Snail	Fe-O	5.1 ± 0.4	1.98 ± 0.01	0.010	-4.3
	Fe-Fe	3.0 ± 0.6	3.11± 0.02	0.017	
	Fe-Fe	0.4 ± 0.2	3.42 ± 0.04	0.004	
Budo-pond	Fe-O	4.8 ± 0.4	1.96 ± 0.01	0.038	-6.7
	Fe-Fe	3.2 ± 0.7	3.07 ± 0.02	0.020	
	Fe-Fe	0.9 ± 0.3	3.42 ± 0.02	0.006	
Mizugami	Fe-O	4.9 ± 0.4	1.97 ± 0.01	0.011	-6.6
	Fe-Fe	3.5 ± 0.6	3.09 ± 0.02	0.020	
	Fe-Fe	1.5 ± 0.6	3.41 ± 0.03	0.016	
Sakuragaoka	Fe-O	4.8 ± 0.4	1.96 ± 0.01	0.011	-6.5
	Fe-Fe	3.5 ± 0.7	3.07 ± 0.02	0.018	
	Fe-Fe	1.9 ± 0.4	3.41 ± 0.03	0.015	
sambe	Fe-O	5.1 ± 0.4	1.97 ± 0.01	0.010	-4.7
	Fe-Fe	3.8 ± 0.9	3.10 ± 0.02	0.024	
	Fe-Fe	0.7 ± 0.3	3.43 ± 0.04	0.009	

[a] Coordination number
[b] Radial distance
[c] Debye Waller parameter
[d] Energy shift
[e] Data from Kikuchi et al. (2014)

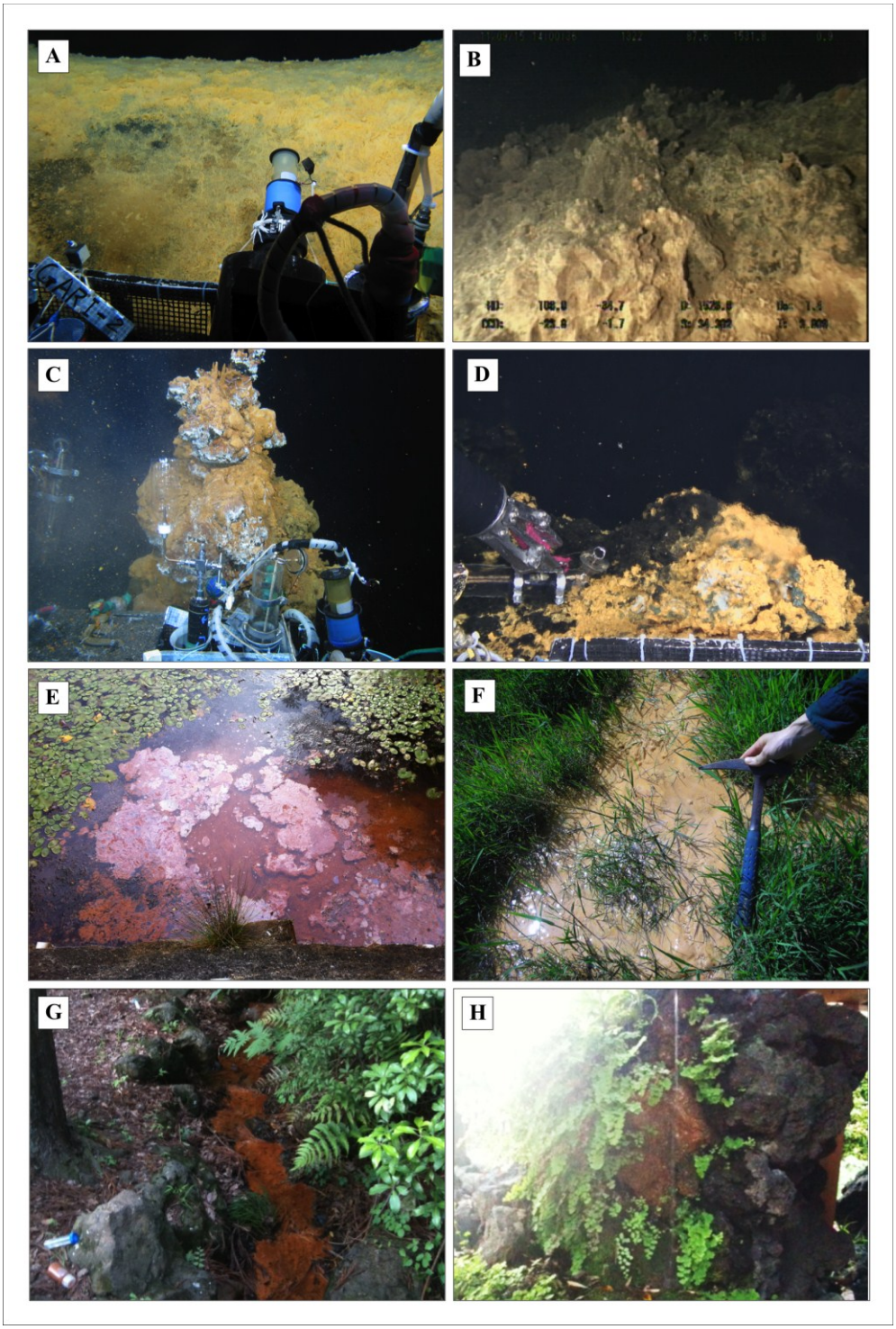

Fig. 2–1. Photographs of sampling locations at (A)NW Eifuku, (B) Tarama, (C) Urashima, (D) Snail, (E) Budo-pond, (F) Sambe, (G) Sakuragaoka, and (H) Mizugami site. Biogenic iron oxyhydroxides show fluffy texture at all sampling site which color are yellowish or orangish.

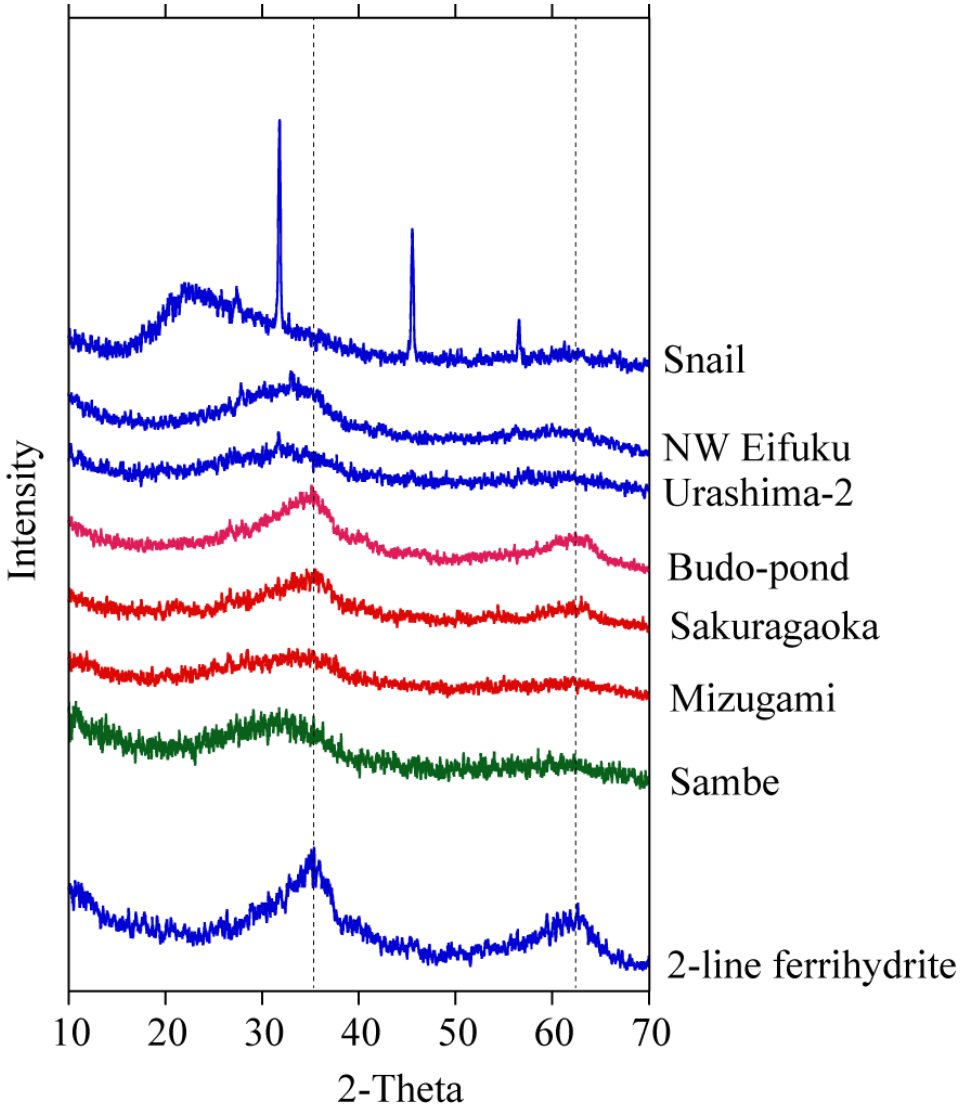

Fig. 2–2. Powder XRD spectra of natural BIOS samples and two-line ferrihydrite. Most of BIOS samples show broad two peaks similar to 2-line ferrihydrite except for Snail site.

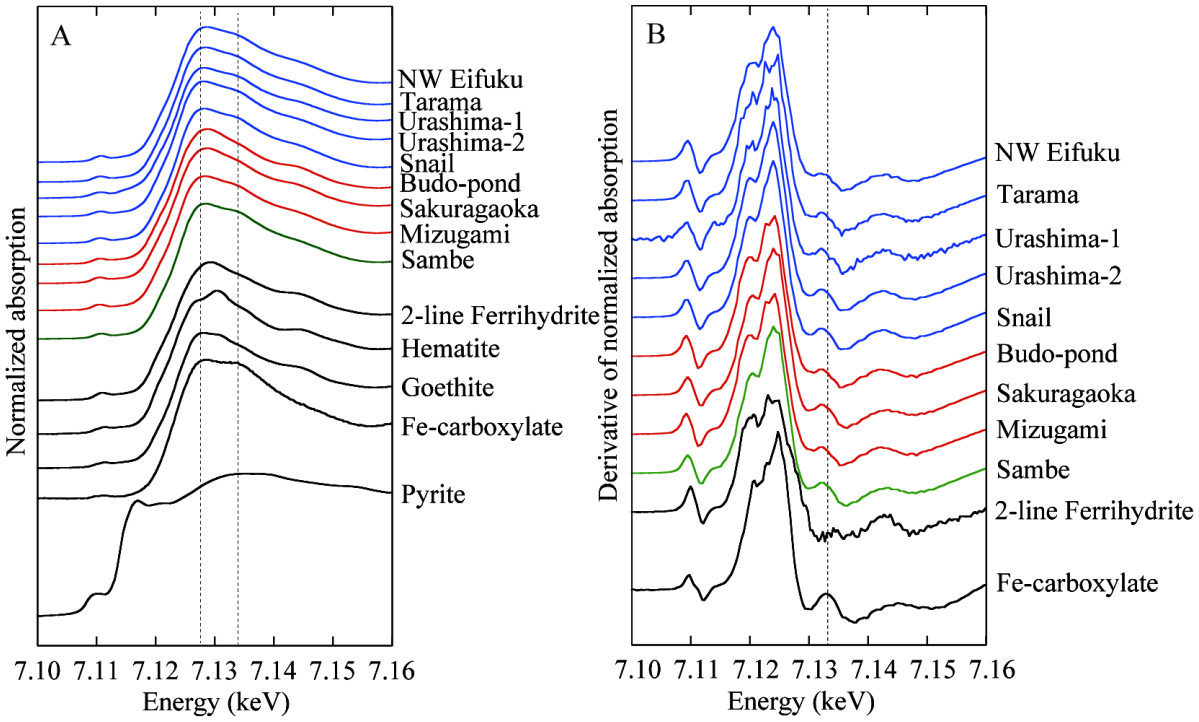

Fig. 2–3. XANES and derivative of normalized absorption of BIOS samples and standard materials. All BIOS samples show similar XANES and derivative of normalized absorption spectra regardless of sampling site. Dashed line represent characteristic features of BIOS that are not similar to that of ferrihydrite. Green, red, and blue spectra indicate hot spring, groundwater discharged points, and hydrothermal vents, respectively.

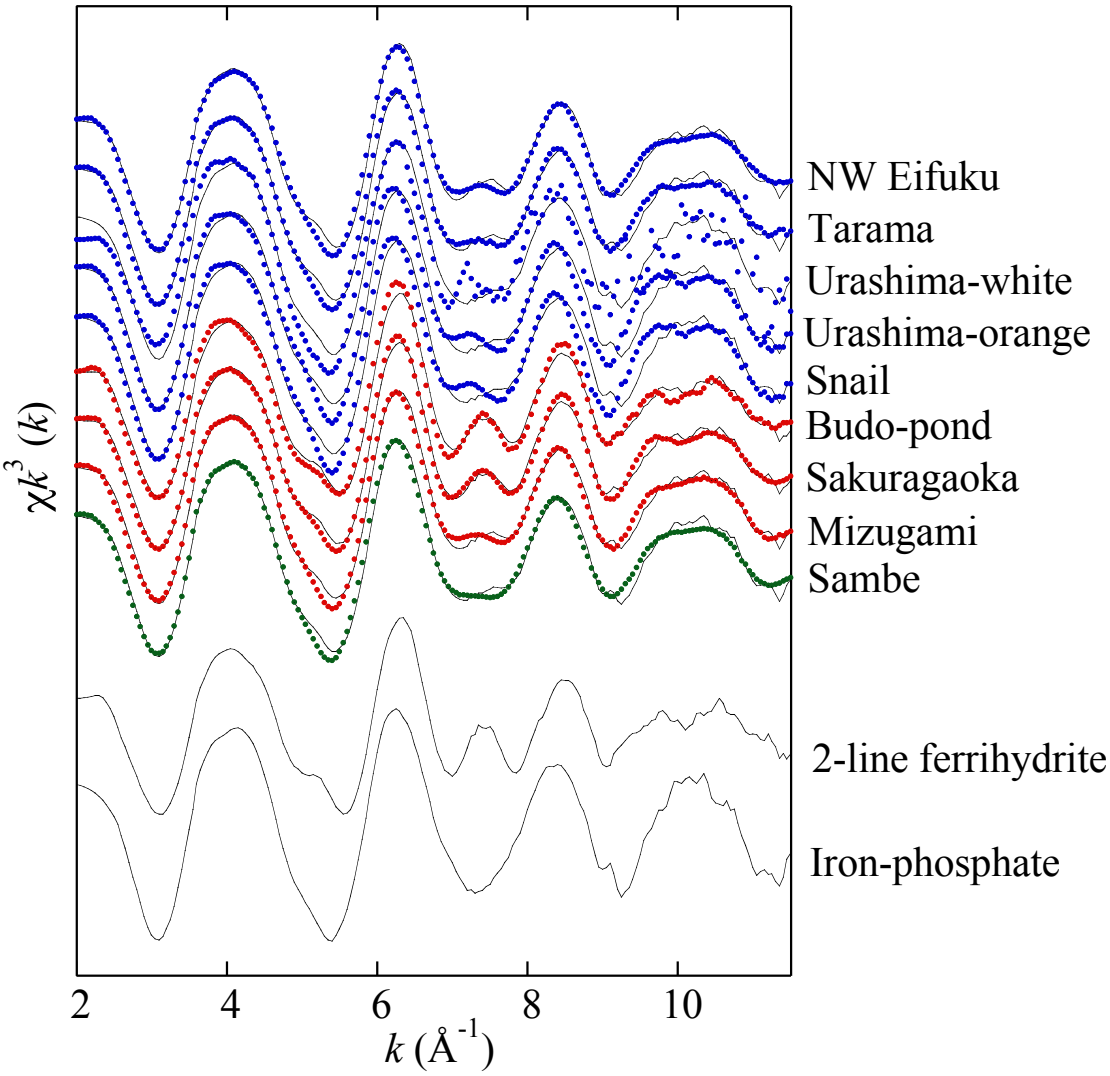

Fig. 2–4. k^3-waithted EXAFS spectra of raw data (circles) and linear-combination fit (solid line) for BIOS collected from various area. Two-line ferrihydrite and iron phosphate are shown as standard material.

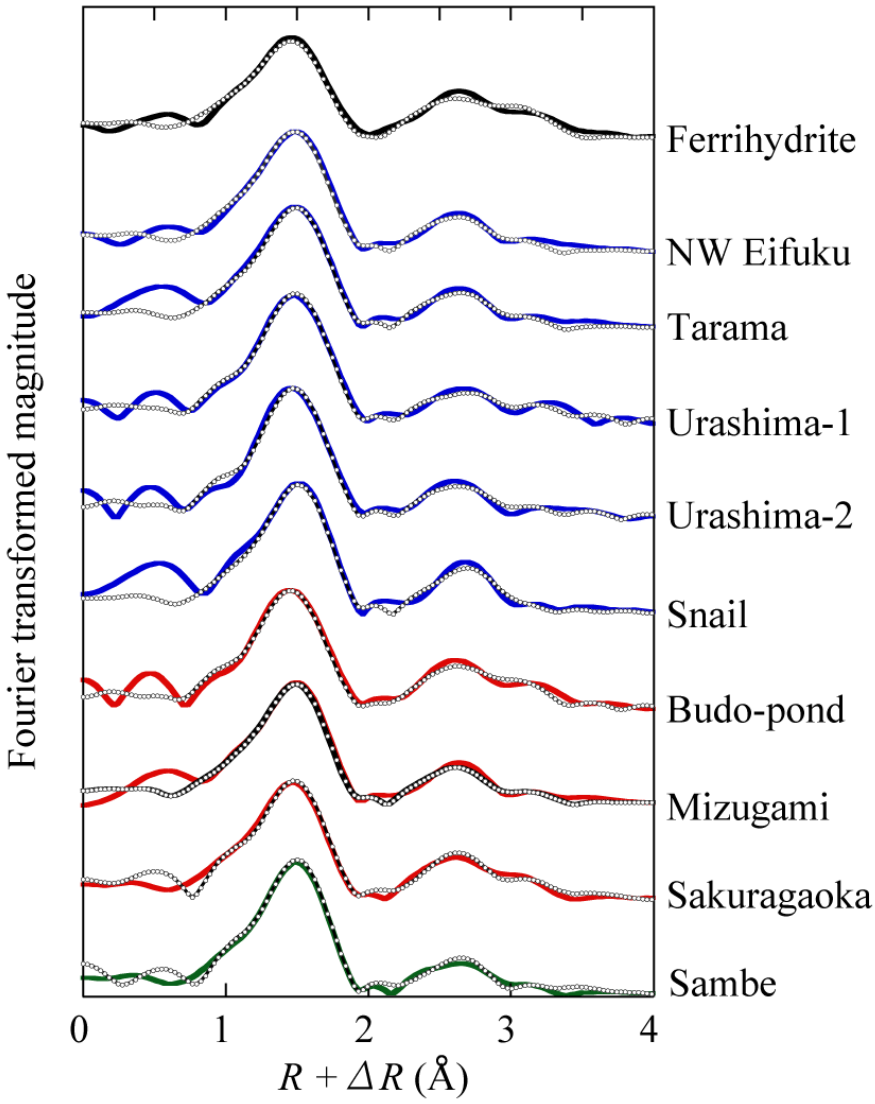

Fig. 2–5. Radial structure function of Fe K-edge EXAFS spectra. Dotted line represents shell-by-shell fitting results.

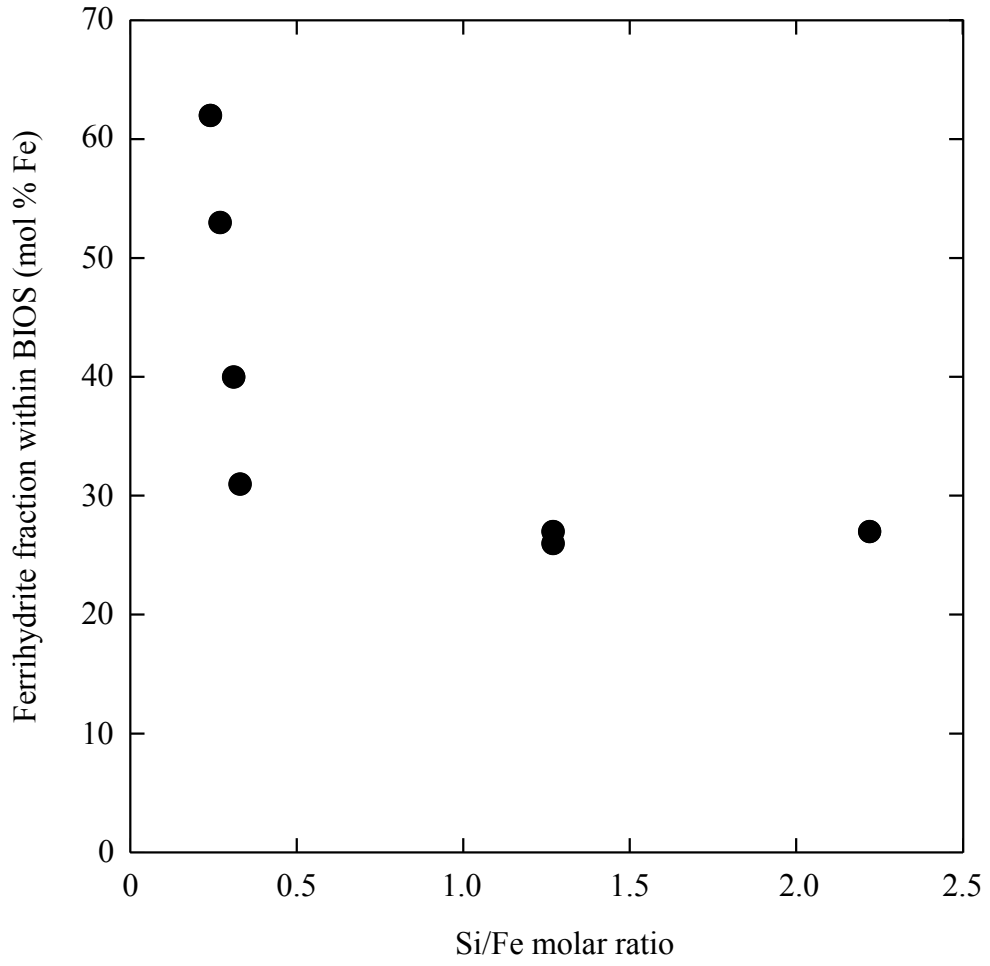

Fig. 2–6. Correlation between ferrihydrite fraction of natural BIOS obtained from EXAFS fittings (Table 2–3) and Si/Fe molar ratio. Strong correlation can be obtained at Si/Fe molar ratio less than 1.0 whereas no correlation at Si/Fe molar ratio larger than 1.0.

Chapter 3. Establishment of new cultivation method for Fe(II)-oxidizing bacteria and characterization of in vitro biogenic iron oxyhydroxides

3.1. Introduction

Biogenic iron oxides (BIOS) are one of the abundant precipitates occurring in natural environments. They are observed at submarine hydrothermal vents (Emerson et al., 2002; Kennedy et al., 2003a, 2003b; Kato et al., 2009; Langley et al., 2009a), groundwater discharge points (Emerson and Revsbech, 1994; Chan et al., 2004, 2009; Duckworth et al., 2009; Gault et al., 2011; Kato et al., 2012), wetlands (Emerson and Weiss, 2004), hot springs (Pierson and Parenteau, 2000; Lalonde et al., 2007; Mitsunobu et al., 2012), and acid mine drainages (Ferris et al., 1989; Clarke et al., 1997; Bruneel et al., 2005). BIOS are complex aggregates of organic material, bacterial cells, and iron (oxyhydr)oxides, in which bacteria play important roles by either biologically controlling or inducing mineral formation (see Konhauser, 1998; Fortin and Langley, 2005 for reviews). Various kinds of acidophilic and neutrophilic iron-oxidizing bacteria have been detected in biologically controlled BIOS, in which the metabolic activities of the bacteria are directly involved in BIOS formation (e.g., nitrate-dependent and photosynthetic iron-oxidizing bacteria; see Weber *et al*., 2006; Hedrich et al., 2011 for reviews). *Gallionella ferruginea* and *Mariprofundus ferrooxydans* are chemolithoautotrophic iron-oxidizing bacteria that are commonly observed within BIOS under neutrophilic conditions (Emerson et al., 2002; Hallbeck and Pedersen, 2005; Duckworth et al., 2009; Gault et al., 2011; Kato et al., 2012). Both bacteria use ferrous iron (Fe^{2+}) as the sole electron donor and produce unique twisted appendages called "stalks" (Hallbeck et al., 1993; Emerson et al., 2007). The distinctive structure of the *Gallionella* and *Mariprofundus* stalks has been investigated, as well as the organisms' biogeographic distributions, energy and carbon metabolism, and possible ecological roles in the global iron cycle (Vatter and Wolfe, 1956; Emerson et al., 2002, 2007; Edwards et al., 2004; McBeth et al., 2011; Singer et al., 2011; Comolli et al., 2011; Saini and Chan, 2013).

BIOS have been also been studied in environmental chemistry, particularly in terms of their mineral species and the adsorptive nature of various ions. The mineral species of BIOS at neutral pH are reported to include ferrihydrite, nano-goethite, nano-lepidocrocite, and

akaganeite (Emerson et al., 2002; Kennedy et al., 2003a, 2003b; Chan et al., 2004, 2009, 2010; Duckworth et al., 2009; Gault et al., 2011), and their amorphous and particulate iron (oxyhydr)oxides are known to have large surface areas (Suzuki et al., 2011b). Thus, the iron (oxyhydr)oxides combined in BIOS can act as adsorbents for various trace elements during or after BIOS formation, and this phenomenon plays an important role in controlling global trace element cycles and the retention of various elements (Kennedy et al., 2003b; Duckworth et al., 2009). Previous studies have also suggested that trace elements, such as cesium, copper, and lanthanides, are effectively adsorbed by the organic components of BIOS (Ferris et al., 2000; Anderson and Pedersen, 2003; Martinez et al., 2003). Thus, an understanding of the adsorption mechanisms of BIOS, especially the detailed functions of their organic materials and iron (oxyhydr)oxides, is crucial to clarifying the distribution and behavior of various elements in natural environments.

Most studies of BIOS at neutral pH have been performed in the field or in the laboratory using BIOS collected from natural environments (Martinez et al., 2003, 2004; Katsoyiannis et al., 2006; Langley et al., 2009b; Rentz et al., 2009; Kennedy et al., 2011). Because natural BIOS usually contain large amounts of inorganic and organic materials (e.g., silica and other ions adsorbed onto the BIOS; Kennedy et al., 2003b; Lalonde et al., 2007), these experiments often encounter difficulties in clearly estimating the contributions of biotic and abiotic factors to the observed results. For example, Katsoyiannis et al. (2006) noted that the reduced adsorption of uranium to BIOS was predominantly caused by the electrostatic repulsion between the negatively charged BIOS and anionic uranium(VI) carbonate species. However, the surface charges of iron (oxyhydr)oxides are readily altered during their adsorption to and/or coprecipitation with various materials, including organic materials (Mikutta et al., 2008), inorganic ions such as phosphate and silicate (Arai and Sparks, 2001; Dyer et al., 2010), and bacteria themselves (Kulczycki et al., 2005). Therefore, BIOS that are experimentally synthesized in the laboratory could be ideal materials for adsorption studies. However, no experimentally synthesized BIOS, especially those formed by *Gallionella* and *Mariprofundus* species, have yet been successfully produced in laboratory cultures because of difficulty in establishing the narrow anoxic–oxic interface required for the growth of these organisms. Emerson and Moyer (1997) developed a culture technique called the “gradient

method", in which certain anoxic–oxic gradients were prepared in an agar-solidified medium. Modified from the original report of Kucera and Wolfe (1957), the gradient method is applicable to many microbiological investigations. However, the quantities of BIOS produced in small- scale agar-solidified medium and the incorporation of agar into the BIOS makes this method inappropriate for the detailed chemical characterization of BIOS.

In this study, I established a new culture method for neutrophilic iron-oxidizing bacteria in a liquid medium using diffusion chambers. I used *M. ferrooxydans* PV-1, which is known to play an essential role in iron and carbon cycles in ocean environments (Emerson et al., 2002; Edwards et al., 2004), as a test microorganism for the newly designed culture method. The mineral species of BIOS produced during the growth of *M. ferrooxydans* PV-1 (designated "*in vitro* BIOS") with this method were determined with both bulk and micro X-ray absorption fine structure (XAFS) analyses. I also compared the amounts of BIOS produced with the culture method developed in this study and with previous culture methods. Finally, I compared the mineralogical and morphological characteristics of the *in vitro* BIOS with those of BIOS samples obtained from deep-sea hydrothermal environments ("*in situ* BIOS")

3.2. Materials and Methods

3.2.1. Culture of iron-oxidizing bacteria by gel-stabilized gradient and batch liquid methods

A chemolithoautotrophic iron-oxidizing bacterium, *M. ferrooxydans* PV-1, was obtained from the American Type Culture Collection (BAA−1020). This strain was precultured in liquid medium (hereafter referred to as the "batch liquid method") or with the agar-stabilized gradient method (Emerson and Floyd, 2005) to draw quantitative comparisons of the formation of *in vitro* BIOS. The artificial seawater (ASW) medium used in this study contained 1.0 mL of trace minerals and 1.0 mL of vitamin supplement per liter of ASW and was buffered with 5 mM sodium bicarbonate (Emerson and Moyer, 2002). Ferrous sulfide (FeS) was also synthesized according to Emerson and Floyd (2005). Both the gel-stabilized gradient medium and batch liquid medium were prepared in a 100 mL glass bottle with a rubber cap. In the gradient medium, 10 mL of FeS with 1.5% agar was first pipetted to the

bottom of the glass bottle and then ASW containing 0.1% agar, which had been bubbled with filter-sterilized (pore size, 0.2 μm; Advantec, Tokyo, Japan) N_2–CO_2 gas (80:20), was added on top of it. The gel-stabilized gradient medium was inoculated with the bacteria using a syringe.

For the batch liquid medium, 100 mL of ASW was dispensed into a 100 mL glass bottle and bubbled with N_2–CO_2 gas (80:20). Filter-sterilized air was added to the headspace to supply O_2 after the lid was closed. A final concentration of 1.8 mM filter-sterilized $FeCl_2$ was added to the glass bottle as the Fe^{2+} source. The bottle was inoculated with the bacteria and Fe^{2+} was then added. No additional Fe^{2+} or O_2 was supplied during incubation. The initial cell densities were the same as those used in the diffusion-chamber method described below.

2.2. Culture of neutrophilic iron-oxidizing bacteria and BIOS precipitation with a diffusion-chamber device

Mariprofundus ferrooxydans PV-1 was cultured with concomitant BIOS synthesis (*in vitro* BIOS), using a diffusion-chamber device containing two chambers separated by a membrane filter (Fig. 3–1). Each chamber was cubic, with 5 cm edges, and the membrane area between the chambers was 7.07 cm^2 (circle with radius 1.5 cm) with a shallow concavity around the hole of the membrane area to set an O-ring. The diffusion chambers were washed with acid and sterilized with UV light (253.7 nm) for about 12 h on a clean bench. A polycarbonate or mixed cellulose membrane filter (pore size, 0.2 μm; Advantec) was then set between the diffusion chambers and tightly closed with screws.

The diffusion chamber was designed to produce a broad anoxic–oxic gradient under conditions of low partial oxygen pressure (pO_2) and high Fe^{2+} concentrations. Before incubation, 10 mL of FeS was mixed with ASW (total volume, 100 mL) and dispensed into one of the cubic chambers (the “anoxic chamber”). Another 100 mL of ASW was added in the other chamber (the “oxic chamber”). Cells were also added to the oxic chamber (final concentration, 8.0×10^6 cell/mL) from the early stationary phase of *M. ferrooxydans* precultured in batch liquid medium. The liquid in both chambers was purged with filter-sterilized (pore size, 0.2 μm; Advantec) N_2–CO_2 gas (80:20) for about 2 min after the addition of ASW, FeS, and bacteria. Each diffusion chamber was then tightly capped with a

silicon plug. Incubations were conducted at 25 °C for a maximum of nine days. During inoculation, the anoxic chamber was constantly mixed with a magnetic stirrer. Two sets of diffusion chambers were removed from the incubator each day to measure the pH and dissolved oxygen (DO). The pH was measured with a pH meter (SS054, Horiba, Kyoto, Japan) and DO was measured with a DO meter (HQ30, Hach, Loveland, CO, USA), which was calibrated with water-saturated air. The medium was then gently mixed and subsampled for Fe^{2+} measurements and cell counts. The Fe^{2+} concentration was measured with a 1, 10-phenanthroline assay (Harvey et al., 1955).

The microbial cell density was evaluated with direct bacterial counts under an optical fluorescence microscope (ECLIPSE 80i, Nikon, Tokyo, Japan). The iron particles in the BIOS were dissolved with a drop of 3.0 M HCl and the BIOS then passed through a membrane filter (pore size, 0.2 μm; Millipore, Billerica, MA, USA). The samples were then washed with Milli-Q water and stained with SYTO 13 (Molecular Probes, Invitrogen, Carlsbad, CA, USA). No disruption of cells was observed during this procedure.

Control experiments for the present method were also conducted in two experimental systems: (i) a cell-free control; and (ii) an azide-treated cell control (dead cells). In the azide-treated controls, a final concentration of 2.0 mM sodium azide was added to the ASW before the addition of the bacteria to the oxic chamber.

2.3. Collection of BIOS

Different procedures were used to collect the BIOS from different culture systems. For the gel-stabilized gradient method, the gradient medium was collected in a glass bottle, which was placed in a hot water bath (approximately 90 °C) to dissolve the agar in the BIOS. The BIOS were collected onto a preweighted membrane. The sample was washed five times with additional hot Mill-Q water and then dried at room temperature (RT). For the batch liquid and diffusion-chamber methods, the precipitates were collected onto preweighed membranes and then washed five times with Mill-Q water. All the samples were dried at RT.

2.4. Natural BIOS collection

Natural BIOS (*in situ* BIOS) were collected from the Northwest Eifuku Seamount in the

northern Mariana Arc (29.223' N, 144°02.567' E) at a water depth of 1545 m, using a remotely operated vehicle (ROV), *Hyper-Dolphin* (dive #1167), owned by the Japan Agency for Marine-Earth Science and Technology, on August 2, 2010. The yellow–orange BIOS had a fluffy texture and extensively covered the seafloor at the summit of the Northwest Eifuku Seamount. The distribution and features of the BIOS were consistent with previous a report by Davis and Moyer (2008). The BIOS samples were collected with a sediment sampler. Immediately after the ROV was recovered onboard, the BIOS samples were processed for each analysis. The portion of the *in situ* BIOS samples intended for XAFS analysis was washed with ultrapure Milli-Q water and then stored at –20 °C to avoid further reaction or transformation. Another portion was fixed with formaldehyde (final concentration, 3.7%) and then stored at 4 °C for observation with scanning electron microscope (SEM).

2.5. SEM observation

The morphological characteristics of the *in vitro* and *in situ* BIOS were examined with SEM. Approximately 0.5 mL of BIOS was transferred to a 1.5 mL plastic tube and centrifuged for about 30 s. The suspension sample was then dehydrated with a graded series of ethanol (30%, 50%, 70%, 80%, 90%, and 100% [v/v] diluted with Mill-Q water). After drying, the sample was mounted on carbon tape on a slide glass and coated with gold. SEM images were obtained with a JEOL JSM-6390 microscope (Tokyo, Japan) at an accelerating voltage of 15 keV.

2.6. Bulk and micro iron K-edge XAFS spectroscopy

2.6.1. Reference materials

Two-line ferrihydrite was synthesized as described by Schwertmann and Cornell (1991). For the synthesis, 1.0 M KOH was added rapidly to a solution containing 0.20 M Fe $(NO_3)_3 \cdot 9H_2O$. Iron phosphate was also synthesized by mixing $FeCl_3 \cdot 6H_2O$ with K_2HPO_4 solution in the same molar ratio. The pH of the $FeCl_3$ solution that contained K_2HPO_4 was increased to 6.5 by the addition of 3.0 M KOH. The synthetic samples were rinsed with Milli-Q water to remove any excess KOH before analysis and were then freeze-dried.

2.6.2. Bulk Fe K-edge XAFS measurement

Iron K-edge XAFS spectra were collected at beamline BL01B1 in SPring-8 (Hyogo, Japan). The reference materials were mixed with boron nitride to reduce the iron concentration to 1-5 wt%. Each mixture was then pressed into a pellet. All BIOS samples were measured in the form of a wet paste, which was converted from the frozen sample at 4 °C. The measurements were made with a fully tuned Si(111) double-crystal monochromator. An rhodiumh-coated Si mirror was also set at an incidence angle of 5.5 mrad to reject higher-order harmonics. The beam size at the sample position was approximately 1 × 0.8 mm^2. The energy was calibrated by setting pre-edge peak maximum of hematite to 7111 eV. The XAFS data for all samples were recorded using ion chambers at RT in transmission mode. The BIOS samples were scanned twice. Photodegradation by incident X-rays during measurement could be ignored because the two spectra were identical. The XAFS data were analyzed using the REX2000 software (Rigaku Co., Ltd.) or the Athena XAFS analysis software package (Ravel and Newville, 2005).

2.6.3. Micro Fe K-edge XAFS measurement

Micro-XRF and Fe K-edge μ-XANES spectra were collected at BL37XU in SPring-8, Japan. The beamline consists of Si(111) double crystal monochromator with Kirkpatric-Baez mirror to obtain X-ray beam with 1.5 × 1.6 μm^2 size at the sample. Spectra of BIOS samples were collected in fluorescence mode using silicon drift detector. Reference spectra were collected in transmission mode measured either at BL37XU or at BL01B1. The Fe XANES collected at both beamlines suggested that the energy resolutions of the spectra were identical between the two beamlines, showing that we can compare the spectra. Measurements in BL37XU were conducted with an energy step 0.5 eV; exposure time 2 or 5 sec. Mapping of Fe by μ-XRF was carried out at irradiation energy at 8 keV. The step size was set to be 1 μm both in x- and y- directions. The measurement time of each pixel was 0.1 s.

3.3. Results and Discussion

3.3.1. Culture of neutrophilic Fe(II)-oxidizing bacteria and BIOS production with a

diffusion-chamber device

Neutrophilic iron-oxidizing bacterium *M. ferrooxydans* PV-1 was cultured with concomitant BIOS production (*in vitro* BIOS) in liquid medium using a newly designed diffusion-chamber device (Fig. 3–1). With this culture method, two different environments were established in each cubic container, designed the "anoxic" and "oxic" chambers. Low levels of DO (DO < 11 μM) were maintained during incubation in the anoxic chamber (Fig. 3–2A). The concentration of Fe^{2+} in the anoxic chamber decreased with time, reflecting the diffusion of Fe^{2+} from the anoxic chamber to the oxic chamber (Fig. 3–2B). On the contrary, the DO level in the oxic chamber was higher than that in the anoxic chamber, with less Fe^{2+}. There was also an oxygen gradient in the oxic chamber. The lowest DO level occurred near the membrane and the highest near the surface of the medium, and the gradient ranged from 11 to 24 μM. The pH in both diffusion chambers showed a normal stable value ranging from 6.1 to 6.8, with a slight increase in pH in the anoxic chamber and a slight reduction in the oxic chamber during incubation. These results suggest that Fe^{2+} diffused from the anoxic chamber into the oxic chamber via the membrane, but each chamber was more or less under pseudoequilibrium conditions. It is also likely that the diffusion of Fe^{2+} was mainly supported by the initial input of FeS solution containing Fe^{2+} (ca. 1.8 mM; Fig. 3–2B) to the anoxic chamber, and the production of Fe^{2+} from FeS was a minor process. We observed no clogging of the membrane during the nine days of the experiment.

Mariprofundus ferrooxydans was successfully cultured with the diffusion-chamber device. The cell density increased from 8.0×10^6 cell/mL to 4.1×10^8 cell/mL during five days of incubation (Fig. 3–3). As the incubation time increased, brownish iron oxides were precipitated at the bottom of the diffusion chamber (Fig. 3–4). The shapes of the stalks found in the oxic chamber were observed by SEM, and had a helical or filamentous structure, ranging in length from a few micrometers to a few dozen micrometers (Fig. 3–5A). These distinctive stalk morphologies were also observed in the batch liquid cultures (Fig. 3–5B) and in BIOS previously produced with the gradient method (Emerson et al., 2007; Singer et al., 2011). However, an SEM analysis showed that the amount of stalks produced was not necessarily associated with the cellular growth of *M. ferrooxydans* PV-1. The stalks were highly encrusted with iron oxides, which could have been produced by both biotic and abiotic

processes. Previous studies have suggested that the stalks are not always biomarkers of biological Fe^{2+} oxidation by stalk-forming iron-oxidizing bacteria (Hallbeck and Pedersen, 2005; Krepski et al., 2012). Moreover, other studies have reported that the chemical oxidation of Fe^{2+} was enhanced by the presence of bacterial cells and stalks, which exerted autocatalytic effects, even when the bacterial cells were sterilized (Kasama et al., 2001; James and Ferris, 2004; Rentz et al., 2007; Druschel et al., 2008).

SEM observation of one of the abiotic controls (cell-free control) revealed 1-2 μm spherical aggregates of iron (oxyhydr)oxides (Fig. 3–5C), which differed in their bulk morphologies from the *in vitro* BIOS (Fig. 3–5A). These aggregates were also seen in the *in vitro* BIOS, although they were smaller. Differences in the size of the iron aggregates in abiotic and biotic systems are commonly observed (Vollrath et al., 2013). It has been reported that iron that is bound to organic materials (i.e., extracellular polysaccharides and stalks) and bacterial cell walls (i.e., carboxylate and phosphate group) inhibits mineral aggregation and crystal growth (Banfield et al., 2000; Kennedy et al., 2004; Chan et al., 2009). Especially in the case of *M. ferrooxydans*, organic materials may play a principal role in defining aggregate size, because the characteristic surface charge and stalk production of the bacterium inhibit surface encrustation (Chan et al., 2010; Saini and Chan, 2013). Because it is difficult to determine whether a precipitate is biotic or abiotic based on its morphology under SEM, we suggest that the *in vitro* BIOS produced during the growth of *M. ferrooxydans* PV-1 in the diffusion-chamber device consisted of iron oxides that were all produced by bacterial energy metabolism, autocatalysis, and chemical oxidation, in addition to the bacterial cells, stalks, and other dissolved organic compounds.

3.3.2. Quantitative estimation of *in vitro* BIOS produced with the diffusion-chamber method and a comparison with previous culture methods

Iron (oxyhydr)oxides production with the diffusion-chamber method was estimated quantitatively under abiotic (cell-free and azide-treated controls) and biotic (*in vitro* BIOS) conditions. The yields of iron (oxyhydr)oxides in the cell-free and azide-treated controls increased gradually with time, exhibiting maximum weight after nine days (Fig. 3–6A). The difference between the cell-free and azide-treated controls was the absence or presence of an

initial autocatalytic effect, respectively (James and Ferris, 2004), and the effect of the different initial production rate in each experiment. The slopes of the Fe^{2+} oxidation rate as a function of incubation time in the two control systems were almost parallel, except during the early incubation period (~2 days), suggesting that the Fe^{2+} oxidation rate as a function of incubation time was similar in the two controls. In contrast to the controls, *in vitro* BIOS production in the diffusion-chamber device increased significantly between day 1 and day 3, and was then stable between days 4 and 9, which seems to correspond to the pattern of the bacterial growth curve (Figs 3–3, 3–6A). Thus, comparison of the production behavior of the *in vitro* BIOS and the control systems indicates the possible involvement of bacterial Fe^{2+} oxidation in the production of *in vitro* BIOS. Considering that biotic iron oxides are simply defined as $W_{\textit{in vitro}\ \text{BIOS}} - W_{\text{azide-treated control}}$ (where W is the amount of iron oxides), the bacterial function accounted for 45% of production during the initial three days of incubation. These ratios are within the range of reported values calculated from the Fe^{2+} oxidation rate using neutrophilic iron-oxidizing bacteria (18%–53% by Neubauer et al., 2002; 4%–88% at various DO concentrations by Druschel et al., 2008).

Although the abiotic and biotic ratios in BIOS are controlled by multiple effects and factors, including DO, Fe^{2+} concentration, pH, and the cellular functions of the bacteria (Neubauer et al., 2002; Druschel et al., 2008), the most notable parameter that affected BIOS production under abiotic and biotic conditions was cell growth as a function of the incubation period in these experiments. The biotic effects were significant during the first 3–4 days of incubation, which corresponded to the early stationary phase of *M. ferrooxydans*. In contrast, the abiotic effects probably dominated in the early exponential and late stationary phases of the bacterium.

I also compared the BIOS production in the diffusion chamber with that in previously used culture methods, such as the gel-stabilized gradient method (Emerson and Moyer, 1997) and batch liquid method (Emerson et al., 2002). I confirmed the cell growth for both previous culture methods (Fig. 3–3). However, with the gradient method, only one datum was covered in both BIOS production and cell concentration because no rusty iron band was clearly visualized during the nine-day incubation period. The initial concentration of Fe^{2+} in the batch liquid method was adjusted to 1.8 mM, which was similar to the Fe^{2+} concentration in

the anoxic chamber in the diffusion-chamber method. Of the three methods I examined, the diffusion-chamber device provided the largest mass of *in vitro* BIOS (Fig. 3–6A, 3–6B). The daily production of *in vitro* BIOS in the batch liquid culture also paralleled the pattern to cell growth (Figs 3–3, 3–6B), but the amount of BIOS recovered was less than that obtained with the diffusion-chamber method. The smallest amount of BIOS was collected with the gradient method.

Although the biotic fractions of BIOS produced with the batch liquid and gradient methods were not estimated quantitatively in this study, I infer that the greater contribution of biotic effects may have led to a greater yield of *in vitro* BIOS with the diffusion-chamber method. The DO and pH values were almost identical or slightly lower in the batch liquid method than the diffusion-chamber method (data not shown). However, the Fe^{2+} concentration in the diffusion-chamber method was lower than in the batch liquid. The yield of *in vitro* BIOS per cell was greatest with the batch liquid method ($1.08 \pm 0.23 \times 10^{-10}$ g iron [oxyhydr]oxides per cell, including both abiotic and biotic precipitates) compared with the diffusion-chamber method ($0.65 \pm 0.19 \times 10^{-10}$ g per cell) and the gradient method ($0.45 \pm 0.03 \times 10^{-10}$ g per cell). These observations suggest that the more BIOS produced by single cells in batch liquid culture can be attributed to the larger abiotic function than was present in the diffusion-chamber culture. The SEM observations of stalks collected from the batch liquid method support this inference because the stalks were more heavily encrusted with iron oxyhydroxides than were those from the diffusion-chamber culture (Fig. 3–5A, 3–5B). Another possible explanation for the lower yields of BIOS from the batch and gradient cultures is the lower cell numbers involved. The growth rate was higher (7 h) in the diffusion-chamber culture than in batch liquid culture (10 h) or the gradient culture (12 h, from Emerson et al., 2007). Therefore, it seems likely that the diffusion-chamber method provided not only a better growth rate and yield of *M. ferrooxydans*, but also more efficient production of BIOS enriched with biotic iron (oxyhydr)oxides.

There are two principal advantages in the newly developed diffusion chamber method: the large size of the anoxic–oxic interface and the appropriate supply of Fe^{2+} in the medium. Iron-oxidizing bacteria grow in a relatively narrow range of anoxic–oxic interface environments, in which they can obtain energy from the redox gradient (Emerson and

Revsbech, 1994). The diffusion-chamber method provides a relatively large space of metabolically available anoxic–oxic gradient for both bacterial growth and concomitant *in vitro* BIOS production, whereas only a narrow range is present in the batch liquid and gradient cultures. Furthermore, because Fe^{2+} is the sole energy source for the growth of *M. ferrooxydans*, a continuous supply of the appropriate concentration of Fe^{2+} in the medium significantly affects bacterial growth and *in vitro* BIOS production. The Fe^{2+} supply was almost constant throughout the incubation period in the diffusion chamber. However, the Fe^{2+} concentration in the batch liquid showed a continuous decline with time (decreasing from 1.8 to 0.3 mM over nine days). A previous study also reported the variability in the Fe^{2+} concentration during bacterial growth in gradient culture (Emerson and Moyer, 1997). It is likely that varying concentrations of Fe^{2+} limit the bacterial oxidation of Fe^{2+} and in turn, accelerate abiotic Fe^{2+} oxidation (Neubauer et al., 2002). It has also been remarked that the formation of a diffusion barrier between the bacteria and Fe^{2+} source inhibits bacterial growth in gradient culture (McBeth et al., 2011). The diffusion-chamber method provides both a large space and a continuous supply of sufficient electron donor for the better growth of *M. ferrooxydans* and its *in vitro* BIOS production.

3.3.3. Morphological observation of *in situ* BIOS

The morphological characteristics of natural (*in situ*) BIOS were compared with those of *in vitro* BIOS. Figure 3–5D shows an SEM image of *in situ* BIOS collected from the Northwest Eifuku Seamount hydrothermal field. Twisted or filamentous structures observed in the sample are similar to the characteristic twisted stalk structures produced by iron-oxidizing bacteria such as *M. ferrooxydans* and *G. ferruginea* (Kucera and Wolfe, 1957; Emerson et al., 2007). Iron (oxyhydr)oxide minerals are localized around the stalk-like structures, and some of these structures are largely masked by the iron (oxyhydr)oxides. Few stalk-like structures lacking iron were identified by SEM. These results indicate that the *in situ* BIOS reflect different stages of iron mineralization and stalk formation along the growth of iron-oxidizing microorganisms as previously demonstrated (Kennedy et al., 2003b; Chan et al., 2004, 2009). Moreover, the morphological characteristics of the *in situ* BIOS are quite similar to those of the *in vitro* BIOS produced by *M. ferrooxydans* PV-1 in the

diffusion-chamber culture (Fig. 3–5A, 3–5D). The morphological similarity between the *in situ* BIOS and the *in vitro* BIOS from *M. ferrooxydans* PV-1 cultured in the diffusion-chamber device suggests that BIOS formation in the deep-sea hydrothermal environment is attributable to the *in situ* function of iron-oxidizing ζ-Proteobacteria, such as members of the genus *Mariprofundus*. A terminal restriction fragment-length polymorphism analysis of the microbial phylotype components of the iron (oxyhydr)oxide precipitates obtained from several Mariana Arc hydrothermal environments showed that the dominant microbial phylotypes were the ζ-Proteobacteria taxa, phylogenetically related to *M. ferrooxydans* (Davis and Moyer, 2008).

3.3.4. Bulk and micro XAFS analysis of mineral species of *in vitro* and *in situ* BIOS

In this study, an XAFS analysis was conducted to identify mineral species of *in vitro* and *in situ* BIOS samples. Because bulk and micro-XAFS studies of *in situ* BIOS (Toner et al., 2008, 2012; Chan et al., 2009; Edwards et al., 2011; Gault et al., 2011; Mitsunobu et al., 2012; chapter 2) or *in vitro* BIOS (Chan et al, 2010) have already been conducted, I focused on the similarities or differences between *in situ* BIOS and the *in vitro* BIOS generated with the diffusion-chamber method. Figure 3–7A shows the extended X-ray absorption fine structure (EXAFS) of BIOS samples and reference minerals. I selected two-line ferrihydrite and goethite as reference minerals to represent the typical components of *in situ* BIOS observed in natural environments. Iron phosphate was selected as the reference mineral to represent iron minerals composed of iron oligomers (Voegelin et al., 2010). Limited Fe(III) hydrolysis in total iron was also observed in the presence of organic material, the iron species of which showed similar EXAFS oscillations to iron phosphate (Karlsson and Persson, 2012; Mitsunobu et al., 2012). The EXAFS spectra of the *in vitro* and *in situ* BIOS (Incubation period: 2 days) had similar oscillation structures in *k* space (Fig. 3–7A). On the contrary, none of the EXAFS oscillations of the reference minerals was identical to those of *in vitro* and *in situ* BIOS, even though BIOS samples had several similar structures with ferrihydrite and iron phosphate. Notable structures (shaded in Fig. 3–7A) were (i) the absence or presence of a shoulder at $k = 5.5$ (Å^{-1}); and (ii) a reduction or increase in the peak around $k = 7.5$ (Å^{-1}). These results indicate that *in vitro* and *in situ* BIOS do not contain single minerals, but

combinations of two or more iron species.

A simulation of iron K-edge EXAFS was performed to determine the contribution of each mineral in the samples. A quantitative simulation was conducted for *k* ranging from 2.5 to 11.5 ($Å^{-1}$) using the Athena software (Ravel and Newville, 2005). I selected the following three standards as proxies for the iron structure to fit the sample spectra: (i) goethite as crystalline iron oxyhydroxide, which consists of iron polymers with edge- and corner-sharing linkages of octahedral iron(III); (ii) ferrihydrite as poorly crystalline iron oxyhydroxide, which consists of iron polymers with edge- and corner-sharing linkages of octahedral iron(III); and (iii) iron phosphate, composed of small iron oligomers. Each reference material can be distinguished by its specific pattern in *k* space. The characteristic EXAFS oscillations of the *in situ* and *in vitro* BIOS fitted reasonably well to those of ferrihydrite and iron phosphate (Fig. 3–7A, Table 1). These results suggest that ferrihydrite is one of the dominant mineral species in both the *in vitro* and *in situ* BIOS. Iron oligomers are predicted to be another predominant iron species. Previous studies have also suggested the presence of amorphous iron oxyhydroxides, such as ferrihydrite, in BIOS (Emerson and Moyer, 2002; Kennedy et al., 2003b; Kato et al., 2009; Gault et al., 2011). My results suggest that *in situ* BIOS and *in vitro*-produced BIOS contained mixtures of several amorphous forms of iron oxyhydroxides.

Mineral species of iron precipitate which located at micro-areas on a single stalk was also identified by micro-XAFS analysis. Fig. 3–8A and 3–8B show SEM images of the stalk. Helical twisted stalks are thought to be the typical products of *M. ferrooxydans* (Chan et al., 2011). Figures 3–8C and 3–8D show the distribution of Fe in the stalk structure. Iron is distributed broadly around stalk, whereas the density of existing Fe is highly different in the location of the stalk at a micro scale. Figure 3–9 shows Fe K-edge XANES spectra at four Fe concentrated spots represented by the number shown in Figures 3–8A and 3–8B. Spectra obtained from different points were approximately identical. The adsorption edge was around 7.13 keV (dashed line in Fig. 3–9) and the feature was similar to that of ferrihydrite. Least-squares fitting of the XANES spectra showed that inclusion of Fe carboxylate species in the fitting in addition to ferrihydrite results in the decrease of R value from 0.00110 to 0.00016 in spectrum1 in Figure 2. This result is consistent with my bulk EXAFS analysis,

suggesting that iron minerals are homogeneously distributed among BIOS.

Shell-by-shell fitting was conducted to further specify the mineral characteristics in the *in situ* BIOS and *in vitro* BIOS. The bulk Fe K-edge EXAFS spectra were Fourier-transformed for a k range from 2.5 to 11.5 ($Å^{-1}$), and fitting was performed with REX2000 (Rigaku). The magnitudes of the Fourier-transformed spectra, together with the fitting results, are listed in Fig. 3–7B and Table 3–3. The EXAFS parameters obtained for ferrihydrite were consistent with those in previous studies, and exhibited edge- and corner-sharing linkages at distances of 3.06 and 3.42 Å, respectively (Toner et al., 2009; Voegelin et al., 2010). These edge- and corner-sharing linkages were also observed in both BIOS samples, suggesting the presence of a structural unit within the BIOS similar to ferrihydrite (Table 3–3). However, the coordination numbers of iron at a distance of 3.42 Å in both the *in situ* and *in vitro* BIOS were lower than that of ferrihydrite, which corresponded to the magnitude of the shells in the Fourier-transform spectra in Fig. 3–7B. These results indicate that both BIOS mainly contained edge-sharing octahedral linkages.

My results are consistent with the previous results of Toner et al. (2009), who suggested that the variation in EXAFS oscillations were attributable to the coordination numbers and structural changes: the reduction in the coordination numbers at the corner-sharing $Fe–O_6$ linkages were linked to (i) the change in spectral shape at k = 5.0–5.8 $Å^{-1}$; and (ii) the reduction in the amplitude of the oscillation at k = 7.0–8.0 $Å^{-1}$. These characteristics were also observed in the EXAFS oscillations in this study, as indicated by the shaded areas in Fig. 3–10A. Although the formation of these characteristic iron oxyhydroxides structures in the BIOS has biological effects (e.g., exopolysaccharides; Toner et al., 2009; Chan et al., 2010; Mitsunobu et al., 2012) and inorganic effects (e.g., phosphate and/or silicate; Toner *et al*., 2009; Suzuki *et al.*, 2011b), my diffusion-chamber method can synthesize minerals similar to those in the *in situ* BIOS collected from deep-sea hydrothermal environments.

3.3.5. Mineral species of *in vitro* BIOS as a function of incubation time and water chemistry

Mineral species of BIOS are further identified at different cultivation time and different phosphate concentration. Figure 3–10 shows EXAFS spectra of *in vitro* BIOS at incubation

time from 2 days to 6 days, and phosphate concentration from 0 mM to 1 mM. Apparent spectral change were obtained at (1) the existence of absence of peak at 7.5 $Å^{-1}$ and (2) change of spectra at 4.0 $Å^{-1}$ to 5.5 $Å^{-1}$. This is attributed by the change of iron mineral species which is shown in Table 3–3. In the absence of phosphate, *in vitro* BIOS contained goethite. However, in the presence of phosphate in culture medium, *in vitro* BIOS mainly consists of oligomeric stage of iron Thus, iron mineral species of BIOS are strongly depends on water chemistry and incubation time.

3.3.6. Application of the new cultivation technique and BIOS production with the diffusion-chamber method

Since the successful isolation of the novel iron-oxidizing chemolithoautotroph *M. ferrooxydans* PV-1 with the gel-stabilized gradient method, this method has been regarded as the most practical culture technique for neutrophilic iron-oxidizing bacteria. Although the technique is applicable to the enrichment, isolation, and basic physiological characterization of neutrophilic iron-oxidizing bacteria from naturally occurring microbial communities, it has several shortcomings in terms of its use in other microbiological, biochemical, and material experiments that require (i) greater yields of cells and bacterial products, such as stalks; and (ii) the purification of BIOS from agar. For example, the contamination of BIOS with agar is not amenable to sensitive chemical analyses, such as organic quantification. The presence of agar also inhibits cell growth (McBeth et al., 2011), which may also inhibit cell mobility. In adsorption experiments, the amount of BIOS collected with the gradient method is relatively small and the removal of agar from the BIOS is also essential for the experiments.

I also tested batch liquid culture, a previously used method that involves no agar, for comparison. However, with this batch method, it was difficult to collect as much BIOS as was collected with the diffusion-chamber method, especially during short incubation periods (within four days). Moreover, neither the gel-stabilized culture method nor the batch liquid method can maintain stable Fe^{2+} concentrations, and their high Fe^{2+} supply may accelerate abiotic effects. All these shortcomings restrict our understanding of the detailed behavior of BIOS as a functional material.

My newly developed diffusion-chamber method allows the successful culture of *M. ferrooxydans* PV-1 and the production of relatively large amounts of BIOS without any

organic compounds other than the by-products of bacterial growth. The culture technique also maintains a stable Fe^{2+} supply under conditions that are much closer to *in situ* conditions. This implies that experiments using diffusion-chamber-synthesized BIOS can more appropriately investigate the *in situ* biogeochemical functions and potential applications of BIOS.

Moreover, the *in vitro* production of BIOS should be very useful for characterizing the physicochemical properties of BIOS, such as their adsorption and coprecipitation behaviors. Chemically synthesized ferrihydrite minerals have long been used to understand the adsorption processes of iron (oxyhydr)oxides in natural systems (Waite et al., 1994; Parida et al., 1997; Raven et al., 1998). Nevertheless, the adsorption behavior of chemically synthesized ferrihydrite minerals towards some trace elements showed different trends from the adsorption of BIOS samples obtained from a groundwater discharge point (Katsoyiannis et al., 2006). This highlights the importance of considering organic functions and bacterial activities when studying the physicochemical properties of iron (oxyhydr)oxides in natural environments, rather than using inorganic ferrihydrite only. My culture method allows the application of *in vitro* BIOS to various adsorption experiments on iron (oxyhydr)oxides, which will provide quantitative and replicable results that are comparable to those of previous studies using natural samples. These will facilitate future applications of *in vitro* BIOS to the removal of various toxic elements and the recycling of valuable trace elements.

Figures and Tables

Table 3–1. Results of EXAFS fitting. Reference material: (i) ferrihydrite (amorphous iron oxyhydroxides with edge- and corner-sharing linkage of octahedral iron(III)); (ii) iron-phosphate (small iron oligomers).

		Fraction(%)		
		Ferrihydrite	Iron-phosphate	R*
sample name				
In vitro BIOS		62±2	38±2	0.023
In situ BIOS	Diffusion chamber method	59±2	41±2	0.019

*The goodness of the fitting calculated by following equation

$$R = \Sigma[k^3\chi_{exp}(k) - k^3\chi_{cal}(k)]^2 / \Sigma[k^3\chi_{exp}(E)]^2$$

Table 3–2. Results of EXAFS through shell-by-shell fitting of ferrihydrite, *in vitro* BIOS (incubation period: 3days), and *in situ* BIOS.

		Atom	R(Å)[a]	CN[b]	σ^2(Å^2)[c]	ΔE_0[d]
ferrihydrite		Fe-O	1.95±0.01	4.3±0.9	0.011	-5.6
		Fe-Fe	3.06±0.02	3.2±0.6	0.020	
		Fe-Fe	3.42±0.02	1.5±0.3	0.011	
In vitro BIOS		Fe-O	1.97±0.01	5.2±0.4	0.011	-5.0
		Fe-Fe	3.09±0.02	2.7±0.6	0.017	
		Fe-Fe	3.41±0.03	0.7±0.3	0.007	
In situ BIOS	Diffusion chamber method	Fe-O	1.97±0.01	5.2±0.4	0.012	-4.9
		Fe-Fe	3.09±0.02	3.3±0.8	0.020	
		Fe-Fe	3.40±0.03	0.8±0.5	0.011	

[a]Radial distance
[b]Coordination number
[c]Debye-Waller factor coefficient
[d]Energy shift

Table 3–3. Results of EXAFS fitting at various incubation time and phosphate concentrations. Reference material: (i) ferrihydrite (amorphous iron oxyhydroxides with edge- and corner-sharing linkage of octahedral iron(III)); (ii) iron-phosphate (small iron oligomers).

Phosphate concentration (mM)	Incubation time (day)	Ferrihydrite	Iron-phosphate	Goethite	Lepidocrocite	R
0	2	68 ± 2	–	32 ±3	–	0.0439
0.001	2	61 ± 3	39 ± 3	–	–	0.0419
1	2	27 ± 2	73 ± 2	–	–	0.0124
0.2	2	66 ± 5	34 ± 5	–	–	0.124
0.2	4	60 ± 3	24 ± 3	–	16 ± 5	0.0581
0.2	6	41 ± 3	23 ± 3	–	36 ± 4	0.0217

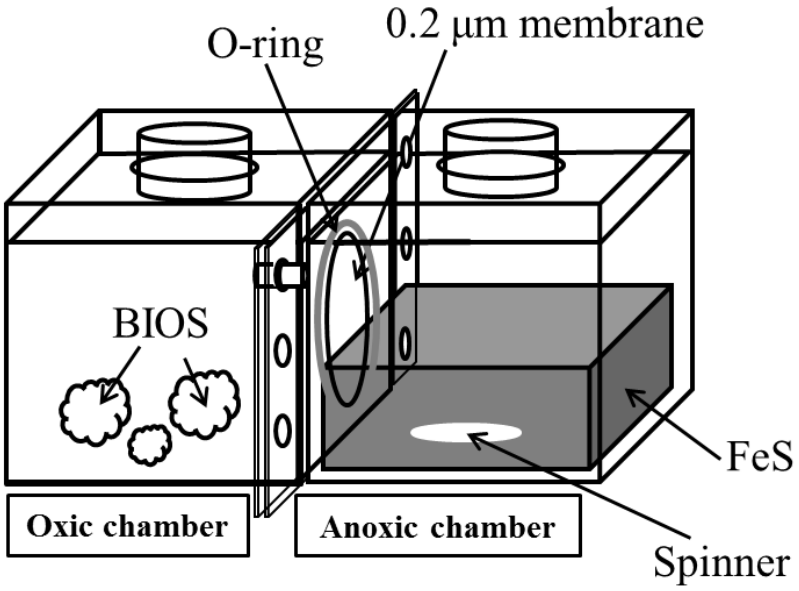

Fig. 3–1. Schematic illustration of diffusion-chamber device. Two chambers are separated and connected by a 0.2 μm membrane. In the anoxic chamber, FeS was added to the ASW medium as a source of soluble Fe^{2+} for the oxic chamber. The oxic chamber works for the medium of iron-oxidizing bacteria and *in vitro* production of BIOS.

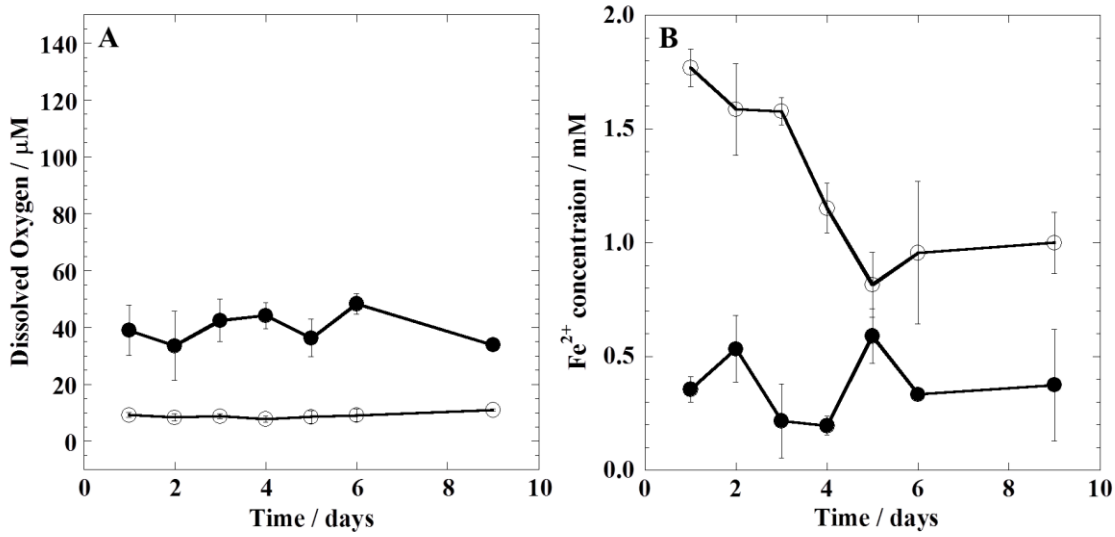

Fig. 3–2. Shift in dissolved oxygen (DO) and Fe2+ concentration in the diffusion-chamber device during incubation. (A) The DO values in the oxic chamber (●) and anoxic chamber (○) are shown. As DO value showed difference in areas within oxic chamber, values at the center of the oxic chamber are plotted. (B) The Fe2+ concentration in the oxic chamber (●) and anoxic chamber (○) is shown.

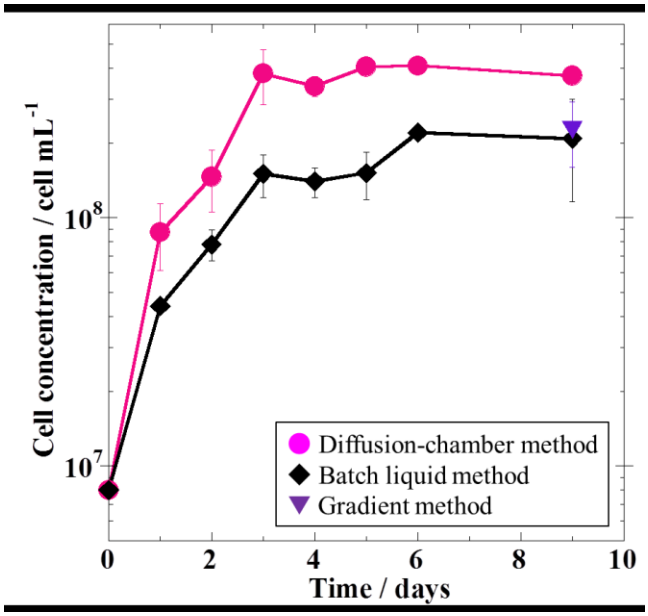

Fig. 3–3. Growth of *M. ferrooxydans* in different culture methods. Growth curves for *M. ferrooxydans* in the diffusion-chamber method (●), the batch liquid method (♦), and the gradient method (▼) are shown. Cell numbers are determined by direct count stained by SYTO 13. Standard error represented here is based on the duplicate experiments.

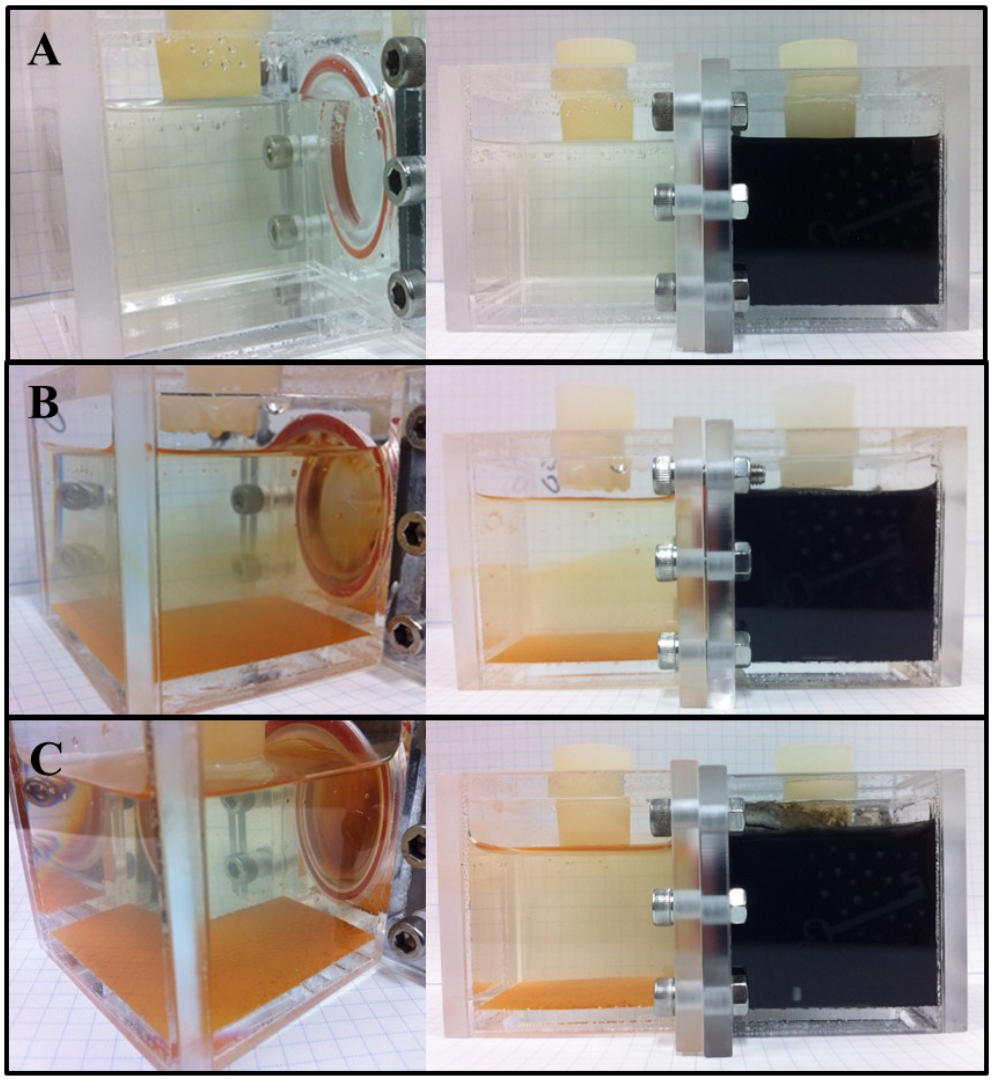

Fig. 3–4. Photographs of the diffusion-chamber device during the growth of *M. ferrooxydans* PV-1. The appearance of the diffusion-chamber device after 0 (A), 3 (B), and 5 (C) days of incubation, respectively, is shown. With increasing incubation period, BIOS were precipitated at the bottom of the oxic chamber.

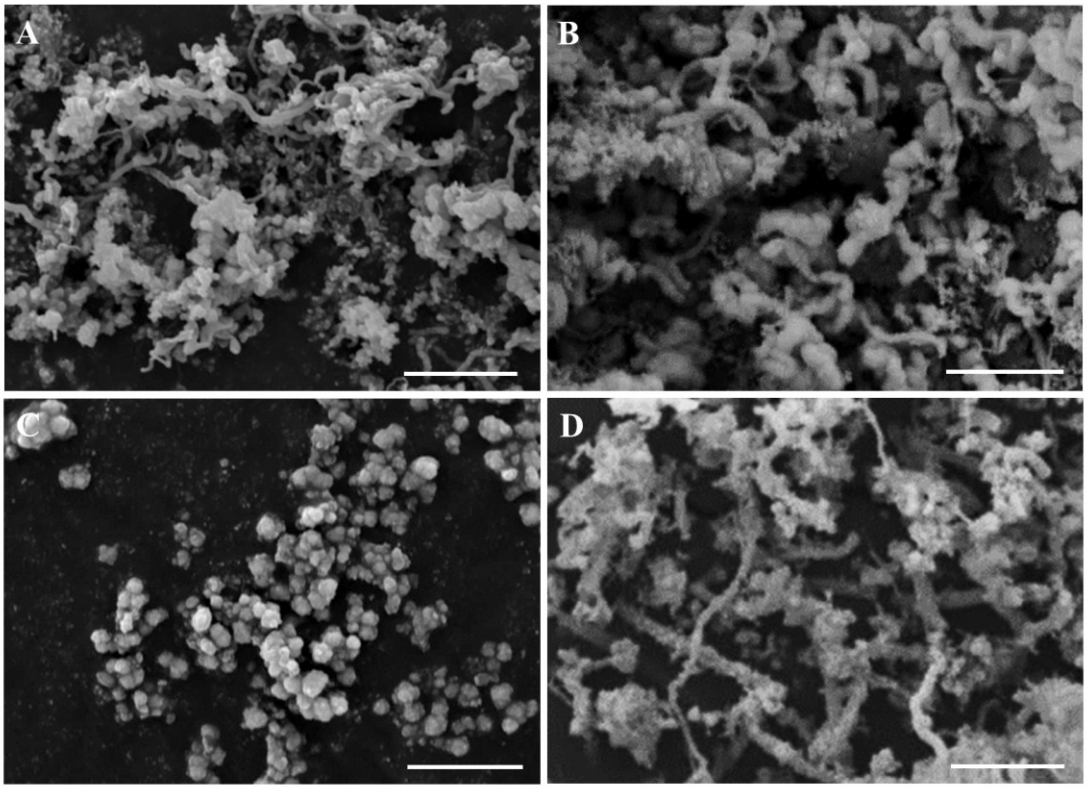

Fig. 3–5. Scanning electron microscope (SEM) images of the BIOS and the precipitates from the abiotic control. (A) SEM image of the *in vitro* BIOS samples collected from diffusion-chamber method with the bacterial growth after the 9 days incubation, (B) SEM image of the *in vitro* BIOS samples collected from batch liquid method with the bacterial growth after the 9 days incubation, (C) SEM image of the precipitates from the cell-free control experiment after the 9 days incubation, and (D) SEM image of the *in situ* BIOS collected from the Northwest Eifuku Seamount. Twisted stalks are the typical materials that are associated with the growth of *M. ferrooxydans* PV-1. Scale bars: 10 μm.

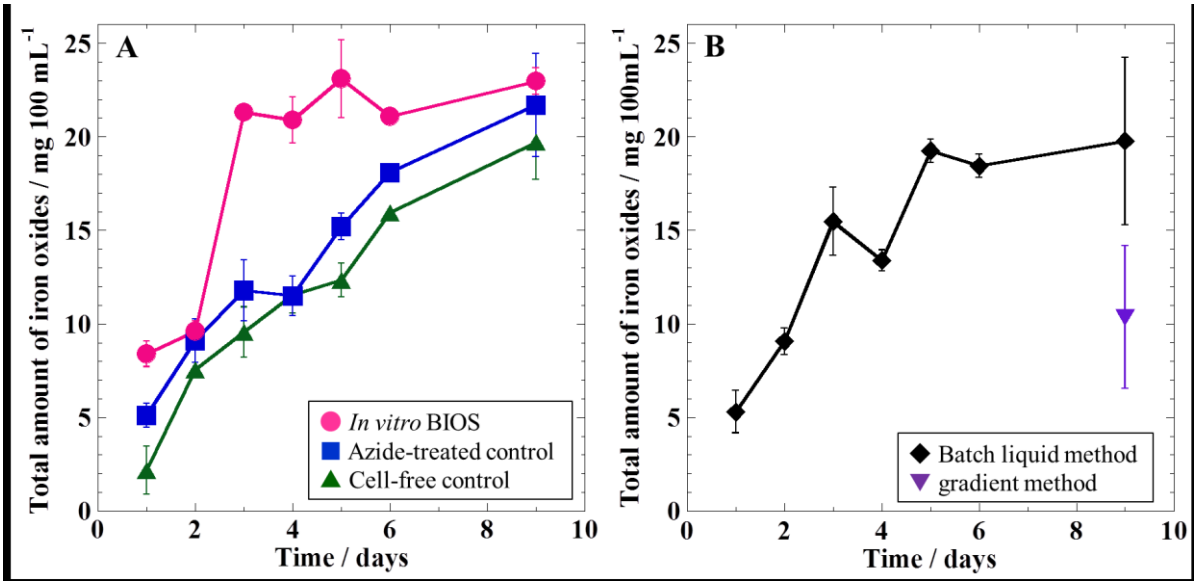

Fig. 3–6. *In vitro* BIOS production of *M. ferrooxydans* PV-1 and iron oxyhydroxides production in control systems. (A) Total amounts of iron oxyhydroxides collected from the diffusion-chamber method with the bacterial growth (●), cell-free control (▲), and the azide-treated control experiments (■) are shown. (B) Total amounts of *in vitro* BIOS collected from the cultivation with the batch liquid method (♦), and the gradient method (▼) are present.

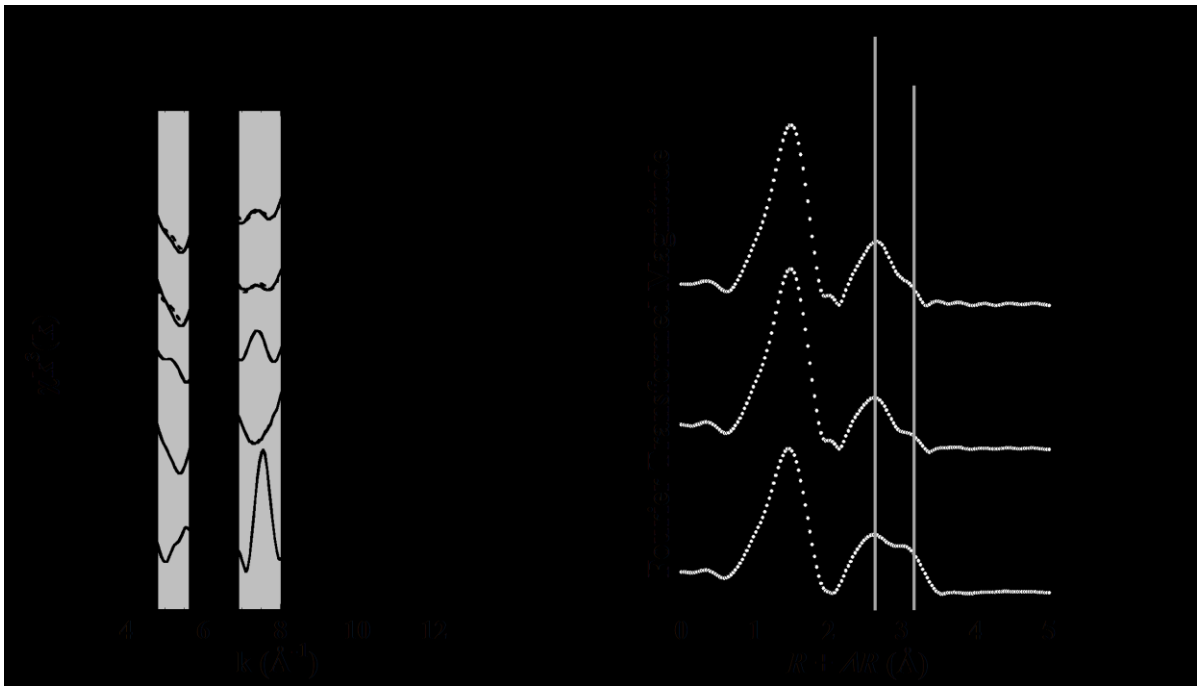

Fig. 3–7. EXAFS spectra and Fourier transformed data of *in vitro* BIOS (Incubation period: 3 days), *in situ* BIOS, and reference minerals. (A) Normalized k^3-weighted EXAFS spectra for samples and reference minerals at the iron K-edge. The dotted lines in the samples show the results of the linear combination fitting using ferrihydrite and iron phosphate (Table 3–1). Shaded areas highlight the spectral features of *in vitro* and *in situ* BIOS. (B) Radial structure function of the spectra shown in (A) after the Fourier transformed for a k range from 2.5 $Å^{-1}$ to 11.5 $Å^{-1}$. The dotted lines represent the model fit lines (Table 3–2).

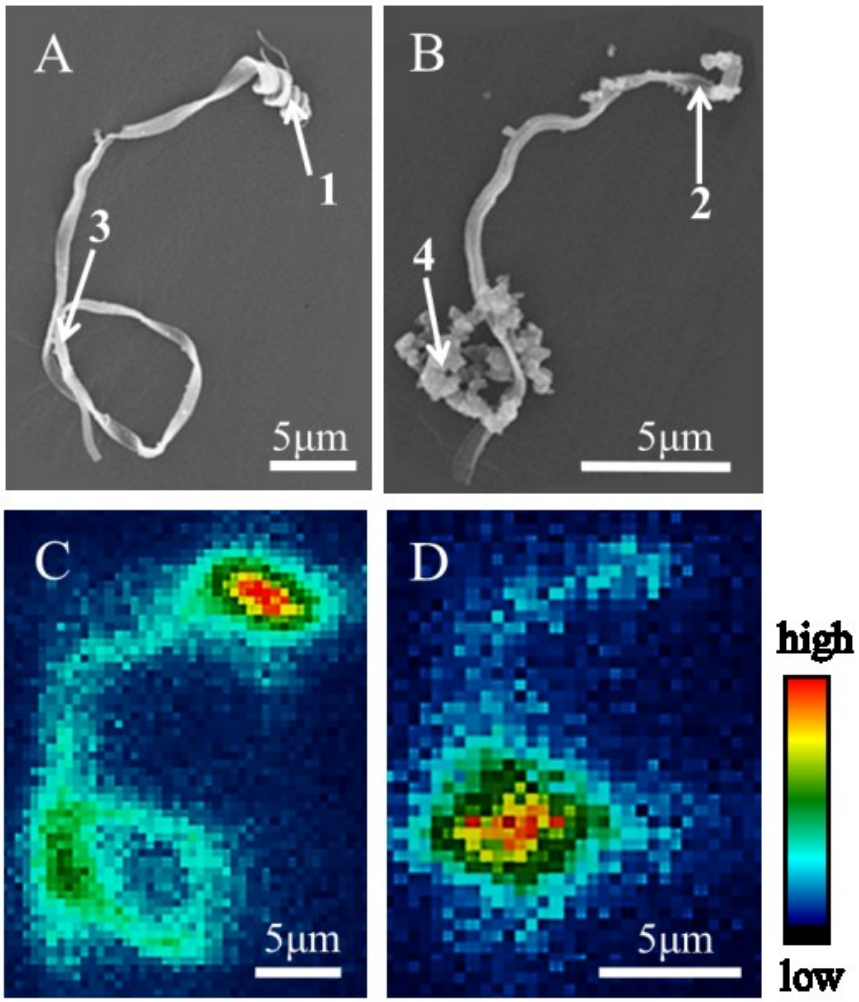

Figure 3–8. SEM and μ-XRF images of samples. (A), (B) SEM images of stalk structure in BIOS. The numbers show the measured points by μ-XANES (C), (D) μ-XRF images of Fe. X-ray beam size, 1.5 ×1.6 μm^2; Step size, 1 μm; Measurement time, 0.1s/point. Figure from Kikuchi et al. Application of synchrotron based XEF-XAFS to the speciation of Fe on single stalk in bacteriogenic iron oxides (BIOS), Chemistry letters, 2011, 40, 680–681.

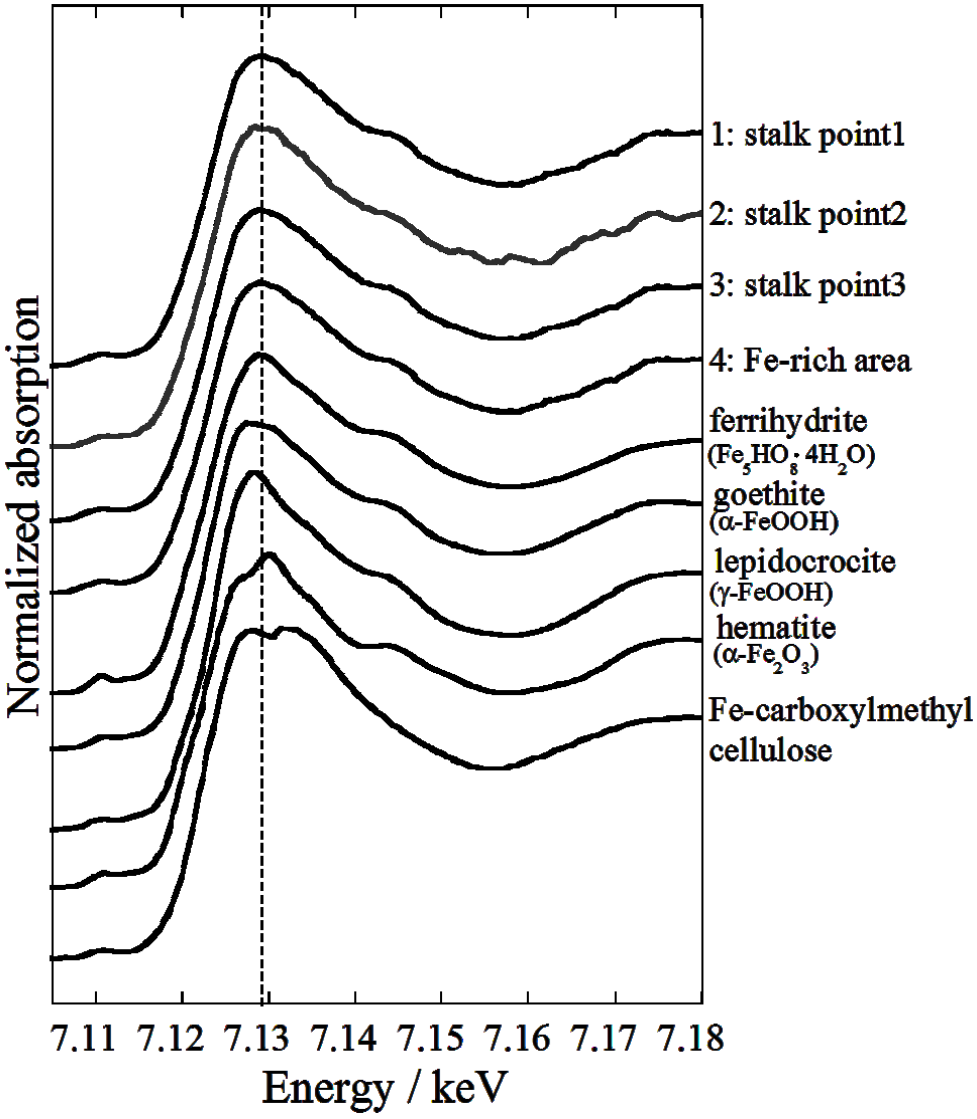

Fig. 3–9. Normalized Fe K-edge μ-XANES spectra of samples and reference minerals. The numbers indicate the measurement points as shown in Figure 3–8. The vertical dashed lines indicate the adsorption edge of samples. Figure from Kikuchi et al. Application of synchrotron based XEF-XAFS to the speciation of Fe on single stalk in bacteriogenic iron oxides (BIOS), Chemistry letters, 2011, 40, 680–681.

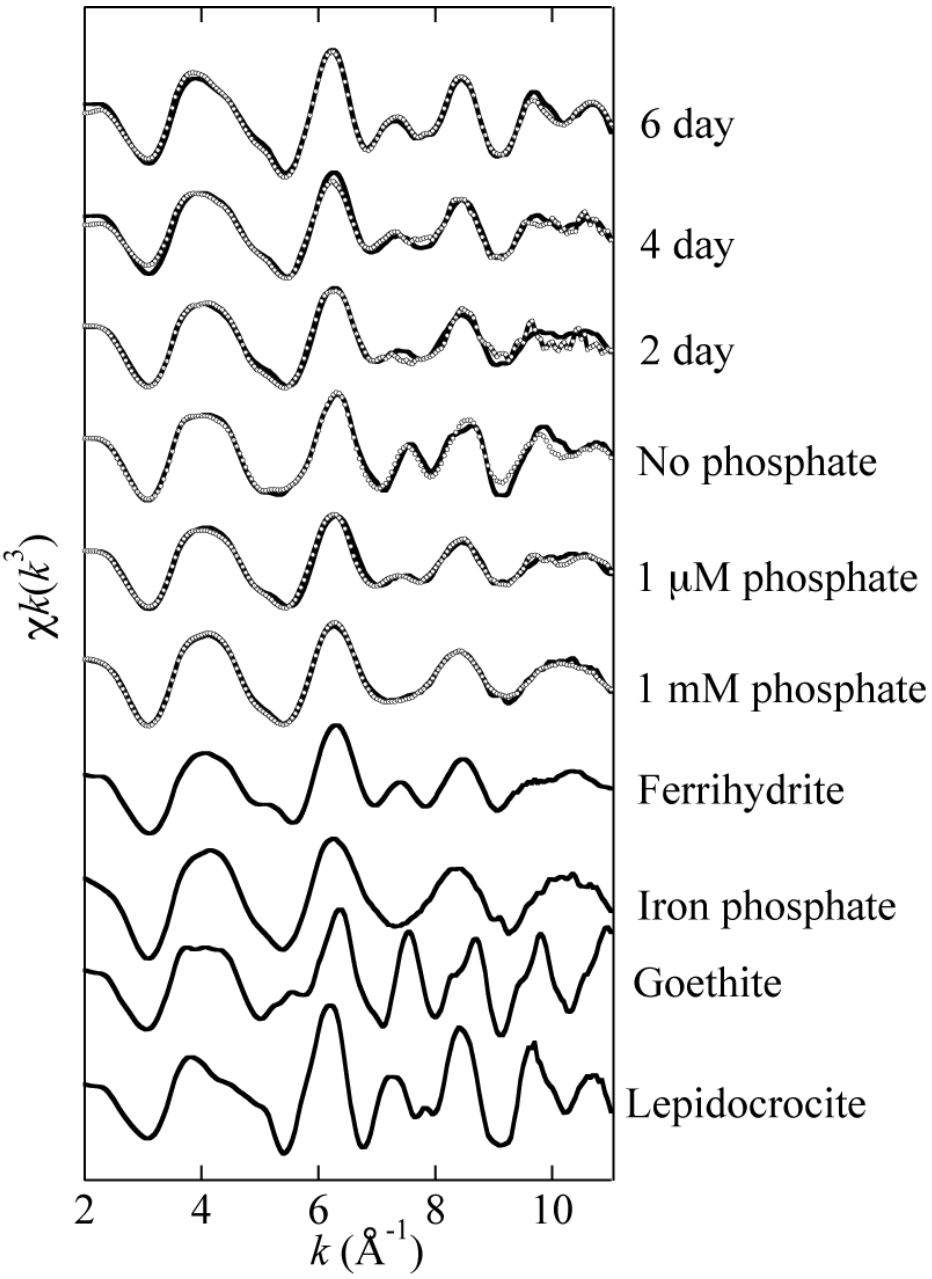

Fig. 3–10. Normalized k^3-weighted EXAFS spectra *in vitro* BIOS at various phosphate concentration and incubation time. The dotted lines in the samples show the results of the linear combination fitting using standard minerals (Table 3–3). The dotted lines represent the model fit lines (Table 3–3).

Chapter 4. Decrease of arsenate adsorption onto biogenic ferrihydrite: Effect of specific surface area and surface charge

4.1. Introduction

Adsorption of toxic element (e.g. arsenic, uranium, and cadmium) onto mineral has a significant influence on the mobility of toxic element in natural environment. Concentrations of toxic element regulated by the adsorption reaction have direct implications on both microbial activities and human health (Bissen and Frimmel, 2003; Sheik et al., 2012). In addition, selective adsorption of toxic element onto specific mineral can be applied to engineering techniques to reduce their aqueous contaminations (Cundy et al., 2008). Thus, understanding of the adsorption behavior of toxic elements onto minerals can contribute to the related fields in geochemistry, human ecology, environmental microbiology, and engineering technology.

Adsorption reactions of arsenic on iron oxyhydroxides is one of the most intensively studied processes in geochemical and engineering field (Pierce and Moore, 1982; Fuller et al., 1993; Bowell, 1994; Manceau, 1995; Raven et al., 1998; Jain et al., 1999; Dixit and Hering, 2003; Sherman and Randall, 2003; Gao et al., 2013). High concentration of arsenic is observed under various environmental conditions such as groundwater, hydrothermal vents, and acid mine drainages (Smedley and Kinniburgh, 2002; Mandal, 2002; Hossain, 2006). Especially, contamination of arsenic in drinking water (mainly groundwater) causes health problems all over the world which is one of the most serious environmental issues we are facing today (Mandal, 2002; Mukherjee et al., 2006). Iron oxyhydroxides works as a dominant adsorbent of arsenic at these arsenic-contaminated areas (Akai et al., 2004). On the contrary, desorption of arsenic from iron oxyhydroxides leads to the mobilization of arsenic into aqueous systems (Nickson et al., 1998). These adsorption-desorption behavior of arsenic controlled by iron oxyhydroxides depends on various factors such as oxidation state of arsenic (arsenate or arsenite), adsorption structure, pH, redox state, ionic strength, and bioavailability of iron oxyhydroxides which have been extensively studied so far (Waychunas et al., 1993; Raven et al., 1998; Goldberg and Johnston, 2001; Lenoble et al., 2002; Dixit and Hering, 2003; Sherman and Randall, 2003; Saalfield and Bostick, 2010; Sharma et al., 2010;

Zhu et al., 2011; Lee et al., 2014; Qi and Pichler, 2014). However, most of the previous studies preformed experiments using inorganically-synthesized iron oxyhydroxides such as goethite and ferrihydrite.

Precipitation of iron oxyhydroxides occurs both abiotic and biotic pathways in natural environment (James and Ferris, 2004; Melton et al., 2014). Although abiotic and biotic Fe(II) oxidation is tightly interconnected, ratio of biotic Fe(II) oxidation exceeds abiotic one at Fe(II)-rich anoxic-oxic transition zone (O_2 concentration approximately <50 μM; Druschel et al., 2008), where we observe such conditions at groundwater discharge points (James and Ferris, 2004; Gault et al., 2011; Kato et al., 2012), hydrothermal vents (Emerson and Moyer, 2002), and plant roots (Weiss et al., 2003; Møller and Sand-Jensen, 2008). Iron oxyhydroxides collected from various natural environment with Fe(II)-oxidizing bacteria (e.g. autotrophic Fe(II)-oxidizing bacteria and nitrate-reducing Fe(II)-oxidizing bacteria; (Anderson et al., 2006; Kato et al., 2012; Hegler et al., 2012) are often called as biogenic iron oxyhydroxides (BIOS). Mineral species of BIOS have been reported as poorly-ordered iron oxyhydroxides: ferrihydrite by X-ray diffraction (XRD) analysis and more detailed analysis by X-ray absorption fine structure (XAFS) identified that BIOS are less poorly-ordered mineral than synthetic ferrihydrite (Toner et al., 2012). These studies indicated that BIOS is common iron oxyhydroxides in natural environment which may work as an important adsorbent for arsenic. BIOS present in hydrothermal vent and groundwater treatment system contain high concentration of arsenic (Katsoyiannis and Zouboulis, 2004; Meyer-Dombard et al., 2013), suggesting that BIOS is indeed an important scavenger for arsenic in natural environment. However, adsorption of arsenic onto BIOS is still not clear, such as (1) whether arsenic adsorption onto BIOS show similar adsorption capacity and pH dependence to that onto synthetic iron oxyhydroxides? and (2) what physicochemical factors cause adsorption characteristic of BIOS? Previous studies proposed models on arsenic mobility using results of arsenic adsorption onto inorganic iron oxyhydroxides (Jain et al., 1999; Swedlund, 1999), but there is no report confirming that the models could be applied to BIOS. Biogenic iron oxyhydroxides is different from synthetic ferrihydrite in that they co-exist with organic materials and bacterial cells (Chan et al., 2009; Wu et al., 2014). Some trace elements preferentially adsorbed onto organic and bacterial phases of BIOS show different adsorption

behavior from that on pure synthetic ferrihydrite (Kennedy et al., 2011). A previous study pointed out the decrease of arsenate (As(V)) retention in iron filtering system in the presence of NO^3-reducing Fe(II)-oxidizing bacteria compared to that in abiotic filtering system, because of the presence of organic materials in the biotic filtering system (Kleinert et al., 2011). The information is beneficial to understand arsenic adsorption processes occurring in BIOS, but might not be valid to BIOS produced by different species of iron-oxidizing bacteria and/or different environmental condition (e.g. ionic strength, water chemistry, and pH).

This study identified differences/similarities of As(V) adsorption between BIOS and synthetic iron oxyhydroxides (ferrihydrite). I focused on BIOS produced by a chemolithoautotrophic Fe(II)-oxidizing bacterium *Mariprofundus ferrooxydans*. *M. ferrooxydans* is a marine autotrophic Fe(II)-oxidizing bacterium which have been suggested to play an important role for the precipitation of iron oxyhydroxides in hydrothermal vent (Emerson and Moyer, 2002; Singer et al., 2011). I used BIOS collected from a hydrothermal vent (hereafter referred to as in situ biogenic iron oxyhydroxides: in situ BIOS) where *M. ferrooxydans* were detected by 16S rDNA analysis. However, in situ BIOS contain various kinds of pre-adsorbed or co-precipitated ions (Ferris et al., 2000; Martinez et al., 2003), making it more complex to understand characteristics of adsorption of metal ions by BIOS. I thus used biogenic ferrihydrite which was collected by the incubation of *M. ferrooxydans* under seawater condition (Kikuchi et al., 2014), to identify the effect of initial adsorption and co-precipitation of elements for As(V) adsorption onto BIOS. The characteristics of both in situ and in vitro BIOS were compared with that of synthetic ferrihydrite. Batch adsorption experiments were conducted in seawater condition (ionic strength = 0.70 M). Adsorption structure was identified using X-ray absorption fine structure (XAFS).

4.2. Materials and Methods

4.2.1. Sample collection and preparation

BIOS in natural environment (in situ BIOS) was collected from Tarama knoll, Okinawa Trough, Japan, where Fe(II)-rich diffusing hydrothermal fluid mixed with seawater. Sample was collected using sediment sampler by remotely operated vehicle (ROV) Hyper-Dolphin,

owned by Japan Agency for Marine-Earth Science and Technology. Prior to adsorption experiments, sample was washed with 0.70 M NaCl three times on board and stored at 4 ˚C.

In vitro BIOS was collected by incubating iron-oxidizing bacteria *Mariprofundus ferrooxydans* strain PV-1 using diffusion chamber. Details for the culturing method were described elsewhere (Kikuchi et al., 2014). After culturing *M. ferrooxydans* for 3 days, BIOS were collected from diffusion chamber and then washed and suspended in 0.70 M NaCl.

Inorganic ferrihydrite was synthesized in laboratory according to Schwertmann and Cornell (1991) by adding 1.0 M KOH solution into 0.20 M $Fe(NO_3)_3 \cdot 9H_2O$ solution. After adjusting pH at 7.5, solid was rinsed with MQ-water for five times, washed with 0.70 M NaCl for two times, and then suspended in 0.70 M NaCl.

4.2.2. Scanning electron microscope and transmission electron microscope observation

Samples were examined by scanning electron microscope (SEM) and transmission electron microscope (TEM) to identify morphology of samples. Samples were dehydrated with a series of ethanol (30, 50, 70, 80, and 90 %). Suspended samples were then mounted on carbon tape or copper grid and stored at desiccator overnight. Samples were then coated with gold and examined by HR-SEM (S-5200, Hitachi, Japan) or TEM (JEM-2010, JEOL, Japan). Chemical composition of the sample was evaluated by energy-dispersive X-ray spectrometer (EDS) attached to SEM and TEM.

4.2.3. Specific surface area

Specific surface area (SSA) was measured by nitrogen adsorption isotherm from Brunauer-Emmett-Teller (BET) method. Before measurements, samples were washed with MQ water and freeze dried. Samples (0.01 g) were then introduced into capillary glass designed for BET measurement and dehydrated at room temperature under 10^{-3} Kbar for 48 h. The N_2 adsorption was measured at 77 K using BELSORP-mini (Bell Japan inc., Osaka, Japan).

4.2.4. Batch adsorption experiments

4.2.4.1. Adsorption experiments of arsenate

Arsenate adsorption experiments for in vitro BIOS, in situ BIOS, and synthetic ferrihydrite were conducted at 25°C. For As(V) adsorption isotherms, experiments were conducted at pH 8.0 at initial As(V) concentrations of 25 mg/L, 55 mg/L, 80 mg/L, 100 mg/L, and 160 mg/L. One mg of each adsorbent was taken from the stock solution and suspended into 5 mL 0.70 M NaCl. After adjusting solution pH at 8, appropriate amount of As(V) solution (concentration of stock solution: 1000 mg/L) was added into the bottle and shaken at 120 rpm for 24 h in a water bath.

Arsenate adsorption at pH from 4 to 10 was examined: total liquid volume was 2.5 mL with 0.5 mg of each adsorbent. Initial concentration of As(V) was adjusted to 50 mg/L. After the addition of adsorbent and adsorbate, pH was adjusted to 4, 6, 7, 8, or 10 using 0.10 M HCl or 0.10 M NaOH. Samples were agitated at 120 rpm for 24 h using a shaker. Arsenate concentration in the liquid phase was measured by inductively coupled plasma mass spectroscopy (ICP-MS). The percentage of As(V) adsorbed onto each adsorbent was calculated by the following equation

$$As_{ads} = (As_{in} - As_{eq})/As_{in} \times 100 \quad (1)$$

where As_{in} and As_{eq} are initial and equilibrium concentration of As(V), respectively. Adsorption experiments were conducted in triplicate.

4.2.4.2. Adsorption experiments of yttrium and cerium

Yttrium (Y) and Cerium (Ce) adsorption experiments for in situ BIOS, in vitro BIOS, and synthetic ferrihydrite were conducted using 5 mg of adsorbent. After the addition of 0.5 mg adsorbent with total 2.5 mL of 0.70 M NaCl sotuion, pH was adjusted to 4, 5, 6, 7, or 8 respectively. Yttrium and cerium solution was then added from stock solution to be the final concentration of Y for 1.6 mg/L and Ce for 5.8 mg/L. Samples were shaken for 5 h at 25°C and equilibrium concentration of Y and Ce were measured by ICP-MS.

4.2.5. Micro XRF mapping of iron and arsenate

Micro-XRF mapping of iron and arsenate were obtained at BL37XU in SPring-8, Japan. The beamline consists of Si(111) double crystal monochromator with Kirkpatric-Baez mirror to obtain X-ray beam with 1.5 × 1.6 μm^2 size at the sample. Mapping of iron and arsenate by μ-XRF was carried out at irradiation energy at 12.8 keV. The step size was set to be 0.3 μm both in x- and y- directions. Measurement time of each pixel was 0.5 s.

4.2.6. Arsenic K-edge X-ray absorption fine structure spectroscopy

Arsenic K-edge XAFS measurement was conducted at BL01B1 at SPring-8, Hyogo, Japan. Wet paste samples were collected from batch adsorption experiment, which was conducted using 100 mg of each adsorbents. The energy was calibrated by setting the maximum peak of $KAsO_2$ at 11865 eV. Measurement was conducted in fluorescence mode. Collected XAFS data were analyzed using REX2000 software (Rigaku Co., Ltd.)

4.2.7. Zeta potential analysis

Analysis of zeta potential was performed using a microscope-type analyzer ZEECOM ZC-3000 (Microtec Co., Chiba, Japan). Samples were washed with 0.01 M KNO_3 for three times and 0.1 mL of each sample was finally diluted in a 10 mL 0.01 M KNO_3 solution. Solution pH was adjusted to 4 to 10 for 24 h. Suspensions were then sonicated for ca. 3 min and final pH was obtained with N_2 gas bubbling. Suspensions were then immediately applied in a glass cell. Particles were identified by laser beam. Zeta potential was measured upper and lower levels of the stationary layer with an average particle number of the 500.

4.3. Results and Discussion

4.3.1. Characterization of metal oxides

Mineral species of in situ and in vitro BIOS used in this study were previously characterized by X-ray fluorescence (XRF) and XAFS analysis (Kikuchi et al., 2014; Makita et al. in prep.; Table 2–2). Iron is major element for in situ BIOS (56 wt%; Table 2–2), followed by the inclusion of silicate (14 wt%) and phosphate (3.7 wt%). Concentration of arsenic for in situ BIOS was 409 mg/kg, suggesting initial accumulation of arsenic before the

adsorption experiment. Phosphate is also accumulated in in vitro BIOS (0.6 to 1.6 wt%) since we added them for bacterial growth. Judging from Fe K-edge extended X-ray absorption fine structure (EXAFS), both in situ and in vitro BIOS were consisted of poorly ordered iron oxyhydroxides, which is ordered to a lesser degree than synthetic ferrihydrite (Toner et al., 2012; Table2–3 in Chapter2) .

My SEM and TEM observations of in situ and in vitro BIOS showed common inclusion of stalks, which were covered by fine grains of iron oxyhydroxides (Fig. 4–1A to E). Fine particles of individual grains consisting of 200 to 350 nm spherical aggregate (Fig. 4–1B). Analysis of TEM-EDS at these iron aggregated area for in situ BIOS detected silicate, phosphate, and carbons in addition to iron (Fig. 4–1E). Specific surface areas (SSAs) of synthetic ferrihydrite, in situ BIOS, and in vitro BIOS were 235 m^2/g, 147 m^2/g, and 153 m^2/g, respectively. Organic content of each BIOS are 1.2 wt% for in situ BIOS and 1.9 wt% for in vitro BIOS.

4.3.2. As(V) adsorption onto synthetic ferrihydrite vs. BIOS

Arsenate adsorption onto synthetic ferrihydrite, in situ BIOS, and in vitro BIOS was rapid reaching equilibrium within 3 h (Fig. 4–2). The adsorption isotherms of As(V) at pH 8 for each adsorbent are shown in Figure 4–3. Data from adsorption isotherms were fitted using Freundlich isotherm models as presented by the following equation:

$$q_e = K_F C_e^{1/n} \quad (1)$$

where q_e is the amount of As(V) adsorbed onto each adsorbent (mmol/g) and C_e is the equilibrium As(V) concentration (mol/L). Both K_F and 1/n are constant values that indicate maximum adsorption capacity and heterogeneity factor of the adsorbent surface, respectively. The results of isotherm parameters are shown in Table 4–1. Synthetic ferrihydrite exhibited largest K_F value among the three adsorbents. The 1/n value also showed minimum value for synthetic ferrihydrite followed by in situ and in vitro BIOS. The Freundlich model thus suggests that BIOS samples possess fewer adsorption capacities even on more heterogeneous surface sites when compared with synthetic ferrihydrite.

Adsorption of As(V) onto each adsorbent in pH range of 4 to 10 are shown in Fig. 4–4.

All adsorbents exhibited similar pH dependence for As(V) adsorption: maximum adsorption at pH 4 and the amount of As(V) adsorption gradually decreased with increasing pH. The adsorption capacity of As(V), however, was larger for synthetic ferrihydrite than both in situ and in vitro BIOS at all experimental pH. The amount of As(V) adsorbed onto in situ and in vitro BIOS at pH range from 4 to 8 were linearly decreased from that of synthetic ferrihydrite, maintaining average decreased ratio of 34% and 25% for in situ BIOS and in vitro BIOS, respectively. In vitro BIOS showed slightly larger As(V) adsorption than in situ BIOS. Hence, both adsorption isotherms and adsorption edges suggest lower sorption affinity of As(V) for BIOS than synthetic ferrihydrite.

4.3.3. Results of μ-XRF and Arsenic K-edge EXAFS

To determine the distribution of As(V) within ferrihydrite and organic carbon complex: BIOS, in vitro BIOS was analyzed by μ-XRF. Light microscope image of in vitro BIOS showed aggregation of iron oxyhydroxides on stalks which was consistent with TEM observation (Fig. 4–5A). The μ-XRF mapping of arsenic and iron are shown in Fig. 4–5B and 4–5C. There was a high correlation between distribution of Fe and As, suggesting that ferrihydrite works as an important adsorbent for As(V) on BIOS. Correlation or decorrelation of As(V) with other components such as organic materials and phosphate cannot be discussed since we have not identified their distribution by μ-XRF mapping. There seems to be less distribution of As(V) in the area of the stalk, which may suggest lesser contribution of stalks itself as a As(V) adsorption site.

Oxidation state and adsorption structure of As(V) in each adsorbent was identified by XAFS analysis. X-ray absorption near edge structure (XANES) spectra from all adsorbents showed one prominent peaks at oxidation state of As(V), confirming that As(V) reduction is not occurring during batch adsorption experiments and XAFS measurements (Fig. 4–6). The EXAFS spectra and radial structure functions (RSFs) are given in Fig. 4–7. All three adsorbents showed nearly identical EXAFS spectra, suggesting similar coordination environment of As(V). The RSFs obtained by FT of the EXAFS spectra in the k range between 2.5 to 11.5 $Å^{-1}$. The results of the shell-by-shell fitting are shown in Table 4–2. The corresponding radial structure functions in three adsorbents showed similar two main peaks

at 1.69 Å and 3.30 Å, respectively. The peak at the distance of 1.69 Å was attributed from the oxygen atoms of AsO_4 tetrahedra. The second RSF peak at distance of 3.30 Å with coordination number of 4 suggests As-Fe shell. These results are common coordination environment of As(V) onto synthetic ferrihydrite, explained by inner-sphere binuclear bidentate complexes (Manceau, 1995; Sherman and Randall, 2003).

4.3.4. Zeta potential

The results of zeta potential for synthetic ferrihydrite, in situ BIOS, and in vitro BIOS are present in Fig. 4–8. I used laser beam to identify and trace each iron particle during the measurements. Given that (1) laser beam can detect particle size between 10 to 400 nm and (2) my TEM observation identified spherical aggregation of iron oxyhydroxides (200 to 350 nm in size) within BIOS (Fig. 4–1B), it is suggested that we measured zeta potential of aggregated ferrihydrite particles. Synthetic ferrihydrite had positive surface charge at pH lower than 8, whereas surface charge shifted to negative at pH higher than 8. The point of zero charge (PZC) thus obtained for the synthetic ferrihydrite (~8.0) in this study agrees with prior studies (Davis and Leckie, 1978). In comparison to synthetic ferrihydrite, positive surface charge was measured only at around pH 4 for both in situ and in vitro BIOS (Fig. 4–8). The PZC obtained from in situ and in vitro BIOS were approximately 4.5 and 5.5, respectively. The results showed that BIOS possess larger negative charges for the broader pH range, compared to synthetic ferrihydrite.

4.3.5. Decrease of As(V) adsorption onto BIOS

My batch As(V) adsorption results for in situ and in vitro BIOS show both BIOS can scavenge As(V) rapidly from solution, by forming inner-sphere complexes. This result is consistent with that of synthetic ferrihydrite. Ferrihydrite has been considered as one of the most common adsorbents for As(V) in natural and synthetic systems and this characteristic is also valid in the case of biogenic ferrihydrite. However, As(V) adsorption onto in situ and in vitro BIOS was 25 to 34% less than that obtained from synthetic ferrihydrite. This result suggests that As(V) adsorption occurring in natural environment is less than what we speculated using abiotic ferrihydrite. My study indicated two important factors to inhibit

As(V) adsorption onto BIOS: SSA and surface charge. Both functions are known to control adsorption amount of trace elements onto various mineral surfaces.

Ferrihydrite is primarily consists of nano-particles (Janney et al., 2000). My TEM observation of BIOS indeed confirmed nanometer-sized iron particles, which is also consistent with the morphologies of BIOS collected from natural environments (Chan et al., 2009; Suzuki et al., 2012). Considering that there is an inverse relationship between particle size and SSA (Wang et al., 2013), BIOS could have similar or even larger surface area than synthetic ferrihydrite. However, BET SSA obtained for both in situ and in vitro BIOS were less than that of synthetic ferrihydrite. It should be noted that BET SSA cant underestimate real wet surface area because aggregation of nanoparticles during drying reduces surface area. Dry sample observation by TEM and SEM indeed revealed spherical aggregation consists of fine iron oxide particles, but we also observed similar spherical aggregation during wet condition by optical microscope. These results suggest that strong aggregation of ferrihydrite is already exist in aqueous condition, which causes decrease of SSA which results in the less amount of adsorption sites for As(V) onto BIOS.

The other effect to inhibit As(V) adsorption onto BIOS is negative surface charge. Commonly, the decrease of As(V) adsorption onto ferrihydrite with increasing pH can be expressed by electrostatic repulsion between oxyanion As(V) and negatively charged surface sites (Raven et al., 1998). This repulsion effect becomes stronger at pH larger than 8.0 for synthetic ferrihydrite because pH_{pzc} for synthetic ferrihydrite is nearly 8.0 (Davis and Leckie, 1978). On the contrary, pH_{pzc} of in situ and in vitro BIOS were 4.5 and 5.5, respectively, suggesting strong surface repulsion between biogenic ferrihydrite and As(V) compared to synthetic ferrihydrite. This repulsion inhibits As(V) adsorption onto BIOS.

4.3.6. Factors to inhibit As(V) adsorption onto BIOS

Important things to consider are the factors to change SSA and zeta potential in BIOS. This study used two kinds of biogenic ferrihydrite: one was from natural hydrothermal vent (in situ BIOS) where various dissolved ions present, while the other was obtained from incubation of *M. ferrooxydans* in artificial seawater (in vitro BIOS) that contains lesser amount of dissolved ions compared to that in hydrothermal vent. Decrease of As(V)

adsorption occurred both types of biogenic ferrihydrite, suggesting ions commonly present in both in situ and in vitro BIOS could to be main candidates to inhibit As(V) adsorption onto BIOS: that is, organic materials and phosphate.

Co-precipitation and adsorption of organic materials with ferrihydrite have been suggested to promote aggregation of particulate iron oxyhydroxides which simultaneously reduce SSA (Kaiser et al., 2003; Mikutta et al., 2008). Aggregation starts from neutralization of ferrihydrite by the adsorption of organic materials onto ferrihydrite (Braunschweig et al., 2014). On the contrary, high input of organic materials led to stabilization of iron oxyhydroxides as colloidal suspension because negatively charged subaggregate repulses each other (Braunschweig et al., 2014). Surface charges of both in situ and in vitro BIOS in this study were negatively charged at pH larger than 4.5 or 5.5, implying each ferrihydrite aggregates in BIOS is within the stage of static colloidal phase which electrostatically repulses As(V). In the meantime, adsorption of organic materials onto BIOS occupy adsorption site of As(V), causing lower affinity for As(V). Gradual increase of organic content in iron oxyhydroxides within BIOS has been suggested in recent study (Bennett et al., 2014). Thus, I speculate that organic materials present within the aggregated ferrihydrite in both in situ and in vitro BIOS play an important role for the decrease of SSA as well as for the increase of electrostatic repulsion between BIOS and As(V).

The other candidate ion to reduce As(V) adsorption onto BIOS is phosphate. Phosphate is a common inhibitor to decrease As(V) adsorption onto iron minerals because it compete for the same adsorption site with As(V) (Zhu et al., 2011). The SEM-EDS analysis of aggregated iron particles detected phosphate in both in situ and in vitro BIOS. To my knowledge, promotion of mineral aggregation by phosphate has not yet been reported. However, phosphate may be involved in mineral aggregation since phosphate adsorption onto ferrihydrite also alters surface charge of ferrihydrite (Arai and Sparks, 2001). Thus, direct occupation of adsorption site and possibly aggregation of iron oxyhydroxides by phosphate can be another cause to decrease As(V) adsorption onto BIOS. This study did not remove the effect of phosphate from in vitro BIOS since low concentration of phosphate in the cultivation medium changed iron mineral species to more crystalline iron oxyhydroxides, which is consistent with previous results (Larese-Casanova et al., 2010). Tone et al. (2012)

reported that mineral species of BIOS in hydrothermal vent have been preserved as amorphous phase due to silica coating (Toner et al., 2012). Silica also reported to reduce arsenate adsorption onto ferrihydrite which could be an additional factor to inhibit As(V) adsorption onto in situ BIOS.

4.3.7. Cerium and yttrium adsorption onto BIOS: further insight into the adsorption characteristics of BIOS

I have further examined adsorption characteristic of BIOS using yttrium and cerium as adsorbate. Based on the negative surface charge in the wide pH range, both in situ and in vitro BIOS may show electrostatically higher affinity to cations than synthetic ferrihydrite. In addition, previous field-base studies have indicated that bacterial and organic functions within BIOS can provide additional adsorption sites for cations (Ferris et al., 1999, 2000; Martinez et al., 2003). A previous study which compared iodine adsorption onto in situ BIOS and synthetic ferrihydrite indeed show stronger adsorption for in situ BIOS than for synthetic ferrihydrite (Kennedy et al., 2011).

Yttrium and cerium adsorption onto synthetic ferrihydrite, in situ BIOS, and in vitro BIOS are shown in Fig. 4–9A and 4–9B. Both yttrium and cerium adsorption onto each adsorbents showed strong pH dependence. Higher yttrium and cerium retention was exhibited at higher pH, suggesting that the adsorption is controlled by electrostatic affinities between adsorbent and adsorbate. The amount of yttrium and cerium adsorbed onto in situ BIOS showed lowest adsorption capacity among the three adsorbents for all the pH range, showing nearly straight-line increase with increasing pH. However, adsorption of yttrium and cerium onto in vitro BIOS did not follow the adsorption trend of in situ BIOS and sudden increase of adsorption exhibited at pH 6. This adsorption trend is more similar to that of synthetic ferrihydrite. Moreover, retention of both yttrium and cerium at pH 6 were highest among the three adsorbent even though SSA of in vitro BIOS is smaller than synthetic ferrihydrite. I thus speculate that adsorption characteristic of trace element onto BIOS can be changed based on how much adsorption site is available. Even if iron mineral species, SSA, and zeta potential showed nearly identical features, availability of adsorption site could be different between in situ and in vitro BIOS. In situ BIOS contains a lot of trace elements before

adsorption experiments, suggesting some of the adsorption site for yttrium and masked have been masked, although it is not valid for in vitro BIOS. Moreover, higher adsorption of yttrium and cerium onto in vitro BIOS than onto synthetic ferrihydrite may suggest additional adsorption site such as adsorption of these two ions onto organic materials and/or formation of ternary complex formation (e.g. Fe-P-cation and Fe-organic material-cation). Alternatively, it can make more sense to imply that iron oxyhydroxides works as a main adsorption site for yttrium and cerium and higher adsorption of these anions onto in vitro BIOS is caused by "trace element free" fine particles of iron oxyhydroxides than synthetic ferrihydrite and in situ BIOS, based on the similar adsorption trend of cations between synthetic ferrihydrite and in vitro BIOS. Although more detail should be mentioned, my study concludes that adsorption of trace elements onto BIOS is different from synthetic ferrihydrite which is caused by the difference of SSA, surface charge, and presence/absence of metal ions that mask adsorption site for initial stage.

4.4. Environmental implications

My study suggests the effect of organic and inorganic ions to inhibit trace element retention, especially for oxyanion As(V). Decrease of As(V) adsorption onto BIOS was also reported in biogenic iron-based groundwater filtering system (Kleinert et al., 2011), which may indicate that lower efficiency of As(V) retention is a common phenomenon in BIOS rather than to restrict this under seawater condition. Since my in vitro BIOS cannot eliminate the effect of phosphate which greatly inhibit As(V) adsorption onto ferrihydrite, I speculate that phosphate inclusion in BIOS is the nature of BIOS in natural environment. Phosphate is an essential element for Fe(II)-oxidizing bacteria so that BIOS precipitation occurs where phosphate is available even if it is at trace concentration. The growth of iron-oxidizing bacteria produces organic materials with the precipitation of biogenic iron minerals. At the same time, BIOS further accumulate phosphate and organic materials by their high adsorptive affinity, which simultaneously promotes aggregation of iron particles and change of surface charge. Indeed, BIOS in natural environment contain a few percentage ranges of phosphate and organic carbon (Rentz et al., 2009; Table 2–2), showing common accumulation of these elements in BIOS.

Since my study targeted As(V), cerium, and yttrium as adsorbates, there are many other elements accumulated in in situ BIOS, such as uranium and lead(Ferris et al., 2000), which may show different adsorption behavior compared to synthetic ferrihydrite. A previous study noted that pH_{pzc} of BIOS reaches 9.6 because of the preferential adsorption of cations onto BIOS, which result is opposite from my study (pH_{pzc}: 4.5-5.5 in this study). It is likely that adsorption feature of BIOS is not a single character but show several different stages on the basis of how much organic and inorganic ions coexist and how these ions affect physicochemical feature of BIOS. This study pointed out the importance to consider not only characteristics of iron mineral in BIOS (such as iron mineral species and size of iron particles) but also interaction of iron to other ions that affect SSA and surface charge. This result will expand our further understanding of the geochemical role of BIOS in natural environment.

Figures and Tables

Table 4–1. Isotherm parameters of Freundlich models (Experimental condition: ionic strength = 0.7 M NaCl; adsorbent = 1 mg; Initial As(V) concentration = 10 to 190 mg/L).

	K_F	1/n	R^2
synthetic ferrihydrite	2.43	5.03	0.98
in situ BIOS	1.02	3.16	0.98
in vitro BIOS	1.17	3.42	0.80

Table 4–2. Results from shell-by-shell fitting of the As K-edge EXAFS spectra of samples.

sample	shell	R(Å)	N	σ(Å)
synFH	As-O	1.69	4.5	0.05
	As-Fe	3.28	2.2	0.11
synBIOS	As-O	1.69	4.7	0.05
	As-Fe	3.29	2.3	0.12
Tarama	As-O	1.69	4.8	0.05
	As-Fe	3.3	2.4	0.12

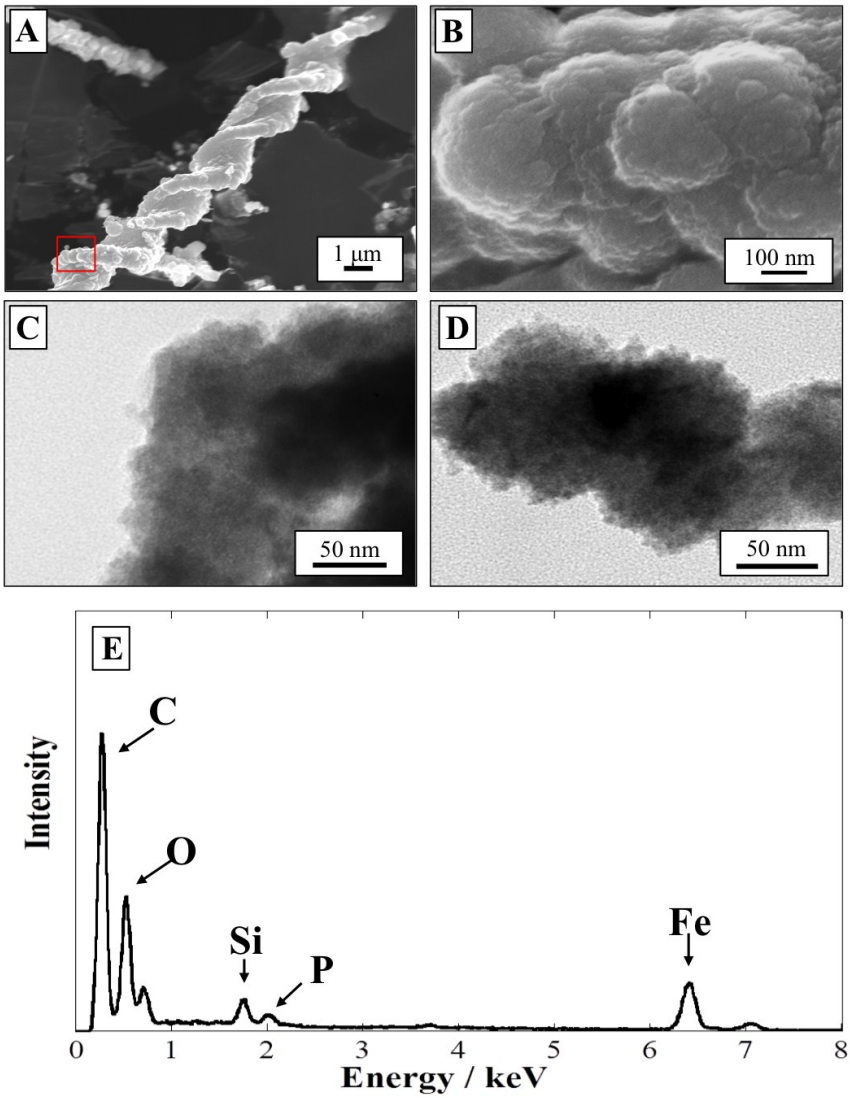

Fig. 4–1. SEM images of in situ BIOS (A, B) and TEM images of in situ BIOS (C) and in vitro BIOS (D). SEM-EDS spectra of aggregated iron hydroxides (E). In situ and in vitro BIOS contain a lot of twisted stalks (A) that are covered by aggregates of iron oxyhydroxides (B). Aggregate are consisted of fine particles of iron oxyhydroxides (C, D) and they contain carbon, silica, and phosphate in addition to iron.

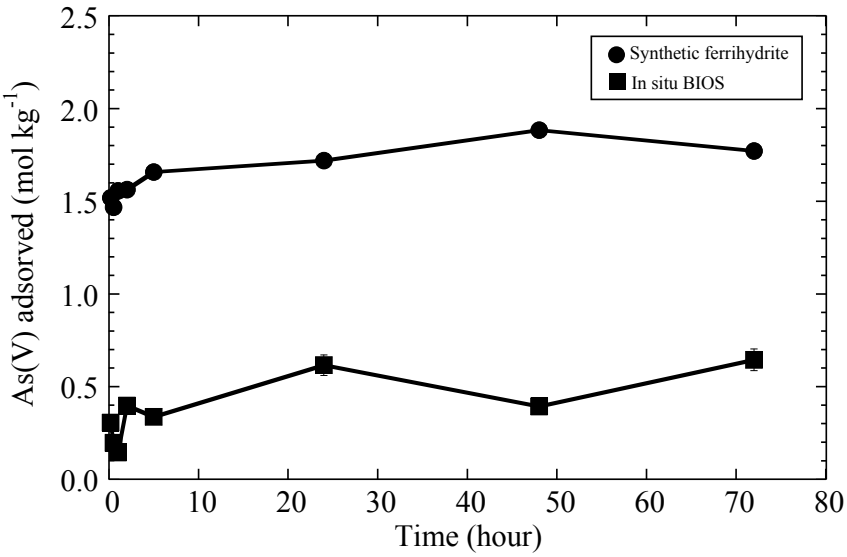

Fig. 4–2. Kinetic of As(V) adsorption by synthetic ferrihydrite and in situ BIOS at pH 8. Adsorption of arsenate in both synthetic ferrihydrite and in situ BIOS reached equilibrium in less than 3 hours. Experimental condition is 1 mg adsorbent; initial As(V) concentration of 50mg/L; I = 0.70 M.

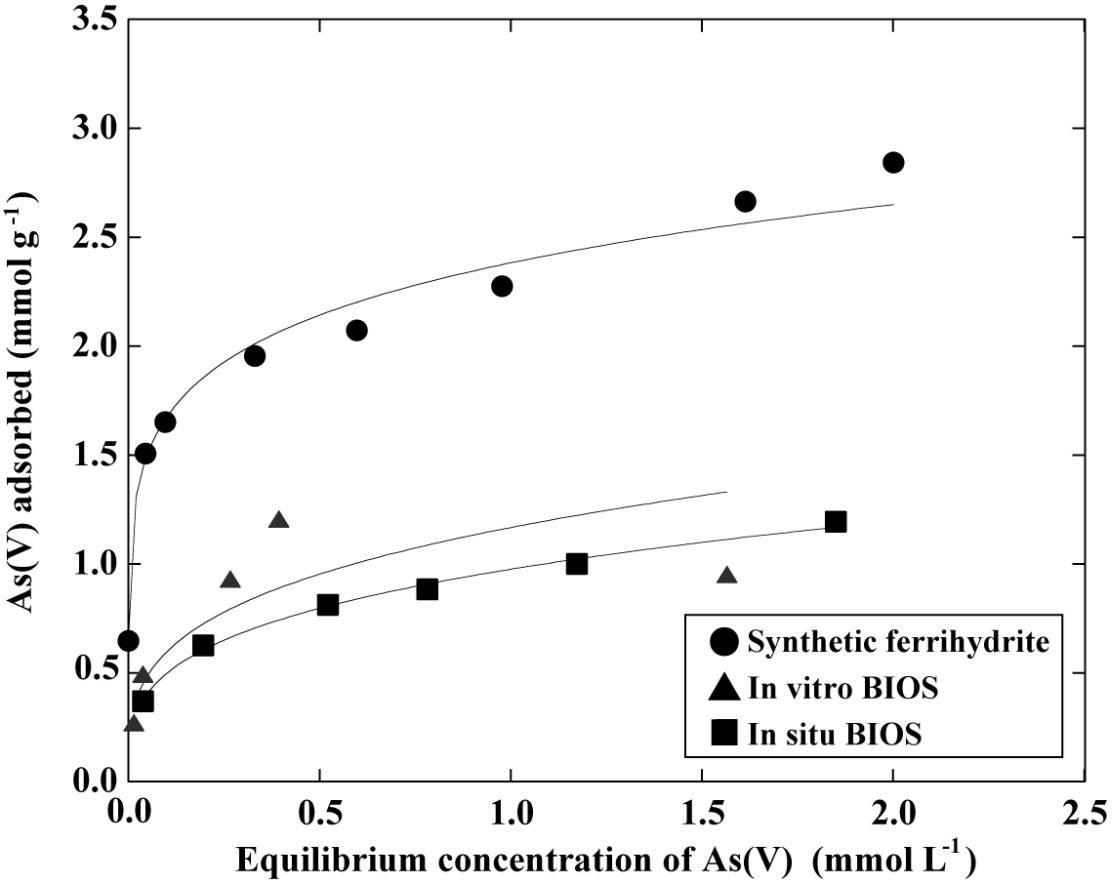

Fig. 4–3. Sorption isotherms of As(V) for synthetic ferrihydrite, in situ BIOS, and in vitro BIOS at pH 8 (sorbent: 1 mg; I = 0.70 M). Solid line represent Freundlich fitting.

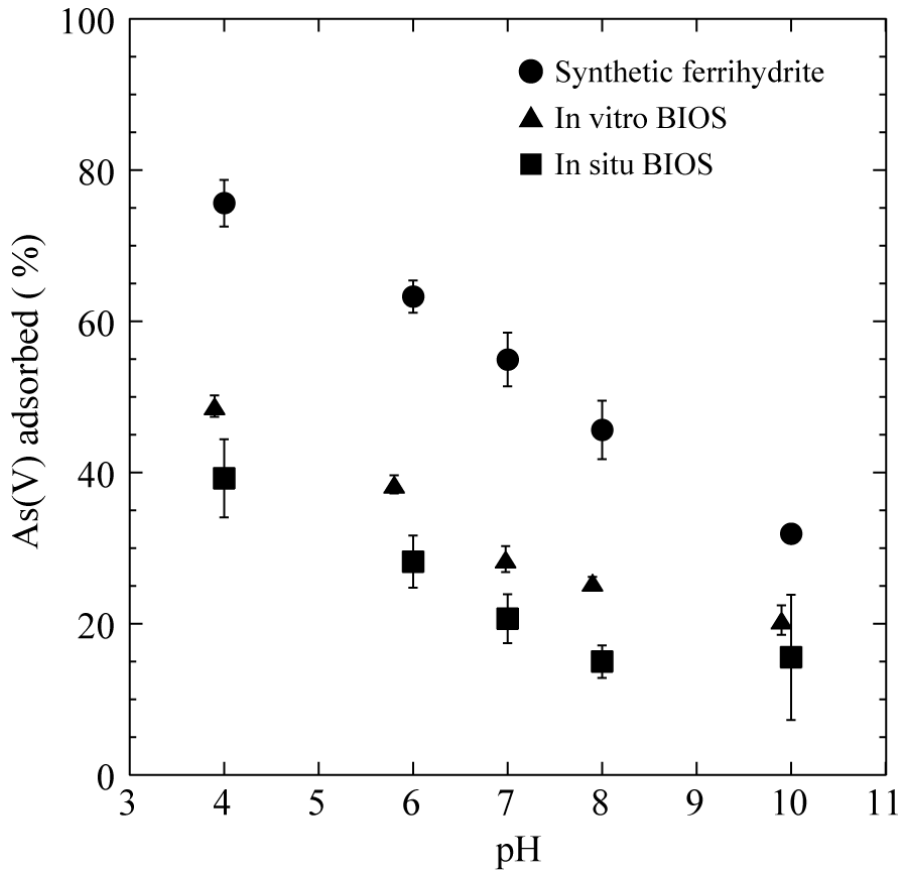

Fig. 4–4. Sorption edges of As(V) by synthetic ferrihydrite, in situ BIOS, and in vitro BIOS (sorbent: 0.5 mg; initial As(V) concentration: 50mg/L; I = 0.70 M NaCl).

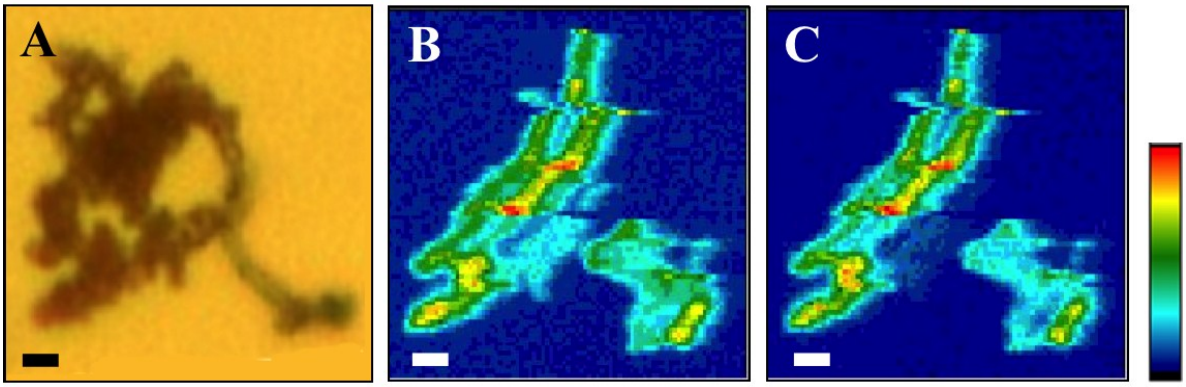

Fig. 4–5. Light micrographs of in vitro BIOS (A) and μ-XRF mapping of iron (B) and arsenic (C) in in vitro BIOS. There is a good correlation between the elemental map of iron and arsenic. Scale bar = 5 μm. X-ray beam size, 0.45 × 0.36 μm^2; Step size, 0.3 μm; Measurement time, 0.5s/point.

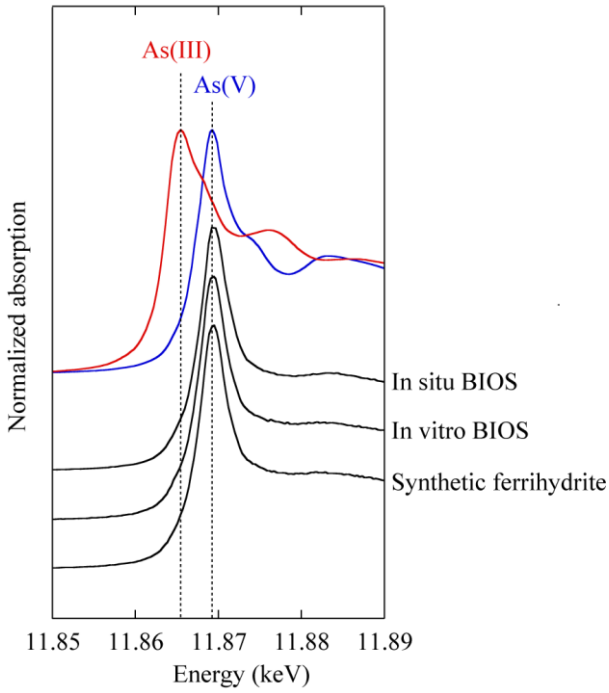

Fig. 4–6. Arsenic K-edge XANES spectra of synthetic ferrihydrite, in situ BIOS, and in vitro BIOS. All adsorbents showed one prominent peaks at oxidation state of As(V), confirming that As(V) reduction is not occurring during batch adsorption experiments and XAFS measurements

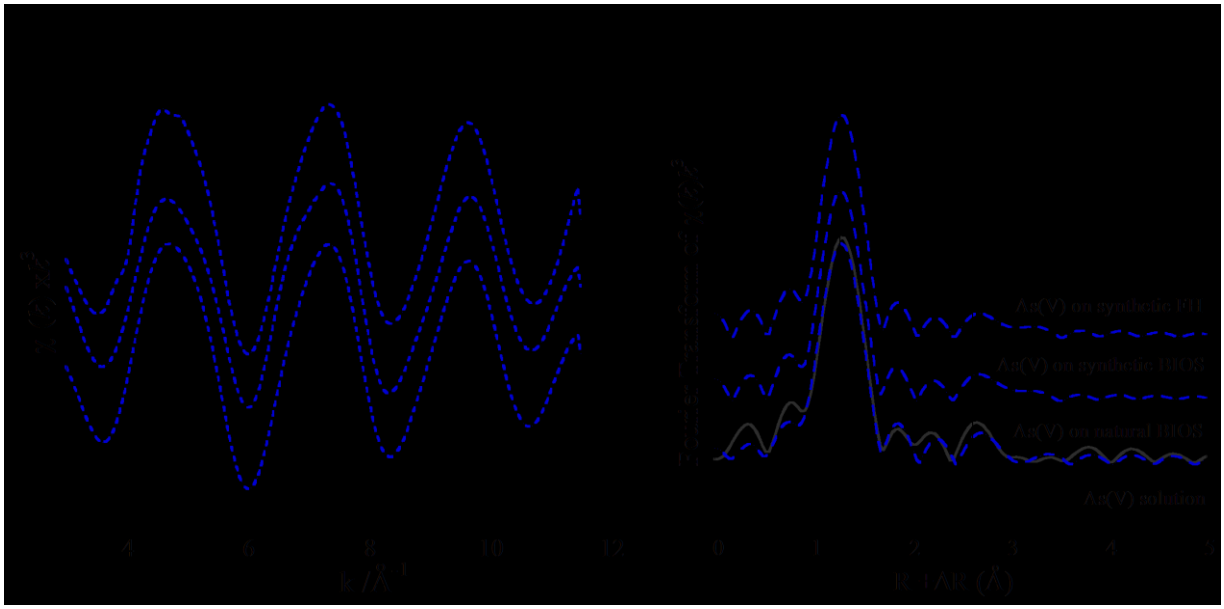

Fig. 4–7. (A) The As K-edge EXAFS spectra collected from As(V) adsorbed onto (i) synthetic ferrihydrite, (ii) synthetic BIOS, (iii) natural BIOS. (B) The magnitude portion of the Fourier transformed data. Solid line represent observed data, while dot line show the fitting.

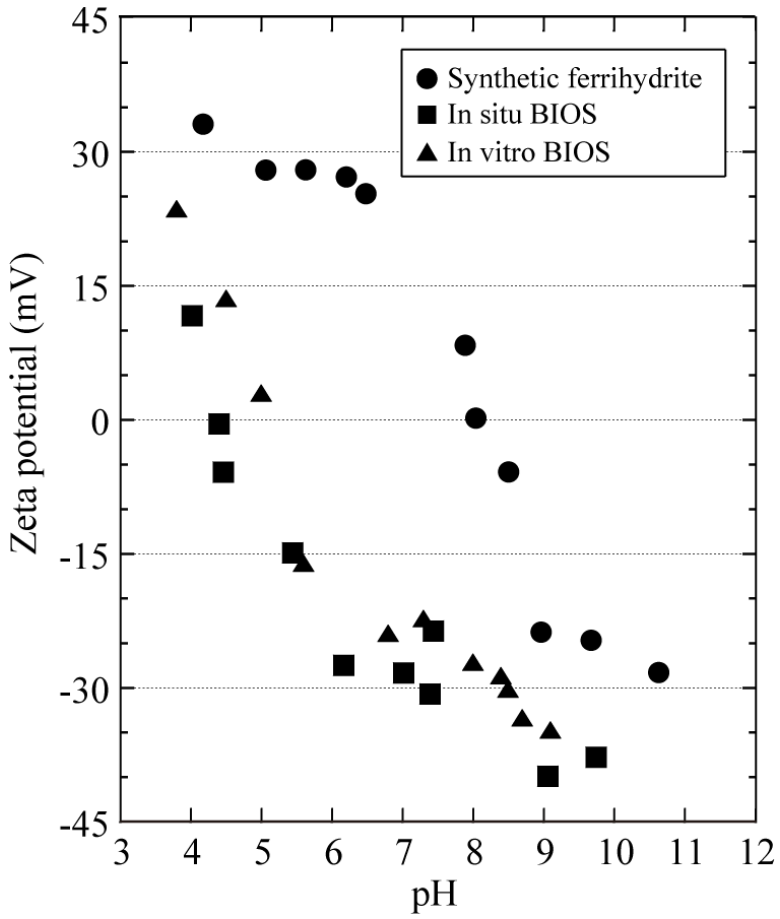

Fig. 4–8. Zeta-potential of synthetic ferrihydrite, in situ BIOS, and in vitro BIOS. Particles were detected by laser-beam. Obtained pH_{pzc} of synthetic ferrihydrite, in situ BIOS, and in vitro BIOS is 8.0, 4.5, and 5.5 respectibely.

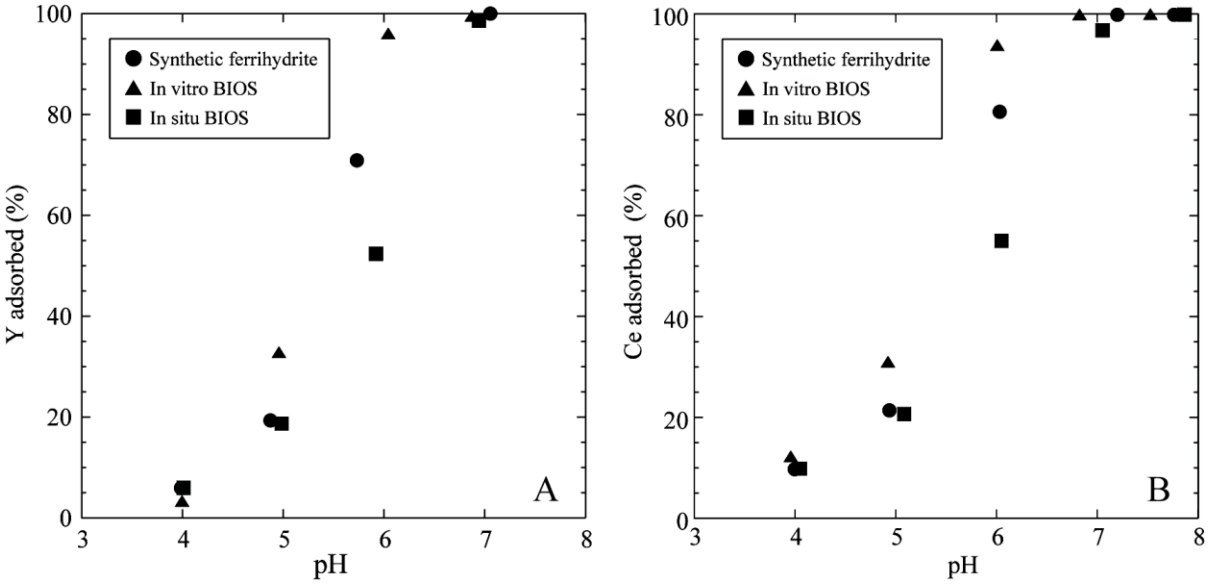

Fig. 4–9. Sorption edges for yttrium (A) and cerium (B) by synthetic ferrihydrite, in situ BIOS, and in vitro BIOS (sorbent: 0.5 mg; initial yttrium and cerium concentration: 1.5 mg/L and 5.5 mg/L; I = 0.70 M NaCl).

Chapter 5. Biogeochemical cycle of iron and carbon during the sedimentation of biogenic iron minerals

5.1. Introduction

Microorganisms play a crucial role in the cycle of various elements (Falkowski et al., 2008) because these microorganisms mediate mineral formation, dissolution, and weathering. Minerals produced by microbial activities adsorb trace elements to a stronger extent than abiotic minerals. Moreover, surface functional groups of bacterial cells (e.g., carboxyl and phosphate groups) and extracellular polymeric substances (EPSs) produced by microorganisms affect trace element behaviors in natural systems (Beveridge, 1989); (Pal and Paul, 2008). Given that microorganisms can grow under various conditions, element cycles driven by microorganisms are ubiquitous phenomena in modern and ancient environments.

Among various element cycles, iron cycle is one of the important processes closely coupled with microbial functions. Iron is an essential element supporting biological processes; this element can also function as both electron donor and acceptor in microbial respiration under various conditions, including circumneutral pH (Kappler and Straub, 2005); (Konhauser et al., 2011) and acidic pH (Baker and Banfield, 2003). Under anoxic and suboxic conditions, the oxidation of Fe^{2+} to Fe^{3+} is mediated by biotic and abiotic processes; however, biotic Fe^{2+} oxidation by bacteria can outcompete abiotic Fe^{2+} oxidation (Druschel et al., 2008). Biogenic iron minerals produced by representative iron-oxidizing bacteria display a poorly ordered nanoparticular form and often co-exist with organic materials, such as stalks, sheaths, and EPSs (Emerson and Moyer, 2002; Toner et al., 2009; Chan et al., 2009; Kikuchi et al., 2011, 2014; Chan et al., 2011; Toner et al., 2012; Wu et al., 2014). The mixture of iron (oxyhydr)oxides and organic materials functions as sorbents of trace elements and enables biogenic iron minerals to control the behavior of various trace elements by adsorption (Ferris et al., 2000).

Once biogenic iron minerals precipitate, these minerals can be utilized as electron acceptors in microbial metabolic processes (Blothe and Roden, 2009; Langley et al., 2009; Emerson, 2009). Some iron-reducing prokaryotes promote the coupling of organic carbon

oxidation with iron reduction; this process is referred to as dissimilatory iron reduction (Lovley, 1991). In addition, iron can be reduced indirectly by sulfate-reducing prokaryotes (Afonso and Stumm, 1992) and humic-reducing prokaryotes (Lovley et al., 1996). The utilization of iron and organic carbon by iron-metabolizing microorganisms can cause secondary iron minerals to precipitate (Fredrickson et al., 1998; Zachara et al., 2002; Hansel et al., 2003). These processes affect the cycles of trace elements present in biogenic iron minerals (Zachara et al., 2001; Muehe et al., 2013). Moreover, other organic carbon oxidation pathways, such as methanogenesis and acetogenesis, may be related to precipitation or dissolution of biogenic iron minerals (Lovley and Phillips, 1986; Roden and Wetzel, 1996; Roden and Wetzel, 2003). Thus, geochemical cycles of trace elements driven by iron oxyhydroxides and organic carbon are likely associated with iron and carbon bioavailability in biogenic iron minerals. Although biomineralization/bioreduction, organic carbon oxidation, and trace element adsorption/desorption of biogenic iron minerals have been investigated in laboratory settings (e.g., Zachara et al., 1998; Ferris et al., 2000; Zachara et al., 2001; Chan et al., 2011), the mechanism by which microbial activities affect iron and carbon biogeochemical processes in natural environments remains uncertain. Previous studies also focused on the coupling of iron-oxidizing and iron-reducing bacteria in biogenic iron-rich sediments (Gault et al., 2011, 2012; Roden, 2012) but failed to address the interrelationship with other microbial metabolic processes and populations. Furthermore, the physicochemical properties of sedimentary habitats (e.g., dissolved oxygen, pH, and Eh) are depth dependent; sedimentary microbial communities remarkably change in a short range (Ludemann et al., 2000). Thus, iron and carbon biogeochemical processes are affected not only by composition and abundance of iron and carbon species but also by physicochemical properties of sedimentary habitats.

Biogenic-iron-associated microbial activity may have also occurred in ancient Fe^{2+}-rich seawater, especially where banded iron formations (BIFs) were formed. Although there has been growing evidence that iron-metabolizing prokaryotes might have involved in the formation of BIFs (Konhauser et al., 2002; Heimann et al., 2010), there is still little information about the microbial populations and functions, the iron phase transformations, and the organic carbon contribution to the deposition and preservation. Nevertheless, it is

quite challenging to obtain the evidences from the ancient, highly metamorphosed BIFs. Biogenic iron sediments and biogeochemical processes in the present Earth may become an excellent modern analog to address the potential interrelations between the microbial development and functions in the deposition and preservation of BIFs.

This study aimed to characterize the depth-dependent changes in iron mineral species, microbial communities, and iron and carbon biogeochemical processes in freshwater biogenic iron-rich sediment. Takahashi *et al*. (2007) and Kato *et al*. (2012) previously studied this site and revealed that abundant fluffy precipitations of biogenic iron minerals in this site are likely produced by iron-oxidizing bacteria. Thus, this biotope is an ideal site to study (i) iron and carbon biogeochemical processes associated with shifts in physicochemical properties of sedimentary habitat, (ii) iron phase transformation, and (iii) microbial community composition in iron-rich sediments. I also determined pore water chemistry and iron mineral species in the sediment by microelectrode analysis, X-ray absorption fine structure (XAFS) analysis, transmission electron microscopy (TEM), and stable CH_4 isotope analysis. I then evaluated the spatial distributions of bacterial and archaeal communities in the sediment by 16S rRNA gene analysis.

5.2. Materials and Methods

5.2.1. Site description and sample collection

Sediment samples were collected from Budo pond at Hiroshima University (34°24.06′ N, 132°42.79′ E) in December 2012 and July 2013 by directly inserting acrylic tubes (15 cm in length) into the sediment. Two cores were collected: one core was used for 16S rRNA gene analysis, mineral speciation, and pore water chemical characterization, and the other core was used for microelectrode analysis. Both sediment cores were collected 30 cm away from the groundwater source, which was located in the flow path of the discharged water in the pond. Each core was treated as described in the following sections. Subsample was prepared in an anoxic chamber (Coy Laboratory Products; Ar:H_2 = 98%:2%; [O_2] < 0.01 ppm).

5.2.2. Microelectrode analysis of pH, Eh, and dissolved oxygen (DO)

Dissolved oxygen (DO), pH, and redox potential (Eh) in the sediment were determined

using a microelectrode in a laboratory. Microelectrode analyses were performed, as described by Shiraishi *et al*. (2010). In brief, DO and redox electrodes were purchased from Unisense (Aarhus, Denmark). The pH electrode was prepared, as described by Gieseke and de Beer (2004). After the cores were collected, the sediment was stored in laboratory at room temperature for approximately 1 h to settle fluffy materials that may have been agitated during sample transport. Microelectrode measurements from depth of 0 cm (water-sediment interface) to depth of 4 cm were conducted at intervals of 1 mm using a motorized micromanipulator (Unisense, Aarhus, Denmark). At depths below 4 cm, microelectrode measurements were conducted at intervals of 2 cm by directly inserting the microelectrodes horizontally into small holes in the acrylic tube.

5.2.3. Pore water sampling and chemical analysis

Sediment cores of 10 cm were sectioned at intervals of 1 cm. Each slurry was then separated into water and sediment phases by vacuum filtration with 0.2 μm membrane filter (Advantec, Tokyo, Japan). After pore water was collected, dissolved (<0.2 μm) Fe^{2+} concentrations were measured spectrophotometrically by 1,10-phenanthroline assay (Harvey *et al*., 1955). The remaining pore water was used to determine major ions, alkalinity, and total organic carbon (TOC). Major cations (Na^+, K^+, Mg^{2+}, and Ca^{2+}) and anions (Cl^-, SO_4^{2-}, and NO_3^-) were identified using an ion chromatograph (Dionex ICS-1100, Thermo Fisher Scientific, Osaka, Japan). Dissolved Mn^{2+} was determined using inductively coupled plasma atomic emission spectrometer (ICP-AES SPS3510, SII Nano Technology Inc., Tokyo, Japan). Alkalinity was determined by Gran titration with 0.10 M HCl. TOC was measured using TOC-V_{CSH} (Shimadzu Corporation, Tokyo, Japan).

5.2.4. Iron content analysis

Two approaches of acid extraction were conducted to quantify the iron content in the sediment. Before analysis was performed, sectioned sediment samples were air-dried (sediment up to 2 cm) or dried in a glove box (sediment deeper than 3 cm). The iron dissolved in 6.0 M HCl was analyzed by ICP-AES. Iron minerals commonly present in sediments (e.g. goethite and hematite) were dissolved in 6.0 M HCl; these dissolved iron

minerals corresponded to total iron content. Poorly crystalline iron oxyhydroxides can be dissolved in 0.50 M HCl.

5.2.5. Scanning electron microscope (SEM) and transmission electron microscope (TEM) observations

The microstructure and mineralogy of the sediment were studied by SEM (JEOL JSM-5390) and TEM (JEOL JEM-2010). The chemical composition of the sediment was evaluated by energy-dispersive X-ray spectrometer (EDS, attached to the SEM and TEM). For both observations, samples were dehydrated with a graded series of ethanol (30%, 50%, 70%, 80%, 90%, and 100%) for 10 min each. A drop of mineral suspension was applied to a carbon tape for SEM, and a copper grid for TEM observations. TEM observation was conducted at an accelerating voltage of 15 kV, and SEM observation was conducted at an accelerating voltage of 200 kV.

5.2.6. Iron K-edge X-ray absorption fine structure (XAFS) measurement

Bulk iron K-edge XAFS spectra were obtained using beamline BL01B1 in SPring-8 (Hyogo, Japan) or beamline BL12C in Photon Factory (PF), KEK (Tsukuba, Japan). Measurements were conducted using fully tuned Si (111) double-crystal monochromator with an Rh-coated or Ni-coated Si mirror at an angle of 5.5 or 6.0 mrad in SPring-8 or PF, respectively. Energy was calibrated by setting the pre-edge peak maximum of hematite to 7111 eV. All of the samples, including standard material (ferrihydrite, goethite, and siderite) and sediment samples, were analyzed in a quick XAFS (Q-XAFS) transmission mode, in which XAFS spectra can be obtained from 6790 eV to 7680 eV for 10 min. Sediment samples were mounted on a mixed cellulose ester membrane (Millipore, Billerica, MA, USA) and then sealed. Q-XAFS spectra were analyzed thrice; my results confirmed that no photon oxidation and reduction occurred during the measurements. Collected XAFS data were also analyzed using Athena XAFS analysis software package (Ravel and Newville, 2005).

5.2.7. 16S rRNA gene analysis of the sediment

Each sediment layer was transferred to a sterilized centrifuge tube and stored at -80°C

before analysis. The 16S rRNA gene analysis of representative layers (1cm and 2 cm, 4 cm, and 10 cm) was conducted to identify change in the microbial community with depth. DNA extractions were conducted using the DNA isolation kit PowderMax Soil kit (MoBio Laboratories, Carlsbad, CA, USA), according to the manufacturer's instructions. Partial 16S rRNA genes were amplified using the universal primers of the 530F and 907R primer set as described in a previous study (Nunoura et al., 2012). These primers target all prokaryotic 16S rRNA genes. A fragment of the 16S rRNA gene was amplified using the polymerized chain reaction (PCR) according to Nunoura et al. (2012). PCR products were checked by gel electrophoresis and purified with the MiniElute Gel Extraction Kit (Qiagen, Tokyo, Japan). PCR products were then transformed into competent *Escherichia coli* strain K12. Clones were incubated overnight at 37°C, and then 94 clones were picked randomly for sequencing. Sequencing was performed using the 3730XL DNA sequencer (Applied Biosystems, Carlsbad, CA, USA).

The 16S rRNA gene sequences with more than 97% identity were grouped into an operational taxonomic unit (OTU). Phylogenetic analysis was performed using the ARB software package (Ludwig et al., 2004) using the ARB-SILVA 106 database (www.arb-silva.de). Coverage was calculated according to Good (1953), using the formula $[1-(n/N)]\times100$, where n is the number of the single-clone out, and N is the total number of clones sequenced. Phylogenetic trees for bacteria and archaea were constructed using the maximum-likelihood method of MEGA5 (Tamura et al., 2011).

5.2.8. Carbon and hydrogen stable isotope analysis of CH_4

Approximately 6 g (wet) of sectioned sediment was inserted in a 20 mL serum bottle and crimp-sealed with a butyl stopper. Afterward, 1 mL of saturated mercuric chloride was added to the bottle to stop any microbial activity. The samples were then mixed vigorously. Before analysis was conducted, the samples were placed in a hot water bath (approximately 80 °C) for 15 min to degas CH_4 dissolved in or adsorbed onto sediment particles. CH_4 concentration and stable isotopic compositions were determined using isotope-ratio-monitoring-gas chromatograph/mass spectrometer. Detailed analytical systems and procedures were described in previous studies (Kawagucci *et al*., 2013). Stable isotope compositions are

reported as δ values (‰) defined by the following equation: $\delta = [(R_{sample}/R_{standard}) - 1] \times 1000$, where R_{sample} denotes the $^{13}C/^{12}C$ or D/H ratio relative to the Vienna Pee Dee belemnite carbonate (V-PDB) and Vienna Standard Mean Ocean Water (V-SMOW) standards, respectively.

5.3. Results

5.3.1. Physicochemical properties of sediment

The sampling site was characterized by copious amounts of iron deposits near the groundwater discharge point (Fig. 5−1A). Groundwater flows from a pipe to an open pond, which passes slowly over the sediment surface. The outer frame and the floor of the pond are covered with concrete, such that the pipe is the only source of groundwater into the pond. The groundwater is enriched in Fe^{2+} and HCO_3^- (Table 5−1), and groundwater temperature is approximately 16 °C throughout the year. The iron sediment is distributed approximately 1.5 m from the groundwater source and found at depths of ca. 15 cm to 120 cm.

Color change was evident depending on sediment depth (Fig. 5−1B). The upper 2 cm layer was rusty-orange. At depths below 2 cm, greenish-brown extended to the remaining sediment layers. Furthermore, the sediments were progressively consolidated from fluffy surface sediment (upper 2 cm) to paste-like texture in deeper layers.

The vertical profiles of pH, Eh, and DO from 0 cm to 10 cm were determined using a microelectrode at intervals of 1 mm or 2 cm (Fig. 5−2). DO continuously decreased as sediment layer deepened; DO completely depleted in the sediment layer below 3 cm. Eh on sediment surface showed a positive value (208 mV) and slightly decreased at a depth of 1 cm. A significant decrease in Eh was observed at depth of 2 cm, where Eh decreased from 123 mV to −92 mV at an interval of 1 cm. At depths below 3 cm, the Eh gradually decreased to −320 mV. Likewise, pH of the sediment depths of 0 cm to 1 cm slightly decreased. By contrast, pH of the sediment at depths of 1 cm to 3 cm slightly increased from 6.3 to 7.4 at an interval of 2 cm. At depths below 4 cm, pH remained almost constant ranging from 6.5 to 7.0.

5.3.2. Pore water profiles of major ions in the sediment

The vertical profiles of major ions in the pore water were determined (Figs. 5−3A to 5−3F).

NO_3^- concentration was almost constant or approximately 12 μM in all sediment layers (Fig. 5−3C). SO_4^{2-} concentration increased at depth of 2 cm (38 μM) and then gradually decreased to 8 μM to 19 μM at depths below 2 cm (Fig. 5−3C). Mn^{2+} concentration reached the maximum value at depth of 3 cm and then decreased as sediment layer deepened below 3 cm (Fig. 5−3C). The lowest dissolved Fe^{2+} concentration was found at depth of 1 cm and then increased at depth of 2 cm (Fig. 5−3A). Fe^{2+} profiles reached maximum values at depth of 4 cm and then decreased substantially as sediment layer deepened. Similar to Fe^{2+} concentration, HCO_3^- concentration increased from 1.4 mM (depth of 1 cm) to 2.5 mM (depth of 4 cm) and decreased to approximately 1 mM at depths below 7 cm. Total dissolved organic carbon and NH_4^+ concentrations increased linearly as sediment layer deepened (Figs. 3D, 3F). The vertical profiles of other ions, such as Na^+, Ca^{2+}, and Cl^-, did not show any prominent change (Fig. 5−3E).

5.3.3. Methane concentration and stable carbon and hydrogen isotopic composition of methane

Pore water CH_4 concentrations in the sediment were almost constant, ranging from 257 μM to 398 μM at depths of 1 cm to 6 cm (Fig. 5−3B). The concentration initially increased at depth of 7 cm, and the maximum value (993 μM) was observed at depth of 8 cm. CH_4 concentration slightly varied at depths of 8 cm to 10 cm.

The stable isotope values of CH_4 obtained from each layer ranged from −59.0‰ to −68.8‰ for $\delta^{13}C$ and from −217‰ to −328‰ for δD (Fig. 5−4A). $\delta^{13}C$ and δD changed simultaneously and showed positive correlation. The ^{13}C- and D-depleted values in CH_4 were obtained at depths of 7 cm to 10 cm. These values were found within the range of biogenic CH_4, particularly of CH_4 produced by aceticlastic and methylotrophic methanogens (Fig. 5−4B), as classified by Whiticar (1999).

$\delta^{13}C$ and δD values simultaneously decreased at depths of 3 cm to 7 cm (Fig. 5−4A). The presence or the absence of microbial CH_4 oxidation was approximated by the ratio of hydrogen versus carbon discrimination ($\Delta\delta D/\Delta\delta^{13}C$): factor Λ at depths of 3 cm to 6 cm. The calculated Λ was 7.7 ($r^2 = 0.97$), which was consistent with Λ of microbial CH_4 oxidation that normally ranges from 3.2 to 12.5 (Feisthauer *et al.*, 2011). By contrast, $\delta^{13}C$ and δD values of

sediment at depths of 1 cm to 2 cm increased; this result indicated the inverse relationship between depths of 3 and 6 cm.

5.3.4. Sediment iron mineralogy

In the stratified iron sediment, iron content was homogeneously distributed throughout the sediment (40wt% to 45 wt%; Table 5−2). The surface sediment treated with 0.50 M HCl showed a high extraction rate. Extraction rate decreased as depth further deepened from 2 cm to 5 cm; furthermore, extraction rate reached <13% at depths below 5 cm. Sediment layers at all of the depths contained filamentous sheaths and twisted stalks, suggesting that sediment are likely composed of continuously deposited biogenic iron minerals.

The surface sediment was characterized by the inclusions of filamentous sheaths and twisted stalks (Fig. 5−5A). Stalks were relatively less abundant than sheaths, which is consistent with a previous observation (Kato et al., 2012). SEM observation of deeper sediment also contained sheaths and stalks (Fig. 5−5B to 5−5D), which allows us to confirm that the sediment is composed of continuous deposition of biogenic iron minerals. Stalks and sheaths at the depths were fragmented to a size of 10–20 μm, compared with those of average size (60 μm) at the surface sediment. It should be noted that these size differences were not related to the preparation procedure, since we treated all samples with the same protocol.

The iron phase transformation in the sediment was specified by iron K-edge extended X-ray absorption fine structure (EXAFS) analysis. The main spatial variations of EXAFS were observed in terms of (i) the absence or the presence of a broad shoulder between k = 5.0 $Å^{-1}$ and 6.3 $Å^{-1}$ and (ii) a change in peak position and magnitude of oscillation at k ranging from 6.9 $Å^{-1}$ to 7.9 $Å^{-1}$ (shadow zones in Fig. 5−6A). Changes in EXAFS spectra were observed in sediment depth layers of 1 cm to 4 cm; the spectra varied slightly at depths below 4 cm. These spectrum changes in EXAFS were related to the presence of secondary minerals, as estimated by least-squares fitting of k^3-weighted EXAFS spectra by the linear combination of the spectra of ferrihydrite, goethite, and siderite (Fig. 5−6B). In sediment at sediment layer of 1 cm to 2 cm, the EXAFS spectra were very similar to those of ferrihydrite. At depths below 3 cm, ferrihydrite transformed into siderite and goethite. The proportion of siderite increased from 3 cm to 4 cm (15% to 25%), and remained relatively constant in deeper layers.

The changes in mineral species within the sediment were also consistent with the result of X-ray diffraction (XRD) analysis (Fig. 5−7).

TEM observations revealed morphological characteristics and spatial arrangements of minerals that precipitated around stalks and sheaths in the sediment. At sediment depth of 1 cm, the surface of stalks and sheaths were covered with fine grains of poorly ordered iron oxyhydroxides consisting of spherical aggregates (25 nm to 50 nm in diameter; Fig. 5−8A). At sediment depths below 3 cm, the surfaces of stalks, sheaths, and microorganism-like structures were encrusted with acicular microstructures (30 nm to 50 nm in length and 5 nm in width; Figs. 5−8B to 5−8D and Fig. 5−7). Although most of these minerals showed broad selected area electron diffraction (SAED) patterns, a ring was identified at 2.8 Å (Fig. 5−6E, 5−8F). Considering the result of EXAFS fittings (Fig. 5−8B) and XRD data (Fig. 5−7), we found that the minerals with a ring pattern of 2.8 Å were siderite. Small amounts of acicular minerals showed d-spacing values of 4.1, 2.6, and 2.4 Å. This observation suggests that acicular minerals include small amounts of goethite.

5.3.5. Bacterial 16S rRNA gene phylotype composition in the sediment

The 16S rRNA gene clone analysis in this study was conducted using a universal PCR primer set. We selected three representative sediment surface layer (both 1 and 2 cm), 4 cm, and 10 cm for the analysis. In total, 250 clones (82 to 86 clones in each layer) were obtained with an average read length of 450 bp. The number of OTUs ranged from 45 to 54 in each layer, and the majority of the OTUs contained only a single clone of sequence. As a consequence, sample coverage was relatively low (47% to 60%), indicating that we could only reveal partial phylogenetic diversity of microbial communities in the sediment.

Most of the sequences (93%) retrieved from the samples were bacterial phylotypes. The phylotypes of *Proteobacteria* dominated the clone libraries (50%) at the phylum level. In particular, the phylotypes of *Betaproteobacteria* (16%), *Gammaproteobacteria* (3%), and *Deltaproteobacteria* (30%) were abundant in the sediment, while there was few sequences of *Alphaproteobacteria* (1%) and no sequence of *Epsilonproteobacteria* in all the samples. Other phyla including *Acidobacteria* (2%), *Bacteroidetes* (3%), *Chlorobi* (4%), *Chloroflexi* (10%), *Nitrospirae* (6%), *Plactomycetes* (3%), and *Firmicutes* (2%) were found in the clone

libraries. All the members listed above constituted 80% of the total bacterial clone sequences.

At surface sediment layer (depth of 1 cm and 2 cm), the phylotypes of *Betaproteobacteria* dominated the clone library (48%) and the phylotypes of *Deltaproteobacteria* (14%) and *Gammaproteobacteria* (10%) were also abundant. The clones affiliated with *Plactomycetes*, *Nitrospirales*, and *Acidobacteria* each represented 4% of the clonal abundance. Within *Betaproteobacteria*, 4 phylotypes (representing 27 clones) were of the *Gallionellaceae* family, which consisted 32% of all the clones. One *Gallionellaceae* phylotypes (11 clones; Layer-A-60(11) in Fig. 5−10A) were closely related to the iron-oxidizing bacterium, *Gallionella capsiferriformans* (Emerson et al., 2013). The other *Gallionellaceae* phylotypes (e.g., Layer-A-65(14) in Fig. 8A) were similar to the sequence of *Sideroxydans lithotrophicus*. In addition, the sequences related with iron-reducing bacteria were also detected in this layer. One phylotype (3 clones; Layer-A-22(3) in Fig. 5−10A) was closely related to *Rhodoferax ferrireducens*, which was affiliated to 4% of the clone library. I also obtained one phylotype (1 clone; Layer-A-92 in Fig. 5−10) with 99% sequence similarity to the sequence of *Georgfuchsia toluolica*, which grows with aromatic compounds using nitrate, manganese, and iron oxyhydroxides as electron acceptors (Weelink et al., 2009). Two phylotypes were affiliated with G*eobacteraceae* in *Deltaproteobacteria*. One phylotype (Layer-A-17 in Fig. 5−10) showed 97% similarity to the 16S rRNA gene sequence of known species *Geoalkalibacter ferrihydriticus* (Zavarzina et al., 2006). Other detected phylotypes were related with methano/methylotrophs in *Methylophilaceae* (4% of the total clone number; e.g., Layer-A-77(2)). Although these phylotypes were distantly related to the known *Methylophilaceae*, they comprised a cluster of clones obtained from lakes, iron-rich mats, and clones from Budo pond which had been analyzed by Kato et al. (2012). We also detected the phylotypes of *Methylococcaceae* (9%) in *Gammaproteobacteria* (e.g., Layer-A-27(3)). Some of the phylotypes were closely related with the cultured methanotrophic bacteria such as *Methylocaldum tepidum* LK6 and *Methylococcus capsulatus* (Ward et al., 2004).

At sediment depth of 4 cm, *Deltaproteobacteria* was the most predominant component in the clone library at the phylum level (38%). The *Chloroflexi* phylotypes were also detected with high clonal abundance (16%) in this layer. Other phyla such as *Plactomycetes, Nitrospirae,* and *Chlorobi* comprised 3%, 6%, and 5% of all the clones, respectively (Fig

5−9). One of the dominant phylotypes retrieved within *Deltaproteobacteria* was related with *Syntrophaceae*. This phylotype represented 12% (9 clones; 3 phylotypes) of the clone library. One *Syntrophaceae* showed similarity to the sequence of *Desulfomonile tiedjei* (1 clone; 96% similarity). The rest of the *Syntrophaceae* phylotypes were related to uncultured lake sediment clones and subsurface sediment clones (e.g., Layer-C-44(7) in Fig. 5−10). Phylotypes related with *Geobacteracea* were also detected in this layer (e.g., Layer-C-17(2) in 5−10). The phylotypes shared 97% similarity with the 16S RNA gene sequences of *Geobacter*

ferrihydriticus and *Geobacter chapellei*. The other *Deltaproteobacteria* phylotypes were affiliated with an unclassified family (Sva0485 in the ARB software). Within *Chloroflexi*, most of the retrieved clones were related with *Anaerolineales*, *Caldilineae*, and *Dehalococcoidetes*. These phylotypes were phylogenetically affiliated with uncultured environmental clones obtained from sludge, freshwater lakes, and iron-rich aggregates.

At 10 cm deep, *Deltaproteobacteria* phylotypes represented 35% of the total sequence, while *Alphaproteobacteria* and *Betaproteobacteria* phylotypes were less than 6%. *Chloroflexi* phylotypes accounted for 7% of the clonal abundance. Sequences related to *Actinobacteria* (4%), *Nitrospirae* (7%), *Plactomycetes* (3%), and *Actinobacteria* (4%) were also detected in this layer. Most of the phylotypes detected in this layer were similar to those observed in layer C, and were distantly related to the sequences of isolated species. One of the predominant phylotypes observed in this layer was unclassified Sva0485 in *Deltaproteobacteria*.

5.3.6. Archaeal community structure in the sediment

A total of 17 archaeal clones were obtained from total layers which comprised 7% of the total clone sequence. Most of the clones were affiliated with *Euryarcheota*, with the exception of one phylotype (one clone) which was affiliated with *Crenarchaeota*. Among all the archaeal clones, 14 clones (2 phylotypes) were obtained from 10 cm deep. One phylotype (10 clones; Layer-I-37(10) in Fig. 5−10B) at 10 cm deep was related to GOM Arc I group in the order *Methanosarcinales*. This phylotype represented 12% of the total microbial community in this layer. Another phylotype (4 clones) was affiliated with the Deep-sea

Hydrothermal Vent group (DHEV8). This phylotype has been detected in a previous study that affiliated 35% of the archaeal clones in the surface sediment (Kato et al., 2012).

5.4. Discussion

5.4.1. Iron oxidation by iron-oxidizing bacteria at the top of the sediment

In this site, iron mineral is present where Fe^{2+}-rich groundwater flows into the oxic water pool. Fe^{2+} consumption was remarkable on sediment surface; as a result, ferrihydrite precipitation occurred. A slight decrease in pH on the surface layer of 1 cm (Fig. 5−2) is consistent with proton production as Fe^{2+} was oxidized; this reaction is generally expressed as follows (Emerson et al., 2010).

$$Fe^{2+} + 0.25O_2 + 2.5H_2O \rightarrow Fe(OH)_3 + 2H^+ \quad (1)$$

Fine ferrihydrite particles precipitated in the vicinity of stalk- and sheath-like structures, which are the distinctive morphological characteristic of biogenic iron minerals observed under neutral pH conditions (Chan et al., 2009; Suzuki et al., 2011). The 16S rRNA gene clone analysis of microbial community in the upper layer revealed the abundant existence of known iron-oxidizing bacterial populations of *Gallionellaceae*. These results suggest that the presence of ferrihydrite in the surface layer is coupled with iron-oxidizing bacterial activity, as observed in previous studies (Takahashi et al., 2007; Kato et al., 2012). Microbial Fe^{2+} oxidation outcompetes abiotic oxidation in suboxic environment (Druschel et al., 2008). Furthermore, iron-oxidizing bacteria grow in oxygenated groundwater trickling filters (de Vet et al., 2011), suggesting that iron-oxidizing bacteria are more widely distributed than previously thought. In this study, dissolved oxygen in the upper sediment layer was aerated (DO: 266 μM); this result may support active biogenic iron oxidation under oxic conditions.

The predominance of iron-oxidizing bacterial phylotypes related to *G. capsiferriformans* and *S. paludicola* in the microbial phylotype composition at 1 cm depth may explain the observation that much less abundant stalk-like structures were found in the surface sediment than sheath-like structures (Fig. 5−5). Neither *G. capsiferriformans* nor *S. paludicola* produces stalks and sheaths during their growth (Weiss et al., 2007; Emerson et al., 2013). It is also important to note that the 16S rRNA gene clone analysis did not detect any phylotypes

affiliated with *Leptothrix* spp., in spite of the abundance of many sheath-like structures in the surface sediment. Previous studies demonstrated the concurrence between the lack of *Leptothrix* phylotypes in the 16S rRNA gene clone analysis and the absence of cells in the sheaths in biogenic iron mineral sediments (Bruun et al., 2010; Gault et al., 2011). Previous studies also indicated potential niche separation between the iron-oxidizing bacterial populations of *Gallionella* and *Leptothrix* spp. (Gault et al., 2012; Fleming et al., 2013). For example, *Gallionella* spp. successfully dominated the microbial community under low organic carbon conditions in winter, rather than under high concentrations of complex organic carbon in summer (Fleming et al., 2013). Since the previous 16S rRNA gene clone analysis of the surface sediment at Budo pond was conducted in autumn and detected considerable abundance of phylotypes related to *Leptothrix* sp. (Kato et al., 2012), the abundant occurrence of sheaths in the surface sediment observed in this study, which is sampled in winter, may be derived from the residual products of possible iron-oxidizing *Leptothrix* spp. that would dominate the microbial community during the seasonal succession of predominant iron-oxidizing populations or from the ongoing production of other sheath-forming iron-oxidizing populations in winter season.

5.4.2. Biological reduction of iron after the precipitation of biogenic iron mineral

A significant increase in pore water Fe^{2+} concentration at depths between 2 and 4 cm suggests that iron reduction occurs in the subsurface zone (Fig. 5−3A). Vertical profiles of pore water Fe^{2+} and HCO_3^- concentrations showed good correlation probably because ferrihydrite dissolution is coupled with organic carbon degradation. Biogenic ferrihydrite, which is more readily reduced than synthetic ferrihydrite, functions as an effective electron acceptor for dissimilatory iron-reducing bacteria (Blöthe and Roden, 2009; Langley et al., 2009; Emerson et al., 2009). Indeed, some iron-reducing bacterial phylotypes related to *Geobacteraceae*, *Comamonadaceae*, and *Rhodocyclaceae* were detected in sediment depths of 1 and 2 cm (upper layer) and depth of 4 cm. In the upper layer, the predominant *Gallionellaceae* phylotypes and *Geobacteraceae*, *Comamonadaceae*, and *Rhodocyclaceae* phylotypes were found in the clone library. However, the detailed distribution pattern of *Gallionellaceae* and iron-reducing bacterial phylotypes cannot be discussed because we

simultaneously treated two separated sediment depths (1 and 2 cm) for the 16S rRNA gene analysis. A possible niche separation of iron oxidizers and iron reducers may be found within the upper 2 cm layer, as indicated by Fe^{2+} concentration change in depth ranging from 1 cm to 2 cm (Fig. 5−3A). Fe^{2+} dissolution by potential bacterial iron reduction did not affect bulk iron mineralogy because ferrihydrite represented the dominant iron species in this layer (Fig. 5−6B). Thus, Fe^{2+} produced by iron-reducing bacteria can be possibly re-oxidized by co-existing *Gallionellaceae* populations and/or by chemical oxidation. The co-occurrence of iron-oxidizing and iron-reducing bacteria is commonly observed in natural samples; this observation suggests that actively driven biogenic iron cycle occurs between soluble and insoluble phases in oxic to suboxic regions of habitats (Emerson et al., 2009; Gault *e*t al., 2011; Sobolev and Roden, 2002; Bruun et al., 2010; Blöthe and Roden, 2009; Roden et al., 2004, 2012).

Only *Geobacteraceae* was observed as the known dissimilatory iron-reducing bacterial genus at sediment depth of 4 cm. This genus represents one of the most common genera of dissimilatory iron-reducing bacteria found in natural environments (Roden et al., 2012) or in laboratory incubation experiments (Snoeyenbos-West et al., 2000; Lentini et al., 2012). Organic carbon (e.g., acetate) oxidation with iron reduction can be expressed in the following reaction:

$$CH_3COO^- + 8Fe(OH)_3 \rightarrow 8Fe^{2+} + 2HCO_3^- + 15OH^- + 5H_2O \quad (2)$$

In this reaction, pH and HCO_3^- concentration increase as ferrihydrite is reduced; this result is consistent with the pore water chemistry profile obtained in this study (Figs. 5−2 and 5−3A). Thus, the presence of *Geobacter* species at depth of 4 cm suggests that biogenic iron mineral dissolution and organic carbon decomposition may be promoted by activities of organo-heterotrophic dissimilatory iron-reducing bacteria. However, the dominant microbial phylotypes at depth of 4 cm were *Syntrophaceae* species, not iron-reducing *Geobacteraceae* species. *Syntrophaceae* species are fermentative organo-heterotrophs that grow syntrophically with hydrogen-utilizing counterparts in various anoxic environments (Kuever et al., 2005).

Fermentative organo-heterotrophs may play an important role in iron and carbon biogeochemistry in the Budo pond sediment. Futhermore, fermentative prokaryotes, such as

Chloroflexi and methanogenic archaea (Benz et al., 1998; Bond and Lovley, 2002; Kawaichi et al., 2013), can reduce iron. The iron reduction activity of microbial community is significantly affected by the amount and the type of organic compounds (e.g., organic acid and sugars) and iron minerals (Lentini et al., 2012). Another possible interpretation is that potentially dominating *Syntrophaceae* may yield additional fermentative products (e.g., lactate, acetate, and H_2) as electron donors for co-existing syntrophic counterparts, such as *Geobacter* iron reducers. Although we could not clarify whether *Syntrophaceae* phylotypes dominating at depth of 4 cm were directly involved in iron reduction, my results suggest that fermentative organo-heterotrophs are implicated in iron and carbon cycles in subsurface sediment layer.

5.4.3. Secondary iron mineralization

Fe^{2+} produced by iron-reducing bacteria was presumably precipitated as secondary iron minerals at depths below 3 cm. Mineral formation followed by microbial iron reduction has been extensively investigated particularly under laboratory conditions; under these condition, various secondary iron minerals precipitate in different water chemistry, initial iron mineral species, and Fe^{2+} concentrations (Fredrickson et al., 1998; Zachara et al., 2002; Hansel et al., 2003; Lentini et al., 2012). In this study, siderite and goethite were detected as the dominant secondary minerals. The mineralization of goethite from ferrihydrite is caused by dissolution/reprecipitation (Cornell and Schwertmann, 1996; Hansel et al., 2003) or aggregation-based crystal growth (Banfield *et al*., 2000). The presence of goethite in the subsurface sediment was associated with the increase in pore water Fe^{2+} concentration (Fig. 3A); this result indicated that goethite is mainly formed by dissolution/reprecipitation processes.

EXAFS fitting and TEM results suggest that siderite, along with goethite, precipitated on the surfaces of sheaths, stalks, and microorganisms (Figs. 5−8B to 5−8D) in suboxic environment. These results suggest that Eh and Fe^{2+} production in very local areas adjacent to the sheaths, stalks, and microbial cells decrease; as a result, siderite can precipitate in the vicinity of these biogenic materials. In addition, the encrustation of ferrihydrite by goethite and siderite may prevent access of iron-reducing bacteria to ferrihydrite as their electron

acceptor. Pore water Fe^{2+} concentration significantly decreased from depths below 4 cm, even though abundant ferrihydrite was still present in the sediment (Fig. 5−6B). Extractable iron at 0.50 M HCl also decreased lineally as sediment depth reached below this layer; this result is consistent with siderite and goethite precipitation. HCl (0.50 M) dissolves ferrihydrite and siderite but does not dissolve goethite (Heron and Christensen, 1994). Although the number of SAED patterns of goethite in encrusting acicular minerals was less than that of siderite, 0.50 M HCl extraction results may indicate common encrustation of goethite around ferrihydrite, in addition to siderite. Thus, the distribution of secondary minerals can be considered as an important factor to control iron bioavailability for potential iron-reducing bacteria in natural microbial communities.

In addition, the morphology of siderite precipitation is interesting. Although rhombohedral siderite formation has been reported during the dissimilatory iron reduction (Fredrickson et al., 1998; Zachara et al., 2002), there were acicular siderite as well as less abundant rhombohedral siderite (Fig. 5−7B). Similar structures of siderite have been observed in peat soils (McMillan and Schwertmann, 1998) and sand flat sediments (Pye et al., 1990), suggesting that acicular siderite would be one of the ubiquitous structures of siderite widespread in natural environments. However, the acicular siderite does not necessarily indicate the function of microbial iron reduction since abiotic siderite synthesis provides a similar morphology (Wiesli et al., 2004). Rather, the precipitation rate and stage of the mineral are likely associated with the morphological characteristics of siderite. Initial rapid precipitation of siderite tends to form small euhedral spherules, which then grow into the well-known rhombohedral forms (Weisli et al., 2004). In sediment, acicular siderite was preserved at depths below 3 cm, which points to the possible mechanisms to prevent further mineral growth, such as trace element substitution and/or adsorption/co-precipitation of organic materials.

5.4.4. Organic carbon oxidation by methane production

In sediment layer deeper than the plateau zone of iron reduction (Fe^{2+} < 0.48 mM; at depths below 7 cm), microbial CH_4 by aceticlastic and methylotrophic methanogens was increased. In freshwater environments, aceticlastic methanogens are predominant compared

with methylotrophic populations; by contrast, these methanogens are outcompeted by dissimilatory iron reducers for the same substrate (Roden and Wetzel, 2003). Thus, the function of aceticlastic methanogens usually dominates in anoxic habitats at layers below the iron reduction zone (Lovley and Phillips, 1986; Roden and Wetzel, 1996, 2003; Teh et al., 2008). Even in sediment layers below the iron reduction zone, the dissolved organic carbon content was increased, and acetate concentration might be sufficient for the methanogenic activity. In addition, aceticlastic methanogens were vertically distributed, as indicated by 16S rRNA gene clone analysis. The 16S rRNA gene phylotype composition at depth of 10 cm contained the phylotypes of GOM Arc I group in *Methanosarcinales*. Although *Methanosarcinales* species utilize various organic carbon molecules, most of these species produce CH_4 from acetate (Liu and Whitman, 2008), as expressed in the following reaction;

$$CH_3COO^- + H_2O \rightarrow CH_4 + HCO_3^- \quad (3)$$

The molar ratios of CH_4 and HCO^- at depths of 8 cm to 10 cm were almost equal (Fig. 5−3A, 3B). These results indicate that the aceticlastic methanogenesis is one of the predominant microbial activities in deeper sediment zones.

5.4.6. Possibility of methane oxidation in the sediment

The vertical profiles of CH_4 concentrations and stable isotope compositions may show another important aspect of carbon cycle in the sediment. $\delta^{13}C$ data are plotted against the reciprocal CH_4 concentration (Fig. 5−4C). If the change in isotopic value of CH_4 in the stratified sediment is derived from a simple mixture of two isotopic end-members, data are plotted on a straight line. The data at depths between 3 and 10 cm were plotted on a straight line ($R^2 = 0.91$); the data at depth of 2 cm was substantially deviated from the mixing line. Hence, the CH_4 profile at depth above 7 cm can be classified into two zones (Fig. 5−4A): (i) CH_4 exhibits lower ^{13}C and D values as depth reaches below the subsurface zone (depth from 3 cm to 7 cm) and (ii) CH_4 is enriched in ^{13}C and D as depth reaches the surface zone (depths of 1 and 2 cm). In the subsurface zone, the ratio Λ indicated methanotrophic activity. The linear correlation between $\delta^{13}C$ and reciprocal CH_4 concentration indicates a simple diffusive mixing of two isotopic values instead of potential methane oxidation.

Several inorganic ions and minerals serve as electron acceptors in microbial anaerobic CH_4 oxidation. Sulfate predominantly contributes to anaerobic oxidation of CH_4 (AOM) in marine environments (Knittel and Boetius, 2009). Nitrate, nitrite, iron oxyhydroxides, and manganese oxides have been proposed as mediators of AOM (Ettwig et al., 2008; Beal et al., 2009). In the study site, SO_4^{2-} and NO_3^- seemed insufficient between depths of 3 cm to 7 cm (SO_4^{2-} < 30 μM; NO_3^- < 12 μM); SO_4^{2-} and NO_3^- profiles did not significantly change. In addition, ferrihydrite became less bioavailable in the subsurface zone. On the basis of these results, the variation of CH_4 concentrations and isotopic compositions in sediment depths between 3 and 10 cm is attributed to the diffusive mixing between the two isotopic end-members of CH_4; one end-member is derived at depth of 10 cm and the other end-member is obtained at depth of 3 cm.

Isotopically lighter CH_4 was found at depth of 1 cm in the oxic surface zone than in subsurface layers. This result indicates that isotopically lighter CH_4 is supplied from the groundwater. In addition to the microbially produced CH_4 derived from deeper zones, another source of CH_4 is presumably found in groundwater. As such, the variation of CH_4 concentrations and isotopic compositions up to 2 cm may be caused by the bacterial oxidation of CH_4 from groundwater. This result is further supported by the microbial 16S rRNA gene phylotype composition in layer A, where a phylotype related to an aerobic CH_4-oxidizing bacterium was detected (Fig. 5−10A). The abundant supply of CH_4 from both groundwater and deeper sediment zone can create a habitat suitable for aerobic CH_4 oxidizers in the iron-rich sediment in Budo pond.

5.5. Conclusion

In this study, changes in iron mineral species and development of potential microbial community in biogenic iron-rich sediment were observed at a depth interval of 10 cm. The combination of 16S rRNA gene clone analysis, XAFS measurement, stable isotope analysis of CH_4, and TEM observations provides important insights into biogeochemical processes of iron and carbon in circumneutral freshwater sedimentary environment.

In the study site, ferrihydrite was precipitated by iron-oxidizing bacteria and CH_4 was oxidized by methanotrophic bacteria in the surface sediment; these processes were supported

by continuous Fe^{2+} and CH_4 supply from the groundwater (I in Fig. 5−11). Ferrihydrite produced by the microorganisms is extractable by 0.50 M HCl, which could function as an electron acceptor for co-existing iron-reducing bacteria. Ferrous iron produced by dissimilatory iron-reducing bacteria is re-oxidized to precipitate ferrihydrite in the surface sediment layer (depth < 2 cm). By contrast, Fe^{2+} produced in subsurface layers is converted into goethite and siderite (II in Fig. 5−11). Siderite selectively precipitates in the vicinity of stalks and sheath; this result suggests that dissimilatory iron reduction occurs in this vicinity. Thus, organic carbon is oxidized in subsurface sediment as dissimilatory iron is reduced. However, iron reduction is restricted to sediment at depths above 5 cm; a large fraction of ferrihydrite remains in the reduced sediment at depths below 6 cm. The bioavailability of biogenic iron mineral is decreased in deeper sediment layers possibly because siderite and goethite around ferrihydrite are encrusted.

Microbial iron reduction is inhibited at depths below 6 cm, resulting in the dominance of microbial aceticlastic CH_4 production (III in Fig. 5−11). Microbially produced CH_4 in deeper sediment layer is then recycled into shallower sediment zone without being consumed during AOM. Thus, iron-reducing bacteria as organic carbon-metabolizing microorganisms are replaced by methanogenic archaea at depth of 10 cm; this shift is controlled by soluble and insoluble phase transformation of iron and carbon substrates in the biogenic iron minerals.

5.6. Implications

Biogenic iron minerals are commonly present in natural environments. They show high reactivity to various trace elements, and the preservation/dissolution associated with microbial functions directly affects the behavior of trace elements in natural environments. My study reveals that the microbial reduction of ferrihydrite may be inhibited in the subsurface area, whereas organic carbon decomposition proceeds to the deeper part of the sediment. This provides further insights into the cycle of trace elements in the biogenic iron sediment.

It may be also possible to extend insights into the microbial ecosystems and the iron phase transformations in ancient environments such as BIFs. While many studies have been conducted, there is not enough information on the formation mechanism of BIFs, possibly

because of the limitations of their modern analogs. Although my study was conducted for the freshwater iron-rich sediment, and may not directly address the processes in the euxinic ancient ocean, we can still extract processes that lead to the formation of iron deposits associated with a variety of microbial metabolisms and functions. Iron oxides (mainly hematite) and siderite are major constituents of BIFs (Klein, 2005). Acicular-like siderite surrounding microorganism-like structures are observed in BIFs (Heaney et al., 1991), which are similar to the structures observed in this study. There are also encrustations of siderite around goethite/hematite in Cretaceous iron formations (Taylor and Konhauser, 2011). These distinctive precipitation morphologies may indicate direct involvement of microbial metabolisms and functions in the mineral formation as indicated by my study. The siderite precipitation mechanisms is of great importance because it may be significantly linked to the iron and carbon biogeochemistry, microbial metabolisms, and components at the time and place of formation (Heimann et al., 2010). Hence, my finding of microbial siderite formation could be an excellent modern analog.

Figures and Tables

Table 5–1. pH and major elements in the groundwater source.

pH	Na^+ (μM)	K^+ (μM)	Ca^{2+} (μM)	Mg^{2+} (μM)	Fe^{2+} (μM)	SO_4^{2-} (μM)	Cl^- (μM)	NO_3^- (μM)	HCO_3^{-*} (mM)	CH_4 (μM)
6.82	482±3	59.3±0.3	228±1	89.6±0.1	292±8	15.3±0.7	229±7	0.895±0.029	1.91±0.07	159±7

*Measured by Gran titration

Table 5−2. Percentage of total iron and 0.50 M HCl-extractable iron in each sediment

Depth (cm)	Total Fe*‡ (%)	0.5 M HCl extractable Fe‡ (%)
1	42	34
2	42	27
3	42	16
4	44	17
5	45	6
6	44	12
7	42	13
8	40	7
9	41	8
10	42	12

*6.0 M HCl extractable Fe
‡Accuracy is ± 3%

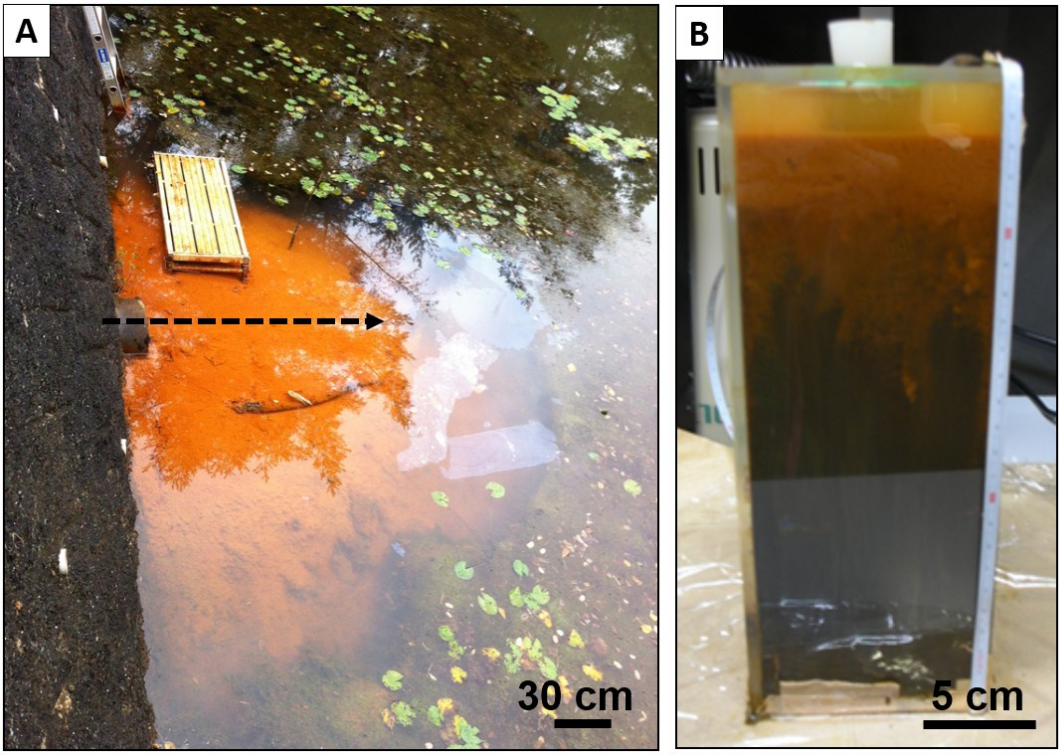

Fig. 5−1. Photographs of (A) biogenic iron-rich sediment at Budo pond, Hiroshima University and (B) sediment collected from the sampling point. The black arrow in (A) shows direction of the groundwater flow. Clear change of color is evident within a series of the collected sediment for (B).

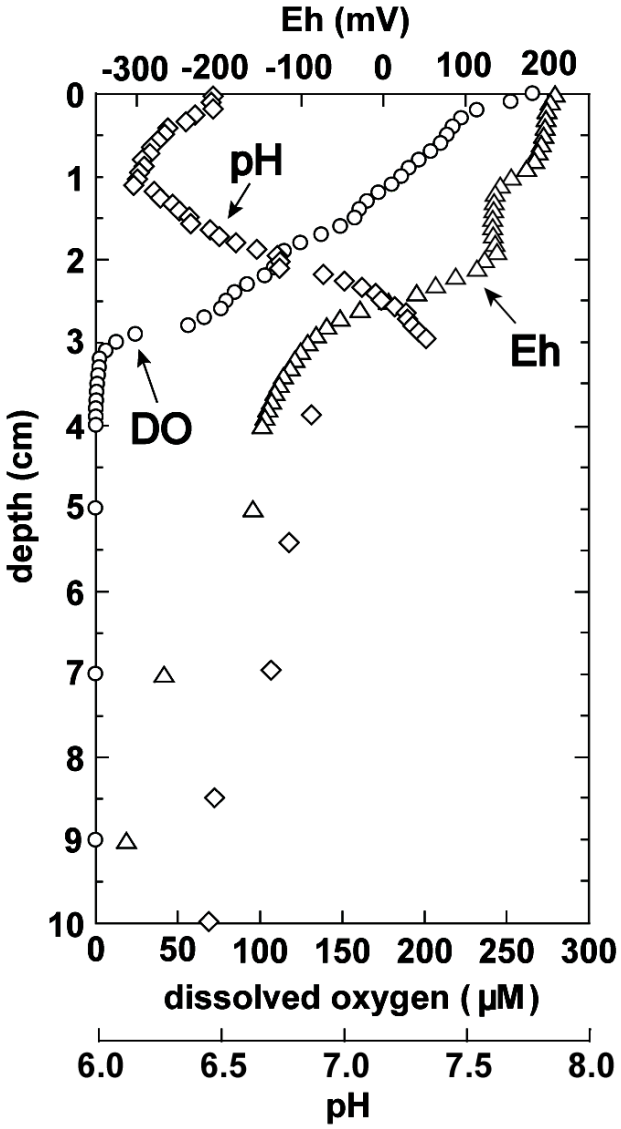

Fig. 5−2. Microelectrode profiles of pH, dissolved oxygen (DO), and redox potential (Eh).

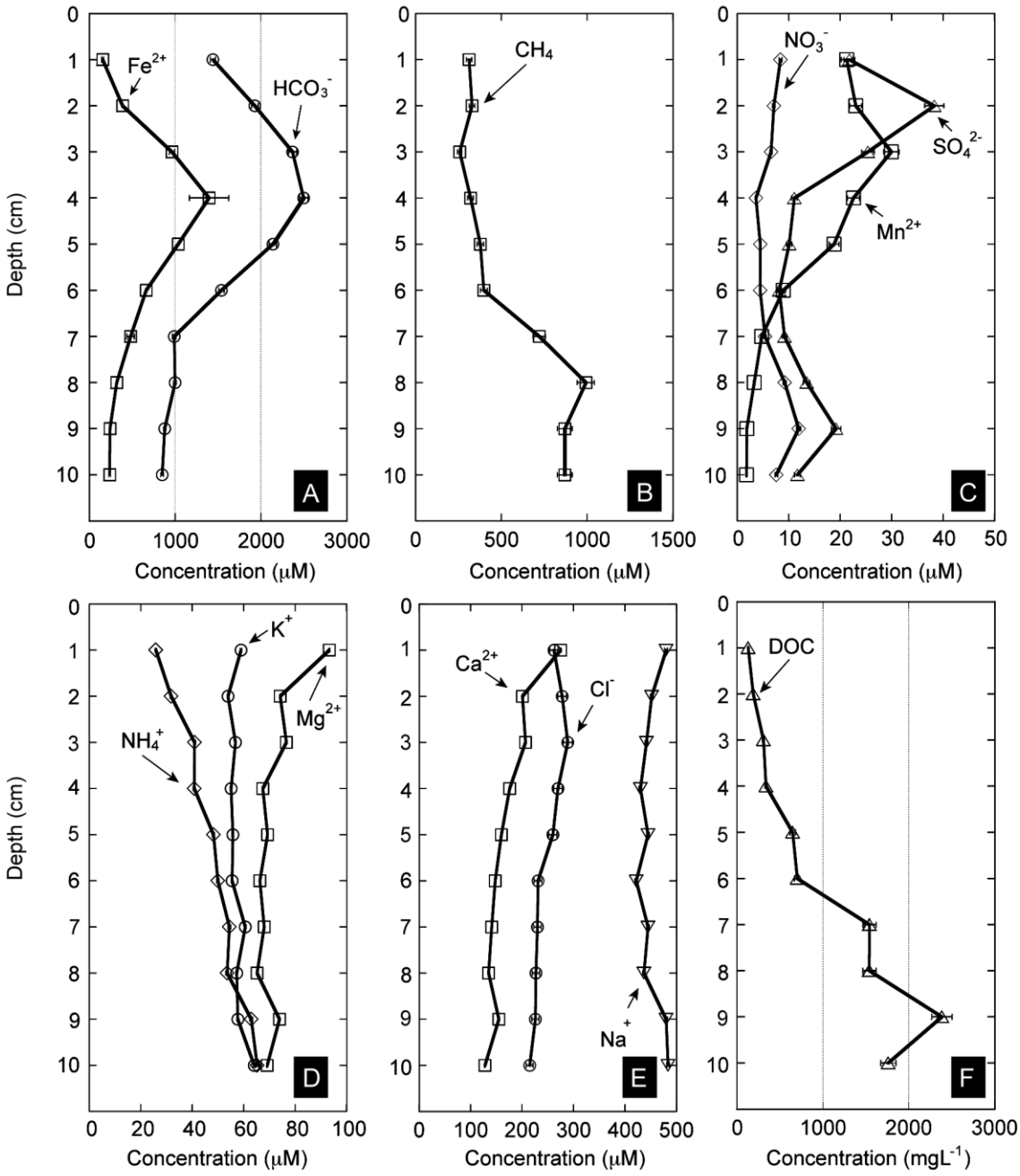

Fig. 5−3. Depth variations of major ions and gas in the sediment

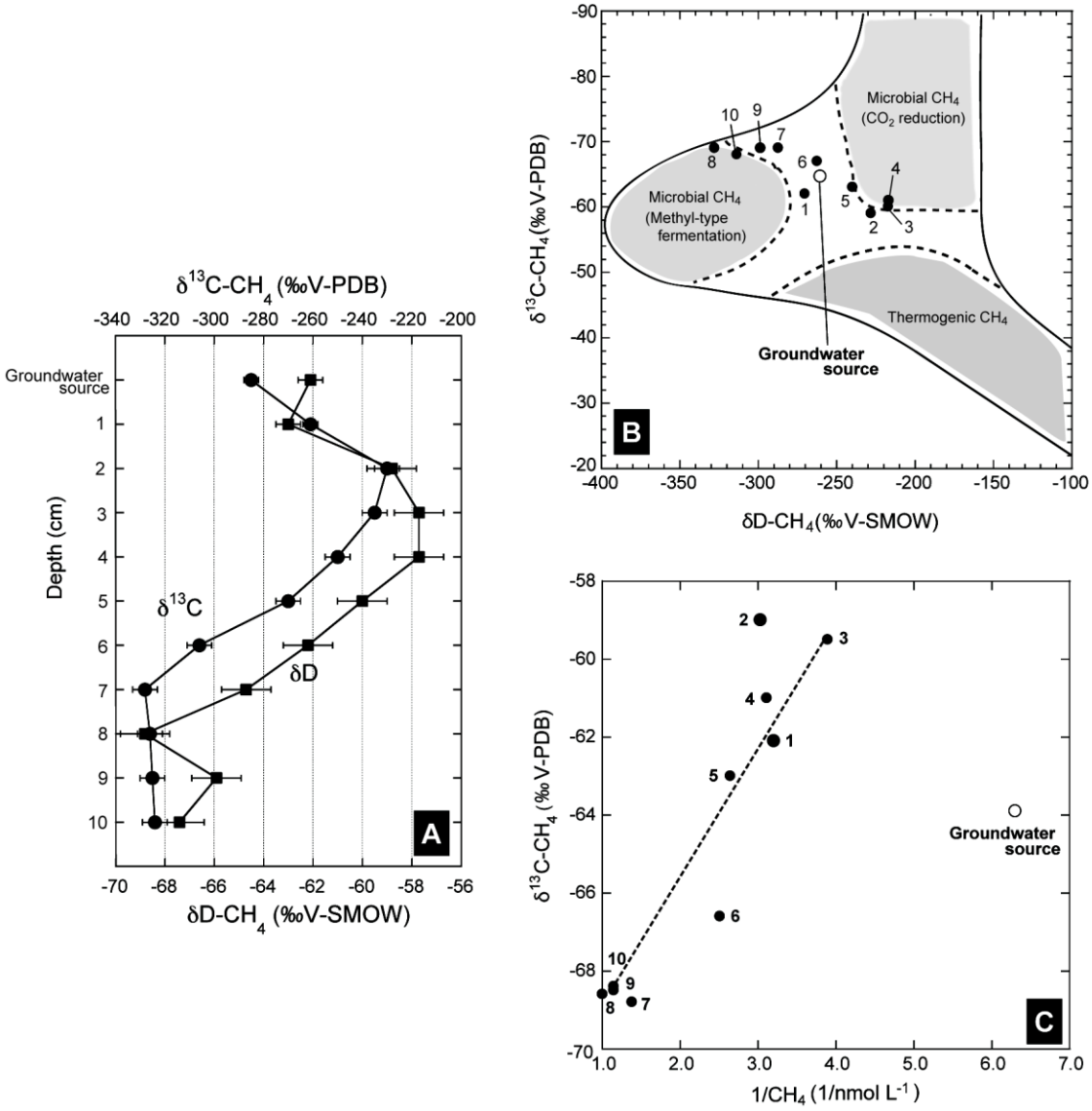

Fig. 5−4. (A) Depth profiles of carbon stable isotopic composition (δ^{13}C) and hydrogen stable isotopic composition (δD) of CH_4. (B) Relationships between δ^{13}C and δD of the sediment samples, based on the classification of Whiticar (1999). The stable isotopic values of δ^{13}C and δD at sediment depths of 8 cm to 10 cm are plotted within the range of CH_4 produce by aceticlastic and methylotrophic methanogens. (C) The composition of δ^{13}C versus reciprocal of CH_4 concentration in each layer. The dotted line indicates mixing trend of depths 3 and 10 cm.

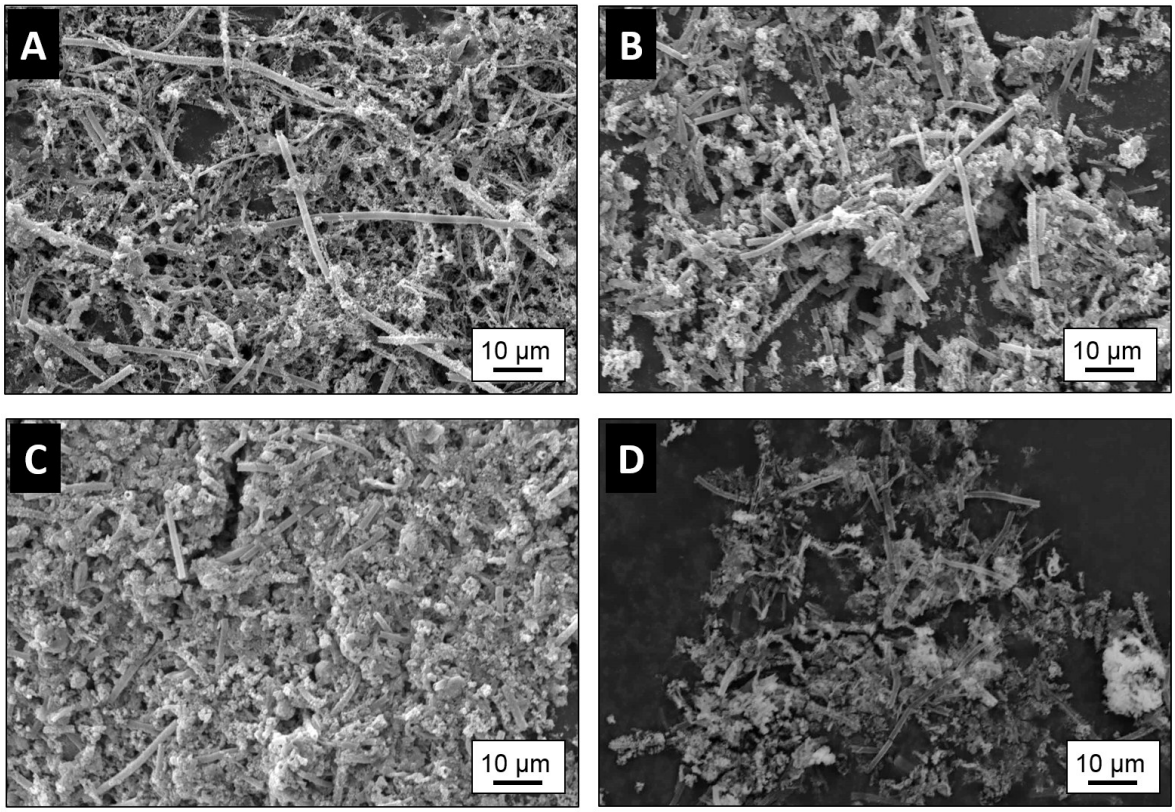

Fig. 5−5. Scanning electron microscopy (SEM) images of the iron deposit at 1 cm (A), 3 cm (B), 6 cm (C), and 8 cm (D). All sediment contains stalks and sheaths which is indicative of biogenic iron minerals.

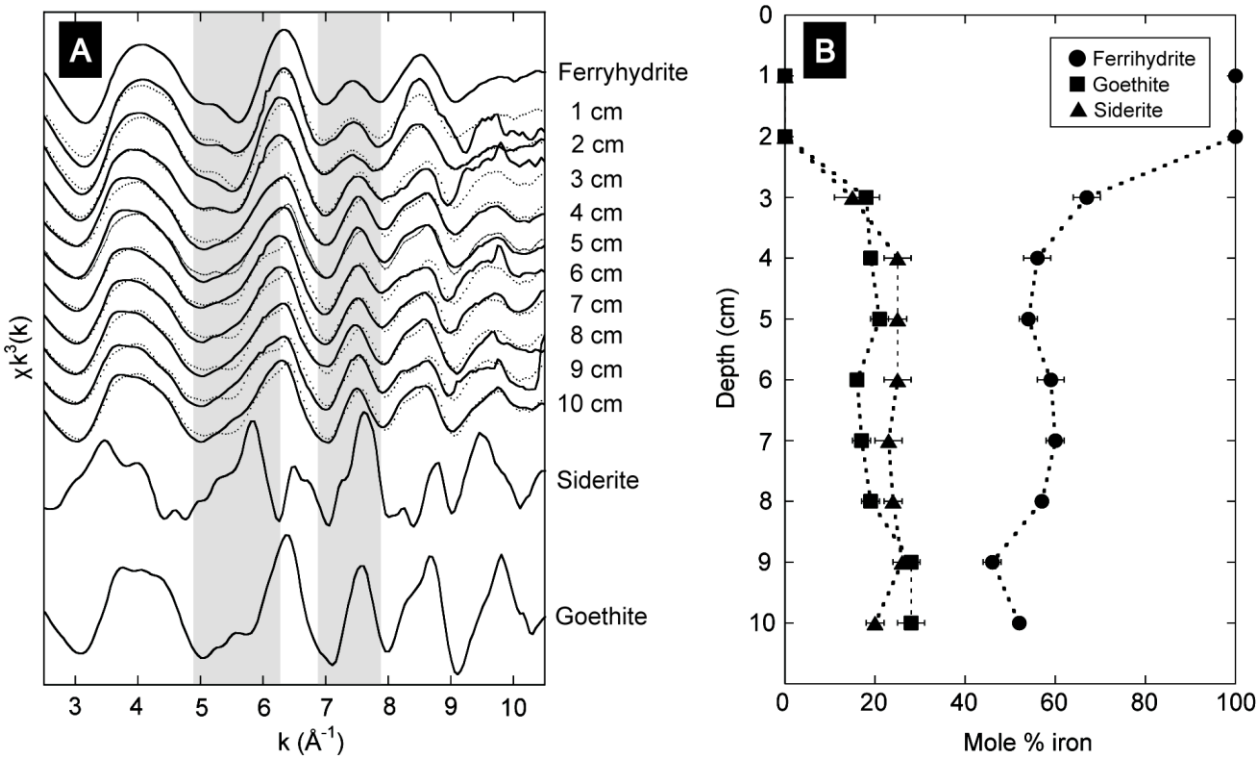

Fig. 5−6. (A) k^3-weighted EXAFS spectra of the sediment samples and reference minerals. The solid line denotes the raw EXAFS spectra and dotted line denotes the linear-combination fitting. The shaded areas highlight the spectral features so that the variations in each layer can be seen, especially for layers from depths of 1 cm to 4 cm. (B) Percentages of minerals in each layer obtained from linear-combination fitting using ferrihydrite, goethite, and siderite as reference minerals.

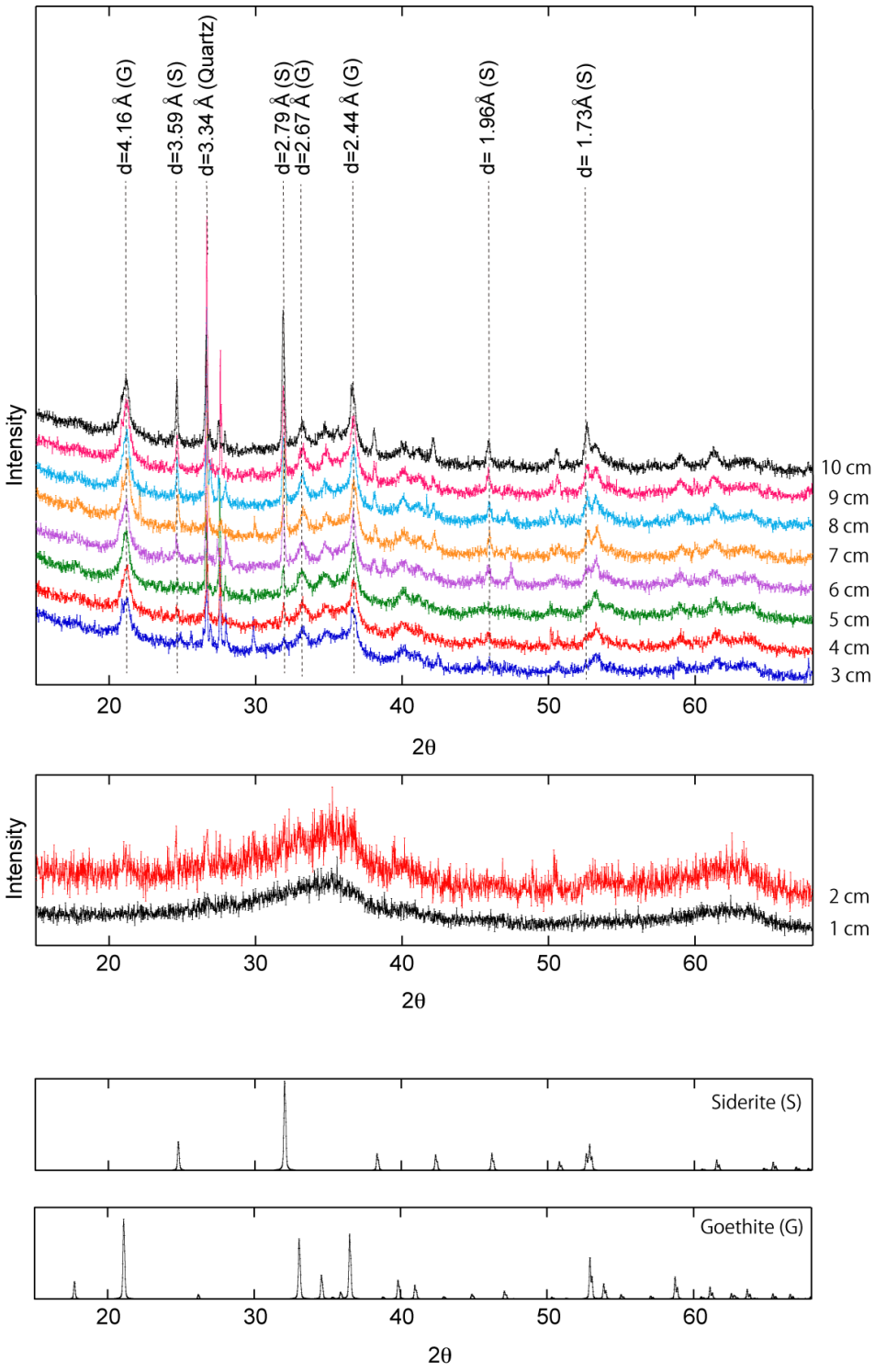

Fig. 5−7. X-ray diffraction patterns of biogenic iron-rich sediment. Reference patterns of siderite and goethite are shown for comparison. Surface sediment (depths of 1 and 2 cm) show two broad peaks, indicative of 2-line ferrihydrite. On the contrary, sediment layers deeper than 3 cm show several sharp peaks which are consistent with siderite and goethite.

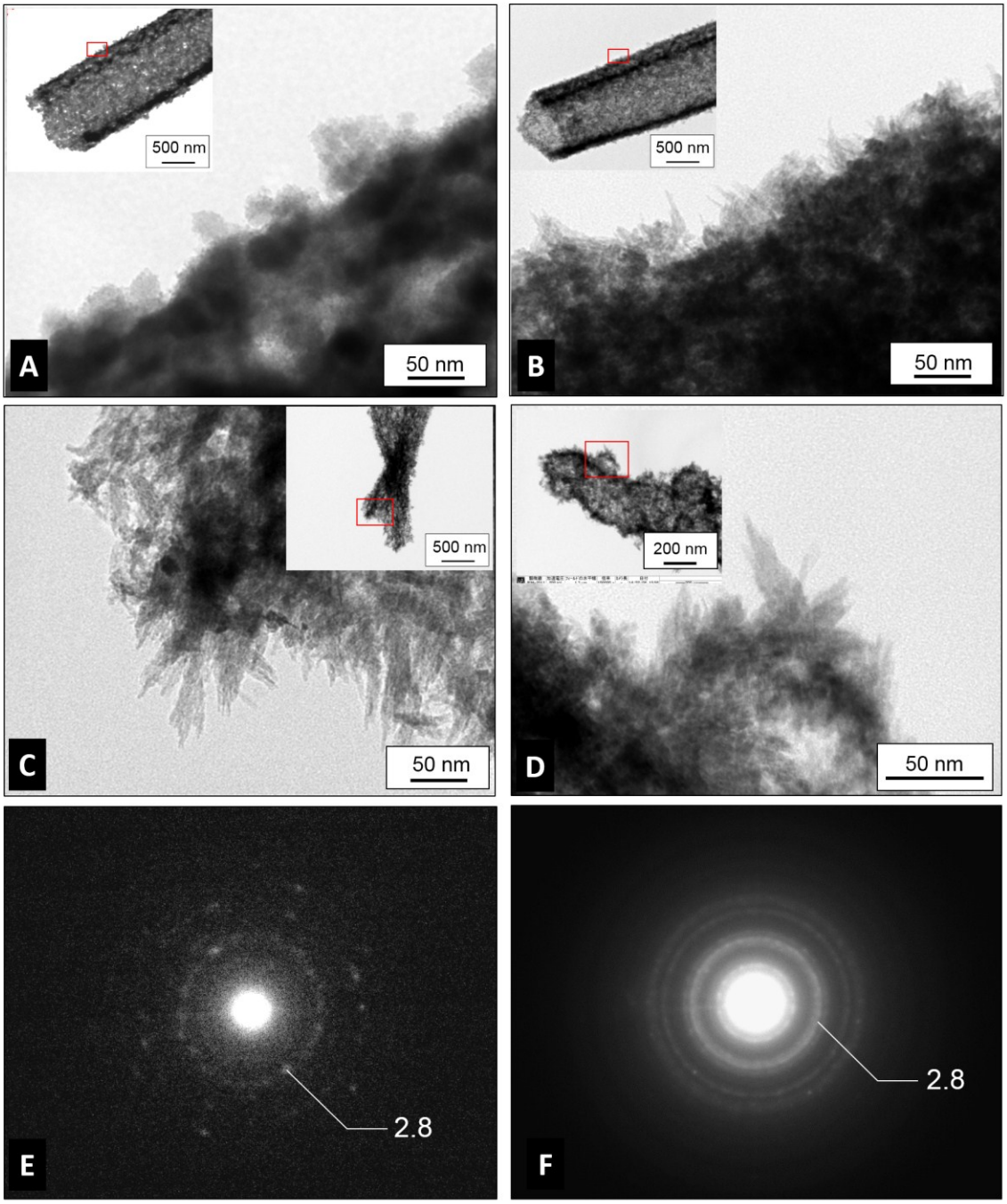

Fig. 5−8. Transmission electron microscope (TEM) images of sheath and stalks in biogenic iron-rich sediment at depth of 1 cm (A), depth of 3 cm (B, C), depth of 7 cm (E) and selected area electron diffraction (SAED) pattern of acicular minerals at depth of 3 cm (E) and depth of 7 cm (F). Poorly-ordered iron oxyhydroxides covers the surfaces of the biogenic organic materials (sheaths) at depth of 1 cm (A), whereas acicular siderite covers the surface of the organic materials (B, C, and D). The SAED ring patterns in E and F are indicative of siderite with 2.8 spacing.

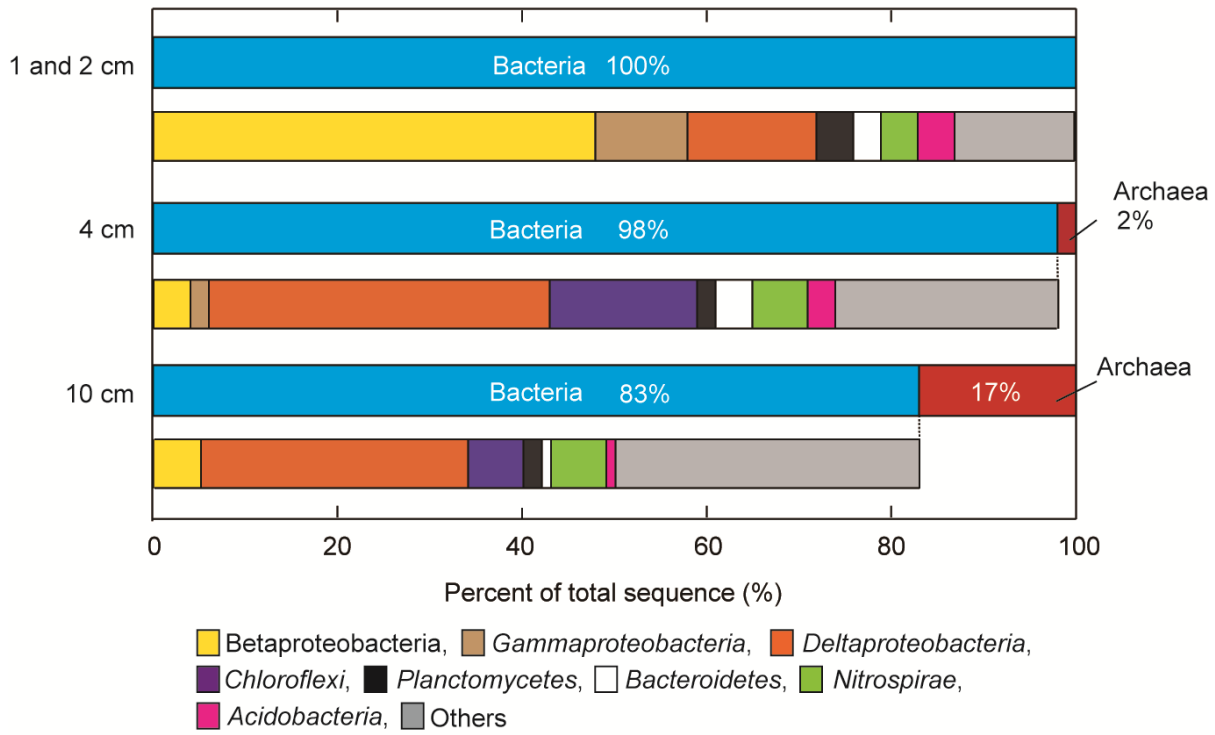

Fig. 5−9. Proportions of bacterial and archaeal numbers and distribution of bacterial phylotypes at sediment depths of 1 and 2 cm (surface layer), 4 cm, and 10 cm.

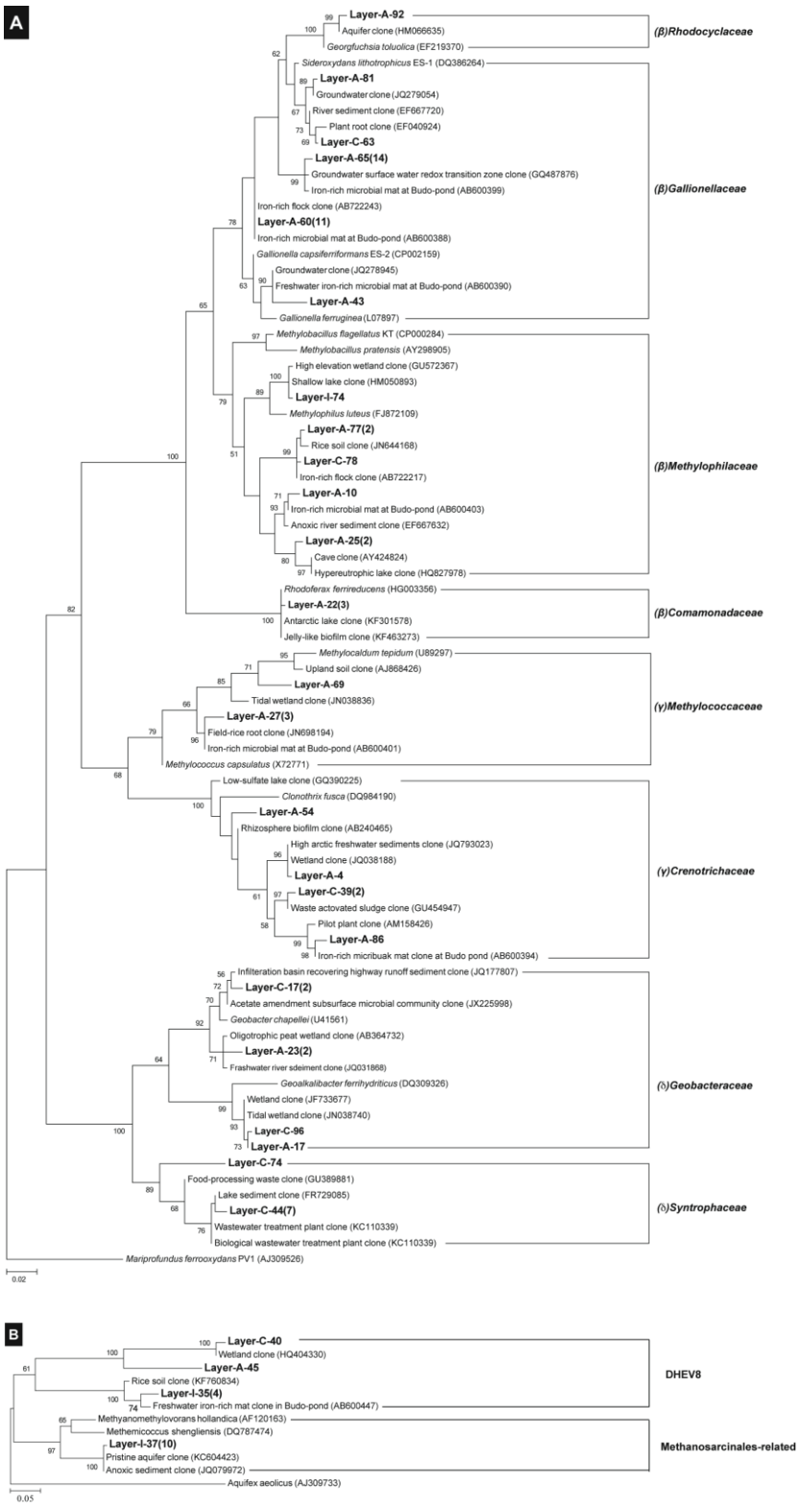

Fig. 5−10. Phylogenetic trees for bacterial (A) and archaeal (B) 16S rRNA genes. Bold letters indicate clones detected in this study. The enclosed numbers shown in the bold letters indicate the number of clones detected. Bootstrap values (higher than 50%) are based on 100 replicates.

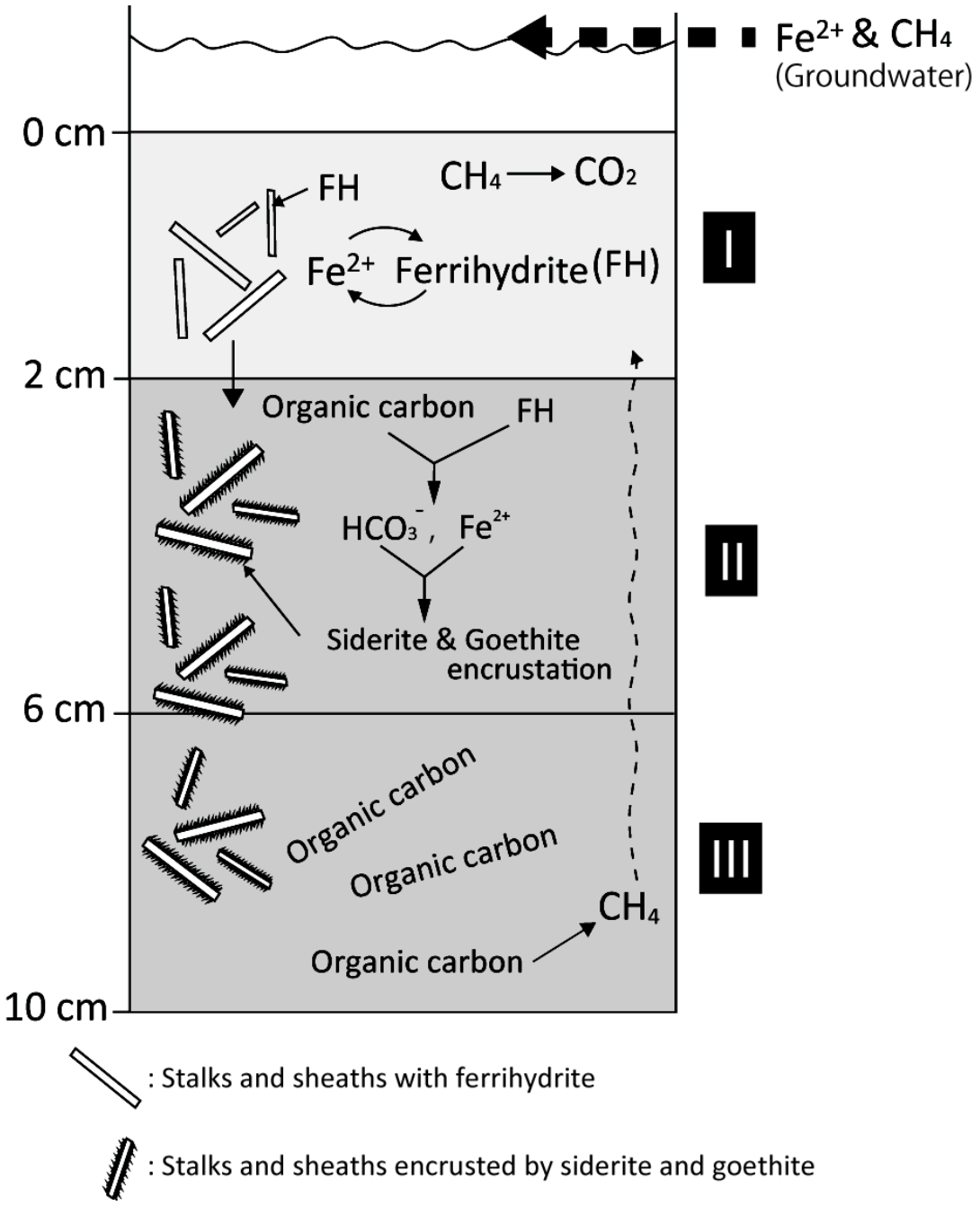

Fig. 5−11. Proposed cycles of iron and carbon in freshwater biogenic iron-rich sediment. Sediment can be sectioned into phase I to III. (Phase I) Precipitation of ferrihydrite by iron-oxidizing bacteria and CH_4 oxidation by methanotrophic bacteria are the main process. Although there is a dissimilatory iron reduction in this zone, Fe^{2+} produced by iron-reducing bacteria is re-oxidized into ferrihydrite. (Phase II) Iron reduction dominates organic carbon oxidation. Ferrous iron and bicarbonate produced in this zone promote precipitation of acicular siderite and goethite. However, iron reduction is restricted in this zone preserving abundant ferrihydrite, possibly because of the surface encrustation of siderite and goethite around ferrihydrite. (Phase III) Microbial aceticlastic CH_4 production dominates organic carbon oxidation.

Chapter 6. Conclusion

In this thesis, I attempted to reveal iron, carbon, and trace element cycles controlled by natural iron oxyhydroxides (BIOS). The geochemical and microbiological importance of iron oxyhydroxides that I summarized in Chapter 1 are following:

1) Iron oxyhydroxides adsorb various trace elements onto their surfaces and control their mobility. They also work as an electron acceptor for iron-reducing microorganisms.
2) Biogenic iron oxyhydroxides (BISO) are minerals precipitated by the activities of microorganisms. Three types of iron-oxidizing bacteria (microaerophilic lithoautotrophic Fe(II)-oxidizing bacteria, anoxic NO_3^--reducing, Fe(II)-oxidizing bacteria, and anoxic photoferrotrophic Fe(II)-oxidizing bacteria) are involved in BIOS formation at neutral pH.

Based on the background above, I firstly identified mineral species and mineral local structures of BIOS that are collected from natural environment and from incubation of Fe(II)-oxidizing bacteria at laboratory apparatus (Chapters 2 and 3). Following findings are summarized as follows:

1) Biogenic iron oxyhydroxides collected from natural environment consist of amorphous iron oxyhydroxides regardless of the sampling site. The iron oxyhydroxides are less ordered than 2-line ferrihydrite which mineral is known as most poorly crystalline mineral among synthesized iron minerals.
2) Poorly-ordered iron oxyhydroxides within BIOS are characterized by smaller amount of corner-sharing octahedral linkages of iron, suggesting more two-dimensional structures of BIOS compared to inorganically synthesized 2-line ferrihydrite.

Adsorptive properties of BIOS are identified using arsenate, yttrium, and cerium as adsorbates (Chapter 4). This study have used three types of adsorbents to identify trace element adsorption characteristics of BIOS: that is (1) synthetic ferrihydrite which has been used to mimic BIOS, (2) BIOS collected from a hydrothermal vent (in situ BIOS), and (3) BIOS incubated by microaerophilic iron-oxidizing bacteria (in vitro BIOS). Following suggestions were obtained:

1) Amount of both arsenate, yttrium, and cerium adsorbed onto in situ BIOS are less than

those onto synthetic ferrihydrite, which indicates that the amount of adsorption of trace element occurring in natural environment is less than that speculated using synthetic ferrihydrite.

2) All adsorbents adsorb arsenate forming inner-sphere complexation. Specific surface areas of both in situ and in vitro BIOS are less than that of synthetic ferrihydrite, even though BIOS consists of iron oxyhydroxides similar or smaller particle size compared to synthetic ferrihydrite. The results suggested that strong aggregation of iron particles reduces active surface sites of BIOS.

To consider long-term diagenesis of BIOS, I have examined sequential changes of iron mineral species and organic carbon composition in a stratified BIOS-rich freshwater sediment (Chapter 5). Following conclusion was suggested.

1) Biogenic iron oxyhydroxides formed by Fe(II)-oxidizing bacteria can be reduced at the subsurface layer (2-5 cm deep) by Fe(III)-reducing bacteria, but most of the ferric iron become inaccessible by siderite encrustation. This limits the degradation of organic materials by Fe(III)-reducing bacteria and enables the microorganisms inhabiting in the deeper sediment to utilize organic materials.

2) Organic carbon is mainly decomposed by Fe(III) reduction at the subsurface sediment (2-6 cm deep) whereas organic carbon decomposed by methanogenesis at the depth below 6cm.

References

Afonso M. D. and Stumm W. (1992) Reductive Dissolution of Iron(Iii) (Hydr)Oxides by Hydrogen-Sulfide. *Langmuir* **8**, 1671–1675.

Akai J., Izumi K., Fukuhara H., Masuda H., Nakano S., Yoshimura T., Ohfuji H., Md Anawar H. and Akai K. (2004) Mineralogical and geomicrobiological investigations on groundwater arsenic enrichment in Bangladesh. *Applied Geochemistry* **19**, 215–230.

Amstaetter K., Borch T. and Kappler A. (2012) Influence of humic acid imposed changes of ferrihydrite aggregation on microbial Fe(III) reduction. *Geochimica et Cosmochimica Acta* **85**, 326–341.

Anderson C. R., James R. E., Fru E. C., Kennedy C. B. and Pedersen K. (2006) *In situ* ecological development of a bacteriogenic iron oxide-producing microbial community from a subsurface granitic rock environment. *Geobiology* **4**, 29–42.

Anderson C. R, Pedersen K. (2003) *In situ* growth of *Gallionella* biofilms and partitioning of lanthanides and actinides between biological material and ferric oxyhydroxides. *Geobiology* **1**, 169–178

Arai Y. and Sparks D. L. (2001) ATR–FTIR Spectroscopic Investigation on Phosphate Adsorption Mechanisms at the Ferrihydrite–Water Interface. *Journal of Colloid and Interface Science* **241**, 317–326.

Baker B. J. and Banfield J. F. (2003) Microbial communities in acid mine drainage. *FEMS Microbiology Ecology* **44**, 139–152.

Balistrieri L. S. and Chao T. T. (1990) Adsorption of selenium by amorphous iron oxyhydroxide and manganese dioxide. *Geochimica et Cosmochimica Acta* **54**, 739–751.

Banfield J. F., Welch S. A., Zhang H., Ebert T. T., and Penn R. L. (2000) Aggregation-based crystal growth and microstructure development in natural iron oxyhydroxide biomineralization products. *Science* **289**, 751–754.

Bauer M. and Blodau C. (2006) Mobilization of arsenic by dissolved organic matter from iron oxides, soils and sediments. *Science of The Total Environment* **354**, 179–190.

Beal E. J., House C. H., and Orphan V. J. (2009) Manganese- and iron-dependent marine methane oxidation. *Science* **325**, 184–187.

Bennett S. A., Toner B. M., Barco R. and Edwards K. J. (2014) Carbon adsorption onto Fe oxyhydroxide stalks produced by a lithotrophic iron-oxidizing bacteria. *Geobiology* **12**, 146–156.

Benz M., Schink B., and Brune A. (1998) Humic acid reduction by *Propionibacterium freudenreichii* and other fermenting bacteria. *Applied and Environmental Microbiology* **64**, 4507–4512.

Benzine J., Shelobolina E., Xiong M. Y., Kennedy D. W., McKinley J. P., Lin X. and Roden E. (2013) Fe-phyllosilicate redox cycling organisms from a redox transition zone in Hanford 300 Area sediments. *Frontiers in Microbiology* **4**, 388.

Bethke C. M. and Yeakel S. (2013) The geochemist's workbench release 9.0 reaction modeling guide. Aqueous solutions, LLC.

Beveridge T. J. (1989) Role of cellular design in bacterial metal accumulation and mineralization. *Annual Review of Microbiology* **43**, 147–171.

Bissen M. and Frimmel F. H. (2003) Arsenic — a Review. Part I: Occurrence, Toxicity, Speciation, Mobility. *Acta hydrochimica et hydrobiologica* **31**, 9–18.

Blothe M. and Roden E. (2009) Microbial Iron Redox Cycling in a Circumneutral-pH Groundwater Seep. *Applied and Environmental Microbiology* **75**, 468–473.

Bond D. R. and Lovley D. R. (2002) Reduction of Fe(III) oxide by methanogens in the presence and absence of extracellular quinones. *Environmental Microbiol*ogy **4**, 115–124.

Bowell R. J. (1994) Sorption of arsenic by iron oxides and oxyhydroxides in soils. *Applied Geochemistry* **9**, 279–286.

Braunschweig J., Klier C., Schroeder C., Haendel M., Bosch J., Totsche K. U. and Meckenstock R. U. (2014) Citrate influences microbial Fe hydroxide reduction via a dissolution disaggregation mechanism. *Geochimica et Cosmochimica Acta* **139**, 434–446.

Bruun A-M., Finster K., Gunnlaugsson H. P., Nørnberg P., and Friedrich M. W. (2010) A comprehensive investigation on iron cycling in a freshwater seep including microscopy, cultivation and molecular community analysis. *Geomicrobiology Journal* **27**, 15–34.

Canfield D. E., Thamdrup B., and Hansen J. W. (1993) The anaerobic degradation of organic matter in Danish coastal sediments: Iron reduction, manganese reduction, and sulfate reduction. *Geochimica et Cosmochimica Acta* **57**, 3867–3883.

Chakraborty A., Roden E., Schieber J. and Picardal F. (2011) Enhanced growth of Acidovorax sp. strain 2AN during nitrate-dependent Fe(II) oxidation in batch and continuous-flow systems. *Applied and Environmental Microbiology* **77**, 8548–8556.

Chan C. S., De Stasio G., Welch S. A., Girasole M., Frazer B. H., Nesterova M. V., Fakra S. and Banfield J. F. (2004) Microbial polysaccharides template assembly of nanocrystal fibers. *Science* **303**, 1656–1658.

Chan C. S., Fakra S. C., Edwards D. C., Emerson D. and Banfield J. F. (2009) Iron oxyhydroxide mineralization on microbial extracellular polysaccharides. *Geochimica et Cosmochimica Acta* **73**, 3807–3818.

Chan C. S., Fakra S. C., Emerson D., Fleming E. J. and Edwards K. J. (2011) Lithotrophic iron-oxidizing bacteria produce organic stalks to control mineral growth: implications for biosignature formation. *ISME J*ournal **5**, 717–727.

Chitrakar R., Tezuka S., Sonoda A., Sakane K., Ooi K., and Hirotsu T. (2006) Phosphate adsorption on synthetic goethite and akaganeite. *Journal of Colloid and Interface Science* **298**, 602–608.

Cismasu A. C., Michel F. M., Tcaciuc A. P., Tyliszczak T., Brown G. E. Jr. and Brown G. E. (2011) Composition and structural aspects of naturally occurring ferrihydrite. *Comptes Rendus Geoscience* **343**, 210–218.

Comolli L. R, Luef B., Chan C. S. (2011) High-resolution 2D and 3D cryo-TEM reveals structural adaptations of two stalk-forming bacteria to an Fe-oxidizing lifestyle. *Environmental Microbiology* **13**, 2915–2929

Cornell R. M. and Schwertmann U. (1996) *The iron oxides: Structure, Properties, Reactions, Occurrence and Uses.* VCH Publishers, NY.

Crosby C. H., Bailey J. V. and Sharma M. (2014) Fossil evidence of iron-oxidizing chemolithotrophy linked to phosphogenesis in the wake of the Great Oxidation Event. *Geology* **42**, 1015–1018.

Crowe S. A., Jones C., Katsev S., Magen C., O'Neill A. H., Sturm A., Canfield D. E., Haffner G. D., Mucci A., Sundby B. and Fowle D. A. (2008) Photoferrotrophs thrive in an Archean Ocean analogue. *Proceedings of the National Academy Sciences* **105**, 15938–15943.

Cundy A. B., Hopkinson L. and Whitby R. L. D. (2008) Use of iron-based technologies in contaminated land and groundwater remediation: A review. *Science of The Total Environment* **400**, 42–51.

Das S., Hendry M. J., Essifie-Dughan J. (2013) Adsorption of selenite onto ferrihydrite, goethite, and lepidocrocite under neutral pH conditions. *Applied Geochemistry* **28**, 185–193.

Davis J. A. and Leckie J. O. (1978) Surface ionization and complexation at the oxide/water interface II. Surface properties of amorphous iron oxyhydroxide and adsorption of metal ions. *Journal of Colloid and Interface Science* **67**, 90–107.

Davis R. E., Moyer C. L. (2008) Extreme spatial and temporal variability of hydrothermal microbial mat communities along the Mariana Island Arc and southern Mariana back-arc system. *Journal of Geophysical Research* **113**, B08S15

DeMaster D. J., Leynaert A. and Queguiner B. (1995) The silica balance in the world ocean: A reestimate. *Science* **268**, 375–379.

Dixit S. and Hering J. G. (2003) Comparison of Arsenic(V) and Arsenic(III) Sorption onto Iron Oxide Minerals: Implications for Arsenic Mobility. *Environmental Science & Technology* **37**, 4182–4189.

Doelsch E., Masion A., Rose J., Stone W. E. E., Bottero J. Y., Bertsch P. M. (2003) Chemistry and structure of colloids obtained by hydrolysis of Fe(III) in the presence of SiO4 ligands. *Colloids and Surfaces A: Physicochemical and Engineering Aspects*. **217**, 121–128.

Druschel G. K., Emerson D., Sutka R., Suchecki P. and Luther G. W. I. (2008) Low-oxygen and chemical kinetic constraints on the geochemical niche of neutrophilic iron(II) oxidizing microorganisms. *Geochimica et Cosmochimica Acta* **72**, 3358–3370.

Duckworth O. W., Holmström S. J. M., Peña J. and Sposito G. (2009) Biogeochemistry of iron oxidation in a circumneutral freshwater habitat. *Chemical Geology* **260**, 149–158.

Dyer L., Fawell P. D., Newman O. M. G. and Richmond W. R. (2010) Synthesis and characterisation of ferrihydrite/silica co-precipitates. *Journal of Colloid and Interface Science* **348**, 65–70.

Edwards K. J., Bond P. L., Gihring T. M. and Banfield J. F. (2000) An archaeal iron-oxidizing extreme acidophile important in acid mine drainage. *Science* **287**, 149–158.

Edwards K. J, Bach W., McCollom T. M., Rogers D. (2004) Neutrophilic iron-oxidizing bacteria in the ocean: their habitats, diversity, and roles in mineral deposition, rock alteration, and biomass production in the deep-sea. *Geomicrobiology Journal* **21**, 393–404.

Edwards K. J., Toner B. M., Glazer B. T., Chan C. S., Rouxel O. J., Bach W., Emerson D., Davis R. E., Tebo B. M., Staudigel H. and Moyer C. L. (2011) Ultra-diffuse hydrothermal venting supports Fe-oxidizing bacteria and massive umber deposition at 5000 m off Hawaii. *ISME J* **5**, 1796–1800.

Egger M., Rasigraf O., Sapart C. J., Jillbert T., Jetten M. S. M., Röckmann T., van der Veen C., Bândă N., Kartal B., Ettwig., and Slomp C. P. (2015) Iron-mediated anaerobic oxidation of methane in brackish coastal sediments. *Environmental Science & Techno*logy **49**, 277–283.

Ehrenreich A. and Widdel F. (1994) Anaerobic oxidation of ferrous iron by purple bacteria, a new type of phototrophic metabolism. *Applied and Environmental Microbiology* **60**, 4517–4526.

Emerson D. and Revsbech N. P. (1994) Investigation of an Iron-Oxidizing Microbial Mat Community Located near Aarhus, Denmark: Field Studies. *Applied and Environmental Microbiology* **60**, 4022-4031.

Emerson D. and Moyer C. (1997) Isolation and characterization of novel iron-oxidizing bacteria that grow at circumneutral pH. *Applied and Environmental Microbiology* **63**, 4784–4792.

Emerson D. and Moyer C. L. (2002) Neutrophilic Fe-Oxidizing Bacteria Are Abundant at the Loihi Seamount Hydrothermal Vents and Play a Major Role in Fe Oxide Deposition. *Applied and Environmental Microbiology* **68**, 3085–3093.

Emerson D. and Weiss J. V. (2004) Bacterial iron oxidation in circumneutral freshwater habitats: findings from the field and the laboratory. *Geomicrobiology Journal* **21**, 405–414.

Emerson D. and Floyd M. M. (2005) Enrichment and isolation of iron-oxidizing bacteria at neutral pH. *Methods in Enzymology* **397**, 112–123.

Emerson D., Rentz J., Liburm T., Davis R., Aldrich H., Chan C., and Moyer C (2007) A Novel Lineage of Proteobacteria Involved in Formation of Marine Fe-Oxidizing Microbial Mat Communities. *PLoS one* **2**, e667

Emerson D. (2009) Potential for iron-reduction and iron-cycling in iron oxyhydroxide-rich microbial mats at Loihi Seamount. *Geomicrobiol. Journal* **26**, 639–647.

Emerson D., Fleming E. J. and McBeth J. M. (2010) Iron-oxidizing bacteria: an environmental and genomic perspective. *Annual Review of Microbiology* **64**, 561–583.

Emerson D., Field E. K., Chertkov O., Davenport K. W., Goodwin L., Munk C., Nolan M., and Woyke T. (2013) Comparative genomics of freshwater Fe-oxidizing bacteria: implications for physiology, ecology, and systematics. *Frontiers in Microbiology* **4**, article 254.

Ettwig K. F., Shima S., van de Pas-Schoonen K. T., Kahnt J., Medema M. H., op den Camp H. J. M., Jetten M. S. M., and Strous M. (2008) Denitrifying bacteria anaerobically oxidize methane in the absence of *Archaea*. *Environmental Microbiol*ogy **10**, 3164–3173.

Fabisch M., Beulig F., Akob D. M. and Kusel K. (2013) Surprising abundance of Gallionella-related iron oxidizers in creek sediments at pH 4.4 or at high heavy metal concentrations. *Frontiers in Microbiology* **4**, 390.

Falkowski P. G., Fenchel T. and Delong E. F. (2008) The microbial engines that drive Earth's biogeochemical cycles. *Science* **320**, 1034–1039.

Feisthauer S., Vogt C., Modrzynski J., Szlenkier M., Krüger M., Siegert M., and Richnow H. H. (2011) Different types of methane monooxygenases produce similar carbon and hydrogen isotope fractionation patterns during methane oxidation. *Geochimica et Cosmochimica Acta* **75**, 1173–1184.

Ferris F. G., Hallberg R. O., Lyven B., and Pedersen K. (2000) Retention of strontium, cesium, lead and uranium by bacterial iron oxides from a subterranean environment. *Applied Geochemistry* **15**, 1035–1042.

Ferris G., Konhauser K. O. and Lyven B. (1999) Accumulation of metals by bacteriogenic iron oxides in a subterranean environment. *Geomicrobiology Journal* **16**, 181–192.

Ferris R. G., Tazaki K., and Fyfe W. S. (1989) Iron oxides in acid mine drainage environments and their association with bacteria. *Chemical Geology*, **74**, 321–330.

Fleming E. J., Cetinić I., Chan C. S., King D. W., and Emerson D. (2013a) Ecological succession among iron-oxidizing bacteria. *ISME Journal* **8**, 804–815.

Fleming E. J., Davis R. E., McAllister S. M., Chan C. S., Moyer C. L., Tebo B. M., and Emerson D. (2013b) Hidden in plain sight: discovery of sheath-forming, iron-oxidizing *Zetaproteobacteria* at Loihi Seamount, Hawaii, USA. *FEMS Microbiology Ecology* **85**, 116–127.

Fredrickson J. K., Zachara J. M., Kennedy D. W., Dong H., Onstott T. C., Hinman N. W., and Li S. M. (1998) Biogenic iron mineralization accompanying the dissimilatory reduction of hydrous ferric oxide by a groundwater bacterium. *Geochimica et Cosmochimica Acta* **62**, 3239–3257.

Froelich P. N., Klinkhammer G. P. K., Bender M. L., Luedtke N. A., Heath G. R., Cullen D., and Dauphin P. (1979) Early oxidation of organic matter in pelagic sediments of the eastern equatorial atlantic suboxic diagenesis. *Geochimica et Cosmochimica Acta* **43**, 1075–1090.

Fuller C. C., Davis J. A., Waychunas G. A., Fuller C., Davis J. and Waychunas G. (1993) Surface chemistry of ferrihydrite: Part 2. Kinetics of arsenate adsorption and coprecipitation. *Geochimica et Cosmochimica Acta* **57**, 2271–2282.

Gao X., Root R. A., Farrell J., Ela W. and Chorover J. (2013) Effect of silicic acid on arsenate and arsenite retention mechanisms on 6-L ferrihydrite: A spectroscopic and batch adsorption approach. *Applied Geochemistry* **38**, 110–120.

Gault A. G., Ibrahim A., Langley S., Renaud R., Takahashi Y., Boothman C., Lloyd J. R., Clark I. D., Ferris F. G., and Fortin D. (2011) Microbial and geochemical features suggest iron redox cycling within bacteriogenic iron oxide-rich sediments. *Chemical Geology.* **281**, 41–51.

Gault A. G., Langley S., Ibrahim A., Renaud R., Takahashi Y., Boothman C., Lloyd J. R., Clark I. D., Ferris F. G., and Fortin D. (2012) Seasonal changes in mineralogy, geochemistry and microbial community of bacteriogenic iron oxides (BIOS) deposited in a circumneutral wetland. *Geomicrobiology Journal* **29**, 161–172.

Gieseke A. and de Beer D. (2004) Use of microelectrodes to measure in situ microbial activities in biofilms, sediments, and microbial mats. *Molecular Microbial Ecology Manual* pp.1–23, Springer, Heidelberg.

Goldberg S. and Johnston C. T. (2001) Mechanisms of arsenic adsorption on amorphous oxides evaluated using macroscopic measurements, vibrational spectroscopy, and surface complexation modeling. *Journal of Colloid and Interface Science* **234**, 204–216.

Good I. J. (1953) The population frequencies of species and the estimation of population parameters. *Biometrika* **40**, 237–264.

Hallbeck L. and Pedersen K. (1990) Culture parameters regulating stalk formation and growth rate of Gallionella ferruginea. *Journal of General Microbiology* **136**, 1675–1680.

Hallbeck L., Stahl F. and Pedersen K. (1993) Phylogeny and phenotypic characterization of the stalk-forming and iron-oxidizing bacterium *Gallionnella ferruginea*. *Journal of General Microbiology* **139**, 1531–1535.

Hallbeck L. and Pedersen K., *Gallionella* (2005) In Brenner D., Kring N., Staley J., editors. *Bergey's Manual of Systematic Bacteriology, 2nd edition*. New York: Springer. pp. 880–886.

Hansel C. M, Benner S. G, Nico P, Fendorf S. (2004) Structural constraints of ferric (hydr)oxides on dissimilatory iron reduction and the fate of Fe(II). *Geochimica et Cosmochimica Acta*. **68**, 3217–3229.

Hansel C. M., Benner S. G., Neiss J., Dohnalkova A., Kukkadapu R. K., and Fendorf S. (2003) Secondary mineralization pathways induced by dissimilatory iron reduction of ferrihydrite under advective flow. *Geochimica et Cosmochimica Acta* **67**, 2977–2992.

Harvey A. E., Smart J. A., and Amis E. S. (1955) Simultaneous spectrophotometric determination of iron(II) and total iron with 1,10-phenanthroline. *Analytical Chemistry* **27**, 26–29.

Heaney P. J. and Veblen D. R. (1991) An examination of spherulitic dubiomicrofossils in Precambrian banded iron formations using the transmission electron microscope. *Precambrian Research* **49**, 355–372.

Hegler F., Losekann-Behrens T., Hanselmann K., Behrens S. and Kappler A. (2012) Influence of Seasonal and Geochemical Changes on the Geomicrobiology of an Iron Carbonate Mineral Water Spring. *Appl. Environ. Microbiol.* **78**, 7185–7196.

Heimann A., Johnson C. M., Beard B. L., Valley J. M., Roden E. E., Spicuzza M. J., and Beukes N. J. (2010) Fe, C, O isotope compositions of banded iron formation carbonates demonstrate a major role for dissimilatory iron reduction in ~2.5 Ga marine environments. *Earth and Planetary Science Letters* **294**, 8–18.

Holden J. and Adams M. W. W. (2003) Microbe–metal interactions in marine hydrothermal environments. *Current Opinion in Chemical Biology*. **7**, 160–165.

Hossain M. F. (2006) Arsenic contamination in Bangladesh—An overview. *Agriculture, Ecosystems & Environment* **113**, 1–16.

Jain A., Loeppert R. H. and Raven K. P. (1999) Arsenite and Arsenate Adsorption on Ferrihydrite: Surface Charge Reduction and Net OH -Release Stoichiometry. *Environmental Science & Technology* **33**, 1179–1184.

Jambor J. L. and Dutrizac J. E. (1998) Occurrence and constitution of natural and synthetic ferrihydrite, a widespread iron oxyhydroxide. *Chemical Reviews* **98**, 2549–2585.

James R. and Ferris G. (2004) Evidence for microbial-mediated iron oxidation at a neutrophilic groundwater spring. *Chemical Geology* **212**, 301–311.

Janney D. E., Cowley J. M. and Buseck P. R. (2000) Transmission electron microscopy of synthetic 2-and 6-line ferrihydrite. *Clays and Clay Minerals* **48**, 111–119.

Kaiser K., Nutrition P., Ecology S. and Guggenberger G. (2003) Mineral surfaces and soil organic matter. *European Journal of Soil Science* **54**, 219–236.

Kappler A. and Newman D. K. (2004) Formation of Fe(III)-minerals by Fe(II)-oxidizing photoautotrophic bacteria. *Geochimica et Cosmochimica Acta* **68**, 1217–1226.

Kappler A. and Straub K. L. (2005c) Geomicrobiological cycling of iron. *Reviews in Mineralogy and Geochemistry* **59**, 85–108.

Kappler A., Benz M., Schink B., and Brune A. (2004) Electron shuttling via humic acids in microbial iron(III) reduction in a freshwater sediment. *FEMS Microbiology Ecology* **47**, 85–92.

Kappler A., Pasquero C., Konhauser K. O. and Newman D. K. (2005a) Deposition of banded iron formations by anoxygenic phototrophic Fe(II)-oxidizing bacteria. *Geology* **33**, 865.

Kappler A., Schink B. and Newman D. K. (2005b) Fe(III) mineral formation and cell encrustation by the nitrate-dependent Fe(II)-oxidizer strain BoFeN1. *Geobiology* **3**, 235–245.

Karlsson T, Persson P. (2012) Complexes with aquatic organic matter suppress hydrolysis and precipitation of Fe(III). *Chemical Geology*. **322-323**, 19–27.

Kasama S, Murakami T (2001) The effect of microorganisms on Fe precipitation rates at neutral pH. *Chemical Geology* **180**, 117–128

Kasama T. and Murakami T. (2001) The effect of microorganisms on Fe precipitation rates at neutral pH. *Chemical Geology* **180**, 117–128.

Kato S., Kobayashi C., Kakegawa T., and Yamagishi A. (2009) Microbial communities in iron-silica-rich microbial mats at deep-sea hydrothermal fields of the Southern Mariana Trough. *Environmental Microbiology* **11**, 2094–2111

Kato S., Chan C., Itoh T., and Ohkuma M. (2013) Functional gene analysis of freshwater iron-rich flocs at circumneutral pH and isolation of a stalk-forming microaerophilic iron-oxidizing bacterium. *Applied and Environmental Microbiology* **79**, 5283–5290.

Kato S., Kikuchi S., Kashiwabara T., Takahashi Y., Suzuki K., Itoh T., Ohkuma M., and Yamagishi A. (2012) Prokaryotic abundance and community composition in a freshwater iron-rich microbial mat at circumneutral pH. *Geomicrobiol. Journal* **29**, 896–905.

Katsoyiannis I. A. and Zouboulis A. I. (2004) Application of biological processes for the removal of arsenic from groundwaters. *Water Research* **38**, 17–26.

Katsoyiannis I. A., Althoff H. W., Bartel H., and Jekel M. (2006) The effect of groundwater composition on uranium (VI) sorption onto bacteriogenic iron oxides. *Water Research* **40**, 3645–3652.

Kawagucci S., Miyazaki J., Nakajima R., Nozaki T., Takaya Y., Kato Y., Shibuya T., Konno U., Nakaguchi Y., Hatada K., Hirayama H., Fujikura K., Furushima Y., Yamamoto H., Watsuji T., Ishibashi J., and Takai K. (2013) Post-drilling changes in fluid discharge pattern, mineral deposition, and fluid chemistry in the Iheya North hydrothermal field, Okinawa Trough. *Geochemistry Geophysics Geosystems* **14**, 4774–4790.

Kawaichi S., Ito N., Kamikawa R., Sugawara T., Yoshida T., and Sako Y. (2013) *Ardenticatena maritima* gen, nov., sp. nov., a ferric iron- and nitrate-reducing bacterium of the phylum 'Chloroflexi' isolated from an iron-rich coastal hydrothermal field, and description of *Ardenticatenia* classis nov. *International Journal of Systematic Evolutionary Microbiology* **63**, 2992–3002.

Kennedy C. B., Gault A., Fortin D., Clark I. D. and Ferris G. (2011) Retention of Iodide by Bacteriogenic Iron Oxides. *Geomicrobiology Journal* **28**, 387–395.

Kennedy C. B., Martinez R. E., Scott S. D. and Ferris G. (2003a) Surface chemistry and reactivity of bacteriogenic iron oxides from Axial Volcano, Juan de Fuca Ridge, north-east Pacific Ocean. *Geobiology* **1**, 59–69.

Kennedy C. B., Scott S. D. and Ferris F. G. (2003b) Ultrastructure and potential sub-seafloor evidence of bacteriogenic iron oxides from Axial Volcano, Juan de Fuca Ridge, north-east Pacific Ocean. *Fems Microbiology Ecology* **43**, 247–254.

Kikuchi S., Makita H., Mitsunobu S., Terada Y., Yamaguchi N., Takai K., and Takahashi Y. (2011) Application of synchrotron μ-XRF-XAFS to the speciation of Fe on a single stalk in bacteriogenic iron oxides (BIOS). *Chemistry Letter* **40**, 680–681.

Kikuchi S., Makita H., Takai K., Yamaguchi N., and Takahashi Y. (2014) Characterization of biogenic iron oxides collected by the newly designed liquid culture method using diffusion chambers. *Geobiology* **12**, 133–145.

Klein C. (2005) Some Precambrian banded iron-formations (BIFs) from around the world: Their age, geologic setting, mineralogy, metamorphism, geochemistry, and origin. *American Mineralogist* **90**, 1473–1499.

Kleinert S., Muehe E. M., Posth N. R., Dippon U., Daus B. and Kappler A. (2011) Biogenic Fe(III) Minerals Lower the Efficiency of Iron-Mineral-Based Commercial Filter Systems for Arsenic Removal. *Environmental Science & Technology* **45**, 7533–7541.

Klueglein N. and Kappler A. (2012) Abiotic oxidation of Fe(II) by reactive nitrogen species in cultures of the nitrate-reducing Fe(II) oxidizer Acidovoraxsp. BoFeN1 - questioning the existence of enzymatic Fe(II) oxidation. *Geobiology* **11**, 180–190.

Klueglein N., Zeitvogel F., Stierhof Y.-D., Floetenmeyer M., Konhauser K. O., Kappler A. and Obst M. (2014) Potential role of nitrite for abiotic Fe(II) oxidation and cell encrustation during nitrate reduction by denitrifying bacteria. *Applied and Environmental Microbiology* **80**, 1051–1061.

Knittel K. and Boetius A. (2009) Anaerobic oxidation of methane: progress with an unknown process. *Annual Review of Microbiology* **63**, 311–334.

Konhauser K. (1997) Bacterial iron biomineralisation in nature. *FEMS Microbiology Reviews* **20**, 315–326.

Konhauser K. O., Hamade T., Raiswell R., Morris R. C., Ferris F. G., Southam G., and Canfield D. E. (2002) Could bacteria have formed the Precambrian banded iron formations? *Geology* **30**, 1079–1082.

Konhauser K. O., Kappler A., and Roden E. E. (2011) Iron in microbial metabolisms. *Elements* **7**, 89–93.

Krepski S. T., Emerson D., Chan C. S., Hredzak-Showalter P. L. and Luther G. W. I. (2013) Morphology of biogenic iron oxides records microbial physiology and environmental conditions: toward interpreting iron microfossils. *Geobiology* **11**, 457–471.

Krepski S. T., Hanson T. E. and Chan C. S. (2012) Isolation and characterization of a novel biomineral stalk-forming iron-oxidizing bacterium from a circumneutral groundwater seep. *Environmental Microbiology* **14**, 1671–1680.

Kucera S. and Wolfe R. S. (1957) A selective enrichment method for *Gallionella ferruginea*. *Journal of Bacteriology* **74**, 344–349.

Kuever J., Rainey F. A., and Widdel F. (2005) Syntrophus, p1033–1036. In Brenner D, Krieg N., Staley J. (ed), Bergey's manual of systematic bacteriology, 2nd ed, vol2. Springer, New York, NY.

Lalonde K., Mucci A., Ouellet A. and Gélinas Y. (2013) Preservation of organic matter in sediments promoted by iron. *Nature* **483**, 198–200.

Langley S., Gault A., Ibrahim A., Renaud R., Fortin D., Clark I. D., and Ferris F. G. (2009a) A comparison of the rates of Fe(III) reduction in synthetic and bacteriogenic iron oxides by *Shewanella putrefaciens* CN32. *Geomicrobiol. Journal* **26**, 57–70.

Langley S., Gault A., Ibrahim Alex, Takahashi Y., Renaud R., Fortin D., Clark I. D. and Ferris G. (2009b) Strontium desorption from bacteriogenic iron oxides (BIOS) subjected to microbial Fe(III) reduction. *Chemical Geology* **262**, 217–228.

Larese-Casanova P., Haderlein S. B. and Kappler A. (2010) Biomineralization of lepidocrocite and goethite by nitrate-reducing Fe(II)-oxidizing bacteria: Effect of pH, bicarbonate, phosphate, and humic acids. *Geochimica et Cosmochimica Acta* **74**, 3721–3734.

Lee W. C., Kim S.-O., Ranville J., Yun S.-T. and Choi S. H. (2014) Sequestration of arsenate from aqueous solution using 2-line ferrihydrite: equilibria, kinetics, and X-ray absorption spectroscopic analysis. *Environmental Science & Technology* **71**, 3307–3318.

Lenoble V., Bouras O., Deluchat V., Serpaud B. and Bollinger J.-C. (2002) Arsenic adsorption onto pillared clays and iron oxides. *Journal of Colloid and Interface Science* **255**, 52–58.

Lentini C. J., Wankel S. D., and Hansel C. M. (2012) Enriched iron(III)-reducing bacterial communities are shaped by carbon substrate and iron oxide mineralogy. *Frontiers in Microbiology* **3**, article 404.

Little C. T. S., Glynn S. E. J. and Mills R. A. (2004) Four-Hundred-and-Ninety-Million-Year Record of Bacteriogenic Iron Oxide Precipitation at Sea-Floor Hydrothermal Vents. *Geomicrobiology Journal* **21**, 415–429.

Liu D., Dong H., Bishop M. E., Wang H., Agrawal A., Tritschler S., Eberl D. D., and Xie S. (2011) Reduction of structural Fe(III) in nontronite by methanogen *Methanosarcina barkeri*. *Geochimica et Cosmochimica Acta* **75**, 1057–1071.

Liu Y. and Whitman W. B. (2008) Metabolic, phylogenetic, and ecological diversity of the methanogenic archaea. *Annuals of the New York Academy of Science* **1125**, 171–189.

Lovley D. R. (1991) Dissimilatory Fe(Iii) and Mn(Iv) Reduction. *Microbiological Reviews* **55**, 259–287.

Lovley D. R. and Phillips E. (1986) Organic-Matter Mineralization with Reduction of Ferric Iron in Anaerobic Sediments. *Applied and Environmental Microbiology* **51**, 683–689.

Lovley D. R., Coates J. D., Blunt-Harris E. L., Phillips E. J. P., and Woodward J. C. (1996) Humic substances as electron acceptors for microbial respiration. *Nature*, **382**, 445–448.

Ludwig W., Strunk O., Westram R., Richter L., Meier H., Yadhukumar, Buchner A., Lai T., Steppi S., Jobb G., Föster W., Brettske I., Gerber S., Ginhart A. W., Gross O., Grumann S., Hermann S., Jost R., Köning A.,

Liss T., Lüβmann R., May M., Nonhoff B., Reichel B., Strehlow R., Stamatakis A., Stuckmann N., Vilbig A., Lenke M., Ludwig T., Bode A., and Schleifer KH. (2004) ARB: a software environment for sequence data. *Nucleic Acids Research* **32**, 1363–1371.

Lüdemann H., Arth I., and Liesack W. (2000) Spatial changes in the bacterial community structure along a vertical oxygen gradient in flooded paddy soil cores. *Applied and Environmental Microbiology* **66**, 754–762.

Manceau A. (1995) The mechanism of anion adsorption on iron oxides: Evidence for the bonding of arsenate tetrahedra on free $Fe(O, OH)_6$ edges. *Geochimica et Cosmochimica Acta* **59**, 3647–3653.

Mandal B. (2002) Arsenic round the world: a review. *Talanta* **58**, 201–235.

Martinez R. E., Pedersen K., and Ferris F. G. (2004) Cadmium complexation by bacteriogenic iron oxides from a subterranean environment. *Journal of Colloid and Interface Science* **275**, 82–89.

Martinez R. E., Smith D. S., Pedersen K. and Ferris G. (2003) Surface chemical heterogeneity of bacteriogenic iron oxides from a subterranean environment. *Environmental Science & Technology* **37**, 5671–5677.

McBeth J. M., Little B. J., Ray R. I., Farrar K. M., and Emerson D. (2011) Neutrophilic Iron-Oxidizing "Zetaproteobacteria" and Mild Steel Corrosion in Nearshore Marine Environments. *Applied and Environmental Microbiology* **77**, 1405–1412.

McMillan S. G. and Schwertmann U. (1998) Morphological and genetic relations between siderite, calcite and goethite in a low moor peat from southern Germany. *European Journal of Soil Science* **49**, 283–293.

Melton E. D., Swanner E. D., Behrens S., Schmidt C. and Kappler A. (2014) The interplay of microbially mediated and abiotic reactions in the biogeochemical Fe cycle. *Nature Reviews Microbiology* **12**, 797–808.

Meyer-Dombard D. R., Amend J. P. and Osburn M. R. (2013) Microbial diversity and potential for arsenic and iron biogeochemical cycling at an arsenic rich, shallow-sea hydrothermal vent (Tutum Bay, Papua New Guinea). *Chemical Geology* **348**, 37–47.

Mikutta C, and Kretzschmar R. (2008b) Synthetic coprecipitates of exopolysaccharides and ferrihydrite. Part II: Siderophore-promoted dissolution. *Geochimica et Cosmochimica Acta*. **72**, 1128–1142.

Mikutta C., Mikutta R., Bonneville S., Wagner F., Voegelin A., Christl I. and Kretzschmar R. (2008a) Synthetic coprecipitates of exopolysaccharides and ferrihydrite. Part I: Characterization. *Geochimica et Cosmochimica Acta* **72**, 1111–1127.

Miot J., Maclellan K., Benzerara K. and Boisset N. (2011) Preservation of protein globules and peptidoglycan in the mineralized cell wall of nitrate-reducing, iron(II)-oxidizing bacteria: a cryo-electron microscopy study. *Geobiology* **9**, 459–470.

Mitsunobu S., Shiraishi F., Makita H., Orchtt B., Kikuchi S., Jorgensen B., and Takahashi Y (2012) Bacteriogenic Fe(III) (oxyhydr)oxides characterized by synchrotron microprobe coupled with spatially-resolved phylogenetic analysis. *Environmental Science & Technology* **46**, 3304–3311.

Moyes L. M., Parkman R. H., Charnock J. M., Vaughan D. J., Livens F. R., Hughes C. R., and Braithwaite A. (2000) Uranium uptake from aqueous solution by interaction with goethite, lepidocrocite, muscovite, and mackinawite: An X-ray absorption spectroscopy study. *Environment Science & Technology* **34**, 1062–1068.

Muehe E. M., Adaktylou I. J., Obst M., Zeitvogel F., Behrens S., Planer-Friedrich B., Kraemer U., and Kappler A. (2013a) Organic carbon and reducing conditions lead to cadmium immobilization by secondary Fe mineral formation in a pH-neutral soil. *Environmental Science & Technology* **47**, 13430–13439.

Muehe E. M., Scheer L., Daus B. and Kappler A. (2013b) Fate of Arsenic during Microbial Reduction of Biogenic versus Abiogenic As–Fe(III)–Mineral Coprecipitates. *Environmental Science & Technology* **47**, 8297–8307.

Mukherjee A., Sengupta M. K. and Hossain M. A. (2006) Arsenic contamination in groundwater: a global perspective with emphasis on the Asian scenario. *Journal of Health* **24**, 142–163

Mustafa G., Singh B., and Kookana R. S. (2004) Cadmium adsorption and desorption behaviour on goethite at low equilibrium concentrations: effects of pH and index cations. *Chemosphere* **57**, 1325–1333.

Møller C. L. and Sand-Jensen K. (2008) Iron plaques improve the oxygen supply to root meristems of the freshwater plant, Lobelia dortmanna. *New Phytologist* **179**, 848–856.

Nevin K. P., Holmes D. E., Woodard T. L., Hinlein E. S., Ostendorf D. W., and Lovley D. R. (2005) *Geobacter bemidjiensis* sp. nov. and *Geobacter psychrophilus* sp. nov., two novel Fe(III)-reducing subsurface isolates. *International Journal of Systematic and Evolutionary Microbiology* **55**, 1667–1674.

Nickson R., McArthur J., Burgess W., Ahmed K. M., Ravenscroft P. and Rahmanñ M. (1998) Arsenic poisoning of Bangladesh groundwater. *Nature* **395**, 338–338.

Nunoura T., Takai Y., Kazama H., Hirai M., Ashi J., Imachi H., and Takai K. (2012) Microbial diversity in deep-sea methane seep sediments presented by SSU rRNA gene tag sequencing. *Microbes and Environments* **27**, 382–390.

Omoregie E. O., Couture R., Van Cappellen P. Corkhill C. L., Charnock J. M., Polya D. A., Vaughan D., Vanbroekhoven K., Lloyd J. R. (2014) Arsenic bioremediation by biogenic iron oxides and sulfides. *Applied and Environmental Microbiology* **79**, 4325–4335.

Pal A. and Paul A. K. (2008) Microbial extracellular polymeric substances: central elements in heavy metal bioremediation. *Indian Journal of Microbiology* **48**, 49–64.

Parida K. M., Gorai B., Das N. N., and Rao S. B. (1997) Studies on ferric oxide hydroxides 3. Adsorption of selenite (SeO_3^{2-}) on different forms of iron oxyhydroxides. *Journal of Colloid and Interface Science* **185**, 355–362.

Parmar N., Gorby Y. A., Beveridge T. J., and Ferris F. G. (2001) Formation of green rust and immobilization of nickel in response to bacterial reduction of hydrous ferric oxide. *Geomicrobiology Journal* **18**, 375–385.

Perret D., Gaillard J.-F., Dominik J. A. and Atteia O. (2000) The Diversity of Natural Hydrous Iron Oxides. *Environmental Science & Technology* **34**, 3540–3546.

Pierce M. L. and Moore C. B. (1982) Adsorption of Arsenite and Arsenate on Amorphous Iron Hydroxide. *Water Research* **16**, 1247–1253.

Pye K., Dickson A. D., Schiavon N., Coleman M. L., and Cox M. (1990) Formation of siderite-Mg-calcite-iron sulphide concretions in intertidal marsh and sandflat sediments, north Norfolk, England. *Sedimentology* **37**, 325–343.

Qi P. and Pichler T. (2014) Closer look at As(III) and As(V) adsorption onto ferrihydrite under competitive conditions. *Langmuir* **30**, 11110–11116.

Ravel B. and Newville M. (2005) ATHENA, ARTEMIS, HEPHAESTUS: data analysis for X-ray absorption spectroscopy using IFEFFIT. *Journal of Synchrotron Radiation* **12**, 537–541.

Raven K. P., Jain A. and Loeppert R. H. (1998) Arsenite and arsenate adsorption on ferrihydrite: Kinetics, equilibrium, and adsorption envelopes. *Environ. Sci. Technol.* **32**, 344–349.

Reiche M., Torburg G., and Küsel K. (2008) Competition of Fe(III) reduction and methanogenesis in an acidic fen. *FEMS Microbiol. Ecol.* **65**, 88–101.

Rentz J. A., Kraiya C., Luther G. W. I. and Emerson D. (2007) Control of ferrous iron oxidation within circumneutral microbial iron mats by cellular activity and autocatalysis. *Environmental Science & Technology* **41**, 6084–6089.

Rentz J. A., Turner I. P., Ullman J. L. and Ullman J. L. (2009) Removal of phosphorus from solution using biogenic iron oxides. *Water Research* **43**, 2029–2035.

Roden E. (2012) Microbial iron-redox cycling in subsurface environments. *Biochemical Society Transactions* **40**, 1249–1256.

Roden E. E. and Wetzel R. G. (1996) Organic carbon oxidation and suppression of methane production by microbial Fe(III) oxide reduction in vegetated and unvegetated freshwater wetland sediments. *Limnology and Oceanogr*aphy **41**, 1733–1748.

Roden E. E. and Wetzel R. G. (2003) Competition between Fe(III)-reducing and methanogenic bacteria for acetate in iron-rich freshwater sediments. *Microbial Ecology* **45**, 252–258.

Roden E. E., McBeth J. M., Blöthe M., Percak-Dennett E. M., Fleming E. J., Holyoke R. R., Luther G. W. III, Emerson D., and Schieber J. (2012) The microbial ferrous wheel in a neutral pH groundwater seep. *Frontiers in Microbiology* **3**, article 172.

Roden E. E., Sobolev D., Glazer B., and Luther G. W. (2004) Potential for microscale bacterial Fe redox cycling at the aerobic-anaerobic interface. *Geomicrobiology Journal* **21**, 379–391.

Rose J., Manceau A., Bottero J. Y., Masion A., and Garcia F. (1996) Nucleation and growth mechanisms of Fe oxyhydroxide in the presence of PO_4 ions: Fe K-edge EXAFS study. *Langmuir* **12**, 6701–6707.

Saalfield S. L. and Bostick B. C. (2010) Synergistic effect of calcium and bicarbonate in enhancing arsenate release from ferrihydrite. *Geochimica et Cosmochimica Acta* **74**, 5171–5186.

Schwertsmann U. and Cornell R. M. (1991) *Iron oxides in the laboratory. Preparation and characterization* VCH, Weinheim, Germany

Schädler S., Burkhardt C., Hegler F., Straub K. L., Miot J., Benzerara K., and Kappler A. (2009) Formation of cell-iron-mineral aggregates by phototrophic and nitrate-reducing anaerobic Fe(II)-oxidizing bacteria. *Geomicrobiology Journal* **26**, 93–103.

Seshadri R., Salzberg S. L., Jensen H. B., Birkeland N. K., Nelson W. C., Dodson R. J., Grindhaug S. H., Holt I., Eidhammer I., Jonasen I., Vanaken S., Utterback T., Feldblyum T. V., Fraser C. M., Lillehaug J. R., and

Eisen J. A. (2004) Genomic insights into Methanotrophy: The complete genome sequence of *Methylococcus capsulatus* (bath). *PLoS Biology* **2**, e303.

Sharma P., Rolle M., Kocar B., Fendorf S. and Kappler A. (2010) Influence of natural organic matter on As transport and retention. *Environmental Science & Technology* **45**, 546–553.

Sheik C. S., Mitchell T. W., Rizvi F. Z., Rehman Y., Faisal M., Hasnain S., McInerney M. J. and Krumholz L. R. (2012) Exposure of Soil Microbial Communities to Chromium and Arsenic Alters Their Diversity and Structure ed. J. A. Gilbert. *PLoS ONE* **7**, e40059.

Sherman D. M. and Randall S. R. (2003) Surface complexation of arsenic(V) to iron(III) (hydr)oxides: structural mechanism from ab initio molecular geometries and EXAFS spectroscopy. *Geochimica et Cosmochimica Acta* **67**, 4223–4230.

Shimizu M., Zhou J., Schröder C., Obst M., Kappler A. and Borch T. (2013) Dissimilatory Reduction and Transformation of Ferrihydrite-Humic Acid Coprecipitates. *Environmental Science & Technology* **47**, 13375–13384.

Shiraishi F., Okumura T., Takahashi Y, and Kano A. (2010) Influence of microbial photosynthesis on tufa stromatolite formation and ambient water chemistry, SW Japan. *Geochimica et Cosmochimica Acta* **74**, 5289–5304.

Singer E., Emerson D., Webb E. A., Barco R. A., Kuenen J. G., Nelson W. C., Chan C. S., Comolli L. R., Ferriera S., Johnson J., Heidelberg J. F. and Edwards K. J. (2011) Mariprofundus ferrooxydans PV-1 the First Genome of a Marine Fe(II) Oxidizing Zetaproteobacterium ed. A. B. Khodursky. *PLoS ONE* **6**, e25386.

Smedley P. L. and Kinniburgh D. G. (2002) A review of the source, behaviour and distribution of arsenic in natural waters. *Applied Geochemistry* **17**, 517–568.

Snoeyenbos-West O. L., Nevin K. P., Anderson R. T., and Lovley D. R. (2000) Enrichment of Geobacter species in response to stimulation of Fe(III) reduction in sandy aquifer sediments. *Microbial Ecology* **39**, 153–167.

Sobolev D. and Roden E. E. (2002) Evidence for rapid microscale bacterial redox cycling of iron in circumneutral environments. *Antonie van Leeuwenhoek International Journal of General and Molecular Microbiology* **81**, 587–597.

Spadini L., Schindler P. W., Charlet L., and Manceau A. Hydrous ferric oxide: evaluation of Cd–HFO surface complexation models combining Cd K EXAFS data, potentiometric titration results, and surface site

structures identified from mineralogical knowledge. (2003) *Journal of Colloid and Interface Science* **226**, 1–18.

Straub K. L., Benz M., Schink B. and Widdel F. (1996) Anaerobic, nitrate-dependent microbial oxidation of ferrous iron. *Applied and Environmental Microbiology* **62**, 1458–1460.

Straub K. L., Schönhuber W. A., Buchholz-Cleven B. E. E. and Schink B. (2004) Diversity of Ferrous Iron-Oxidizing, Nitrate-Reducing Bacteria and their Involvement in Oxygen-Independent Iron Cycling. *Geomicrobiology Journal* **21**, 371–378.

Stumm, W., and J. J. Morgan. (1981) Aquatic chemistry, 2nd ed. John Wiley & Sons, New York, N.Y.

Sudek L. A, Templeton A. S., Tebo B. M., and Staudigel H. (2009) Microbioal ecology of Fe(hydr)oxide mats and basaltic rock from Vailulu'u Seamount, American Samoa. *Geomicrobiology Journal* **26**, 581–596.

Suzuki T., Hashimoto H., Itadani A., Matsumoto N., Kunoh H. and Takada J. (2012) Silicon and phosphorus linkage with iron via oxygen in the amorphous matrix of Gallionella ferruginea stalks. *Applied and Environmental Microbiology* **78**, 236–241.

Suzuki T., Hashimoto H., Matsumoto N., Furutani M., Kunoh H., and Takada J. (2011) Nanometer-scale visualization and structural analysis of the inorganic/organic hybrid structure of Gallionella ferruginea twisted stalks. *Applied and Environmental Microbiology* **77**, 2877–2881.

Swedlund P. (1999) Adsorption and polymerisation of silicic acid on ferrihydrite, and its effect on arsenic adsorption. *Water Research* **33**, 3413–3422.

Sánchez-Román M., Fernández-Remolar D., Amils R., Sánchez-Navas A., Schmid T., Martin-Uriz P. S., Rodríguez N., and McKezie J. A. (2014) Microbial mediated formation of Fe-carbonate minerals under extreme acidic conditions. *Scientific Reports* **4**, 4767.

Takahashi Y., Hirata T., Shimizu H., Ozaki T., and Fortin D. (2007) A rare earth element signature of bacteria in natural waters? *Chemical Geology* **244**, 569–583.

Tamura K., Peterson D., Peterson N., Stecher G., Nei M., and Kumar S. (2011) MEGA5: molecular evolutionary genetics analysis using maximum likelihood, evolutionary distance, and maximum parsimony methods. *Molecular Biology and Evolution* **28**, 2731–2739.

Taylor K. G. and Konhauser K. O. (2011) Iron in Earth Surface Systems: A Major Player in Chemical and Biological Processes. *Elements* **7**, 83–88.

Teh Y. A., Dubinsky E. A., Silver W. L., and Carlson C. M. (2008) Suppression of methanogenesis by dissimilatory Fe(III)-reducing bacteria in tropical rain forest soils: implications for ecosystem methane flux. *Global Change Biol*ogy **14**, 413–422.

Thibault P.-J., Evans R. J., Dutrizac J. E. and Rancourt D. G. (2009) Mineralogical confirmation of a near-P:Fe=1:2 limiting stoichiometric ratio in colloidal P-bearing ferrihydrite-like hydrous ferric oxide. *Geochimica et Cosmochimica Acta* **73**, 364–376.

Toner B. M., Bequó T. S., Michel F. M., Sorensen J. V., Templeton A. S., and Edwards K. J. (2012) Mineralogy of iron microbial mats from Loihi Seamount. *Frontiers in Microbiology* **3**, article 118.

Toner B. M., Santelli C. M., Marcus M. A., Wirth R., Chan C. S., McCollom T., Bach W. and Edwards K. J. (2009) Biogenic iron oxyhydroxide formation at mid-ocean ridge hydrothermal vents: Juan de Fuca Ridge. *Geochimica et Cosmochimica Acta* **73**, 388–403.

Trivedi P., Dyer J. A., and Sparks D. L. (2003) Lead sorption onto ferrihydrite. 1. A microscopic and spectroscopid assessment. *Environmental Science & Technology*, **37**, 908–914

Vatter A. E. and Wolfe R. S. (1956) Electron microscopy of *Gallionella ferruginea*. *Journal of Bacteriology* **72**, 248–252.

Voegelin A., Kaegi R., Frommer J., Vantelon D. and Hug S. J. (2010) Effect of phosphate, silicate, and Ca on Fe(III)-precipitates formed in aerated Fe(II)- and As(III)-containing water studied by X-ray absorption spectroscopy. *Geochimica et Cosmochimica Acta* **74**, 164–186.

Waite T. D., Davis J. A., Payne T. E., Waychunas G. A., and Xu N. (1994) Uranium (VI) adsorption to ferrihydrite: Application of a surface complaxiation model. *Geochimica et Cosmochimica Acta* **58**, 5465–5478.

Wang S. and Mulligan C. N. (2006) Effect of natural organic matter on arsenic release from soils and sediments into groundwater. *Environmental Geochemistry and Health* **28**, 197–214.

Wang X., Li W., Harrington R., Liu F., Parise J. B., Feng X. and Sparks D. L. (2013) Effect of Ferrihydrite Crystallite Size on Phosphate Adsorption Reactivity. *Environmental Science & Technology* **47**, 10322–10331.

Ward N., Larsen Ø., Sakwa J., Bruseth L., Khouri H., Durkin A. S., Dimitrov G., Jiang L., Scanlan D., Kang K. H., Lewis M., Nelson K. E., Methé B., Wu M., Heidelberg J. F., Paulsen I. T., Fouts D., Ravel J., Tettelin H., Ren Q., Read T., DeBoy R. T., Seshadri R., Salzberg S. L., Jensen H. B., Birkeland N. K., Nelson W. C.,

Dodson R. J., Grindhaug S. H., Holt I., Eidhammer I., Jonasen I., Vanaken S., Utterback T., Feldblyum T. V., Fraser C. M., Lillehaug J. R., and Eisen J. A. (2004) Genomic insights into Methanotrophy: The complete genome sequence of *Methylococcus capsulatus* (Bath) *PLoS Biology* **2**. 10

Waychunas G. A., Rea B. A., Fuller C. C. and Davis J. A. (1993) Surface chemistry of ferrihydrite: Part 1. EXAFS studies of the geometry of coprecipitated and adsorbed arsenate. *Geochimica et Cosmochimica Acta* **57**, 2251–2269.

Weber K. A., Achenbach L. A. and Coates J. D. (2006) Microorganisms pumping iron: anaerobic microbial iron oxidation and reduction. *Nature Reviews Microbiology* **4**, 752–764.

Weber K. A., Pollock J., Cole K. A., O'Connor S. M., Achenbach L. A. and Coates J. D. (2006) Anaerobic Nitrate-Dependent Iron(II) Bio-Oxidation by a Novel Lithoautotrophic Betaproteobacterium, Strain 2002. *Applied and Environmental Microbiology* **72**, 686–694.

Weelink S. A. B., van Doesburg W., Saia F. T., Rijpstra W. I. C., Röling W. F. M., Smidt H., and Stams A. J. M. (2009) A strictly anaerobic betaproteobacterium Georgfuchsia toluolica gen. nov., sp. nov. degrades aromatic compounds with Fe(III), Mn (IV) or nitrate as an electron acceptor. *FEMS Microbiology Ecology* **70**, 575–585.

Weiss J. V., Emerson D., Backer S. M. and Megonigal J. P. (2003) Enumeration of Fe(II)-oxidizing and Fe(III)-reducing bacteria in the root zone of wetland plants: Implications for a rhizosphere iron cycle. *Biogeochemistry* **64**, 77–96.

Weiss J. V., Rentz J. A., Plaia T., Neubauer S. C., Merrill-Floyd M., Lilburn T., Bradburne C., Megonigal J. P., and Emerson D. (2007) Characterization of neutrophilic Fe(II)-oxidizing bacteria isolated from the rhizosphere of wetland plants and description of *Ferritrophicum radicicola* gen. nov. sp. nov., and *Sideroxydans paludicola* sp. nov. *Geomicrobiology Journal* **24**, 559–570.

Whiticar M. J. (1999) Carbon and hydrogen isotope systematics of bacterial formation and oxidation of methane. *Chemical Geology* **161**, 291–314.

Wiesli R. A., Beard B. L., and Johnson C. M. (2004) Experimental determination of Fe isotope fractionation between aqueous Fe(II), siderite and “green rust” in abiotic systems. *Chemical Geology* **211**, 343–362.

Woyke T., Munk C., Nolan M., Emerson D., Field E. K., Chertkov O., Davenport K. W. and Goodwin L. (2013) Comparative genomics of freshwater Fe-oxidizing bacteria: implications for physiology, ecology, and systematics. *Frontiers in Microbiology* **4**.

Wu W., Swanner E. D., Hao L., Zeitvogel F., Obst M., Pan Y. and Kappler A. (2014) Characterization of the physiology and cell-mineral interactions of the marine anoxygenic phototrophic Fe(II) oxidizer Rhodovulum iodosum- implications for Precambrian Fe(II) oxidation. *FEMS Microbiology Ecology* **88**, 503–515.

Yee N. (2006) The rate of ferrihydrite transformation to goethite via the Fe(II) pathway. *American Mineralogist* **91**, 92–96.

Zachara J. M., Fredrickson J. K. and Li S. M. (1998) Bacterial reduction of crystalline Fe^ 3^+ oxides in single phase suspensions and subsurface materials. *American Mineralogist* **83**, 1426–1443.

Zachara J. M., Fredrickson J. K., Smith S. C., and Gassman P. L. (2001) Solubilization of Fe(III) oxide-bound trace metals by a dissimilatory Fe(III) reducing bacterium. *Geochimica et Cosmochimica Acta* **65**, 75–93.

Zachara J. M., Kukkadapu R. K., Frerickson J. K., Gorby Y. A., and Smith S. C. (2002) Biomineralization of poorly crystalline Fe(III) oxides by dissimilatory metal reducing bacteria (DMRB). *Geomicrobiology Journal* **19**, 179–207.

Zavarzina D. G., Kolganova T. V., Boulygina E. S., Kostrikina N. A., Tourova T. P., and Zavarzin G. A. (2006) *Geoalkalibacter ferrihydriticus* gen. nov. sp. nov., the first alkaliphilic representative of the family *Geobacteraceae*, isolated from a soda lake. *Microiol*ogy **6**, 673–682.

Zhu J., Pigna M., Cozzolino V., Caporale A. G. and Violante A. (2011) Sorption of arsenite and arsenate on ferrihydrite: effect of organic and inorganic ligands. *Journal of Hazardous Materials* **189**, 564–571.

de Vet W. W. J. M., Dinkla I. J. T., Rietveld L. C., and van Loosdrecht M. C. M. (2011) Biological iron oxidation by Gallionella spp. in drinking water production under fully aerated conditions. *Water Research* **45**, 5389–5398.

Acknowledgements

The work of this thesis is supported by many people.

First of all, I would like to thank Professor Yoshio Takahashi for his supervision. I am very proud that I could be a member of his laboratory. He always encouraged me and gave me many advices for my whole 6 years of research. He also gave me a lot of research opportunity outside the university.

I am grateful to Dr. Kazuya Tanaka and Dr. Aya Sakaguchi, and for their helpful comment in laboratory seminar.

I am grateful to Dr. Makita Hiroko and Dr. Ken Takai (JAMSTEC) for their supervision to my research. I leaned a lot of molecular and cultivation techniques from them which greatly expand my research topics. They also give me many suggestions during my whole PhD study.

I would like to express my profound thanks to Professor Andreas Kappler at Tübingen University. He kindly gave ma a chance to study at his laboratory. It was really precious time for me to spend three months at his laboratory. I also would like to say special thanks to my research buddy, Elif Köksoy. She supported all my research woks at the laboratory and also my private life at Tübingen.

I wish to thank following people for their technical support and helpful comments on my PhD work, Dr. Makoto Maeda for TEM and SEM observations, Dr. Yutaka Mouri for CHN analysis, Dr. Tomoya Uruga, Hajime Tanida, and Dr. Kiyofumi Nitta (BL01B1, SPring-8), and Dr. Yasuko Terada (BL27XU) for XAFS measurements, Dr. Takuro Nunoura and Dr. Zyunichi Miyazaki for 16S rRNA gene analysis, Dr. Uta Konno for isotope analysis, and Dr. Ijiri Akira for acetate measurement.

This PhD thesis was supported by JSPS research fellowships for young scientists (DC1). Also,

a part of my traveling fees was provided by Strategic Fostering program for Strategic Fostering Program for Young Researchers Engaged in Natural Sciences toward the Establishment of the Sustainable Society. My one-month stay at JAMSTEC was supported by Trans-crustal Advection and In-situ reaction of Global sub-seafloor Aquifer (TAIGA) project Mentorship on Research and Education.

Finally, I greatly appreciate my father, my mother, and my sisters. They always encouraged me and love me for what I am. I am so proud to belong with you all.

公表論文

1) Application of synchrotron based μ-XRF-XAFS to the speciation of Fe on single stalk in bacteriogenic iron oxides (BIOS)
S. Kikuchi, H Makita, S Mitsunobu, Y Terada, N Yamaguchi, K Takai, and Y Takahashi
Chemistry Letters, **40**, (2011), 680–681.

2) Characterization of biogenic iron oxides collected by the newly designed liquid culture method using diffusion chambers
S. Kikuchi, H Makita, S Mitsunobu, N Yamaguchi, K Takai, and Y Takahashi
Geobiology, **12**, (2014), 133–145.

参考論文

1) Bacteriogenic Fe(III) (oxyhydr)oxides characterized by synchrotron microprobe coupled with spatially resolved phylogenetic analysis
S Mitsunobu, F Shiraishi, H Makita, BN Orcutt, S Kikuchi, BB Jorgensen, Y Takahashi
Environmental Science & Technology, **46**(2012), 3304–3311.

2) Prokaryotic abundance and community composition in a freshwater iron-rich microbial mat at circumneutral pH
S Kato, S Kikuchi, T Kashiwabara, Y Takahashi, K Suzuki, T Itoh, M Ohkuma A Yamagishi
Geomicrobiology Journal, **29**(2012), 896–905.